Molecular characterization of known and novel olfactory subsystems in the zebrafish

Inaugural-Dissertation

zur

Erlangung des Doktorgrades

der Mathematisch-Naturwissenschaftlichen Fakultät

der Universität zu Köln

vorgelegt von

Gaurav Ahuja

aus Faridabad, Indien

Köln 2014/15

Molecular characterization of known and novel olfactory subsystems in the zebrafish

Inaugural-Dissertation

zur

Erlangung des Doktorgrades

der Mathematisch-Naturwissenschaftlichen Fakultät

der Universität zu Köln

vorgelegt von

Gaurav Ahuja

aus Faridabad, Indien

Köln 2014/15

Berichterstatter: Prof. Dr. Sigrun I. Korsching

Prof. Dr. Peter Kloppenburg

Tag der mündlichen Prüfung: 27-January-2015

Dedicated to my family and teachers

मेरे परिवार और शिक्षकों को समर्पित

Table of Contents

I. Acknowledgement..8

II. Introduction..9

A. Mammalian olfactory architecture is characterized by segregation..9

in several olfactory organs..9

B. Fish possess a single olfactory organ..11

C. Principles of olfactory processing in vertebrates..12

D. All olfactory receptor gene families, except one are GPCRs......................................13

1. ORA (v1r-related) olfactory receptors..13

2. TAARs olfactory receptors..14

3. OlfC (V2R-related) olfactory receptors...15

4. OR (Odorant receptors) olfactory receptors..16

5. FPR (formyl peptide receptors) olfactory receptors..16

6. Membrane Guanylate Cyclase (GC-D) olfactory receptors.....................................17

E. Expression of different receptor gene families is segregated to different OSN types..............17

F. Each OSN subtype expresses distinct signaling Gα proteins.......................................18

G. Olfactory axon convergence to target glomeruli..19

III. Aims of the study..21

....21

IV. Publications of the Dissertation...22

Ahuja G et al (2013). Sci. Rep. 3, 2063; DOI:10.1038/srep02063...23

Ahuja G et al (2014). Sci. Rep. 4, 4037; DOI:10.1038/srep04037...37

Hussain A*, Saraiva L.R*, Ferrero D.M*, Ahuja G*, Krishna V.S, Liberles S.D, and Korsching S.I (2013). PNAS, doi/10.1073/ pnas. 1318596110...46

Behrens M, Frank O*, Rawel H*, Ahuja G*, Potting C, Hofmann T, Meyerhof W and Korsching

S.I (2014). J Biol Chem.pii: jbc.M114.573162....57
Ahuja G and Korsching S.I (2014). doi:10.4161/19420889.2014.970501....69
V. Discussion....75
Zebrafish crypt neurons project to a single, identified mediodorsal glomerulus....75
Kappe neurons, a novel population of olfactory sensory neurons....78
Zebrafish olfactory receptor ORA1 recognizes a putative reproductive pheromone....80
High-affinity olfactory receptor for the death-associated odor cadaverine....81
Coding strategies in small olfactory subsystems may be different from....83
those employed in large subsystems....83
A distinct behavioral response may be generated by activation of a single....84
high- affinity receptor....84
VI. References....85
VII. Abstract....94
VIII. Zusammenfassung....95
IX. Author Contributions....97
X. ERKLÄRUNG....100
XI. Curriculum vitae....101
XII. Appendix....105
List of abbreviations....105

This page was intentionally left blank.

I. Acknowledgement

This study was conducted in the system neurobiology laboratory of Prof. Dr. Sigrun I. Korsching at the Institute for Genetics, University of Cologne, Germany. My research was supported by the generous grant from the International Graduate School in Developmental Health and Diseases (IGSDHD) at the Institute for Genetics. Foremost, I pay my sincere gratitude to Prof. Dr. Sigrun I. Korsching for being a great mentor. I am very thankful to her for the support, advices and trust she bestowed on me. I learned from her the meanings of patience, coordination, candidness and how to tackle daily life of a science laboratory. I am very contented that I had the opportunity to spend these years in learning, from culture to science, at her laboratory.

I will extend my acknowledgement to Prof. Dr. Ansgar Büschges and Prof. Dr. Peter Kloppenburg for accepting to be in my thesis committee, for their interest in my research work, and for kindly serving as my thesis referees. I greatly appreciate Prof. Dr. Wolfgang Meyerhof and Dr. Maik Behrens at German Institute of Human Nutrition Potsdam-Rehbruecke for our successful collaboration.

Many thanks to Prof. Dr. Matthias Hammerschmidt for providing Loligo motion tracking software. I was humbled and honored for being accepted in the class of 2010 of the International Graduate School of Health and Disease. Many thanks to Dr Isabell Witt, Cathy Joergens and Joanna Majczak for their support in all walks of life at graduate school. I was fortunate to have cooperative and ambitious lab fellows like Dr. Yuichiro Oka, Dr. Ashiq Hussain, Ivan Ivandic, Syed Adnan, Venkatesh Krishna, Daniel Kowatschew, Milan Dieris, Kanika Sharma, Vladimir Shiryagin and Dr Veronika Zapilko to whom I am in debt for a great deal of valuable feedback and collaborations. Sincere thanks to Mehmet Saltürk for taking care of all lab equipments, fish room, computers and experimental material supplies.

I am in lack of words to thank my father who had a vision for the education of his children. I am greatly thankful to him for financially and morally supporting me in my life. A great deal of thanks to my mother for taking care of the family, for staying awake with us during exams nights and for all her great sacrifices that she made with my father for their children education. I would also like to give a big thank to my elder brother for igniting the passion in me to pursue a career in biological sciences. Very special thanks to my wife Tripti Mishra Ahuja for being a loving, supportive, caring and understanding life companion.

II. Introduction

The sense of smell (olfactory sense) plays a vital role in many essential behaviors such as prey detection, predator evasion and reproduction. Most vertebrate species possess a specialized olfactory system to detect and discriminate diverse odorants such as amino acids, nucleotides, bile salts, gonadal steroids, and prostaglandins (Speca et al. 1999). However, the molecular understanding of fish olfaction is lagging behind, since the seminal discoveries were mostly made in the mammalian olfactory system.

In 1991, the groundbreaking research from then postdoc Linda Buck in Richard Axels laboratory led to the discovery of the first olfactory receptors. In subsequent work Linda Buck and Richard Axel could show that olfactory receptors constitute a huge gene family, and are expressed in olfactory sensory neurons (OSNs), which are grouped in distinct expression zones (Buck & Axel 1991). Furthermore they deorphanized many olfactory receptors and began the characterization of olfactory brain circuits activated by these receptors (Buck 2005). This pioneer work was recognized by the Nobel committee, who in 2004 awarded Linda Buck and Richard Axel with the Nobel prize in Physiology or Medicine.

A. Mammalian olfactory architecture is characterized by segregation in several olfactory organs

Five to six different olfactory receptor gene families that are expressed in two major and possibly several minor cell types carry the complexity of odor detection in mammals (reviewed in (Gaillard et al. 2004; Fleischer et al. 2009; Hayden & Teeling 2014)). Most mammals, including rodents, exhibit a bipartite olfactory system that is anatomically segregated into two main olfactory surfaces (main olfactory epithelium; MOE and vomeronasal organ; VNO). Each organ expresses distinct olfactory receptor gene families and recognizes distinct classes of odorants. Apart from these, rodents also possess two other olfactory subsystems **(Figure 1b)** which are known to express olfactory receptors, i.e. the septal organ (SO) and the Grueneberg ganglion (GG), *cf*. (Hayden & Teeling 2014; Fleischer et al. 2009)

The MOE mostly contains ciliated neurons, which express a large repertoire of olfactory receptors (odorant receptors, *ORs*) (Mombaerts et al. 1996), as well as the much smaller *taar* gene family (Johnson et al. 2012) and their axons project to the main olfactory bulb (OB) (Mombaerts et al. 1996; Johnson et al. 2012). The VNO contains microvillous neurons that express two families of vomeronasal receptors (*v1rs* and *v2rs*) and their axons projects to the accessory olfactory bulb (AOB) (Wagner et al. 2006). Furthermore, a recently characterized small family of rodent-specific olfactory receptors, i.e. formyl-peptide receptors are also known to be expressed in VNO **(Figure 1b)** (Rivière et al. 2009).

In rodents, the grueneberg ganglion is localized at the tip of the nose, close to the opening of the naris. The neurons of grueneberg ganglion are spherical shaped and possess thirty to forty primary cilia per neuron (Brechbühl et al. 2008). Furthermore, their cell bodies are ensheathed by glial cells (Brechbühl et al. 2013). Grueneberg ganglion neurons project their axons to a small number of glomeruli in the caudal main olfactory bulb (Fleischer et al. 2009; Brechbühl et al. 2008; Brechbühl et al. 2013). These neurons express elements of a cGMP second messenger pathway, including the cGMP-specific cyclic nucleotide-gated channel *CNGA3* and the cGMP-stimulated phosphodiesterase *PDE2* (Juilfs et al. 1997; Meyer et al. 2000; Leinders-Zufall et al. 2007). Recent findings in rodents suggest the functional role of grueneberg ganglion neurons as a fine-tuned cold sensor or alarm pheromone sensor (Munger et al. 2010; Schmid et al. 2010; Brechbühl et al. 2008).

The septal organ is a small patch of olfactory neuroepithelium at the ventral base of the nasal septum found in many mammals (Kratzing 1978; Kociánová et al. 2006). Initial characterization of the septal organ suggests the involvement of two signaling cascades, which was later confirmed with the identification of corresponding fitting receptors i.e. *ORs* and *GC-D* (Kaluza et al. 2004) .

However, the receptor segregation as described above is not without exceptions. A few V1R transcripts have been detected in the MOE of humans and goats (Rodriguez et al. 2002; Wakabayashi et al. 2007) . Similarly, one particular V2R subtype-V2R83- is also expressed outside VNO in the neurons of the grueneberg ganglion (Fleischer et al. 2009). Interestingly, whole-genome sequencing revealed the ectopic expression of *ORs* in non-chemosensory tissues e.g. MOR23 and testicular hOR17-4 (Kang & Koo 2012). Moreover, TAAR1 is the only TAAR subtype which is not expressed on the olfactory epithelium, but indeed express in stomach, kidney, lungs and some brain regions (amygdala) (Babusyte et al. 2013; Bradaia et al. 2009; Hussain et al. 2009a; Panas et al. 2012).

B. Fish possess a single olfactory organ

The fish olfactory system consist of a single olfactory organ which is known to express orthologs of all known mammalian olfactory receptor families except formyl-peptide receptors (*FPRs*) (Korsching 2009). Furthermore, fish possess the same main types of olfactory sensory neurons, ciliated neurons, which harbor olfactory receptors of *or* and *taar* gene families, and microvillous neurons which express *v1rs* and *v2rs* olfactory receptor gene families (Sato et al. 2005) **(Figure 1a)**. In addition to these well known cell types, fishes possess a third type of olfactory sensory neuron, crypt neurons, which were originally identified morphologically by electron microscopy (Hansen & Zeiske 1998; Parisi et al. 2014). In rodents, novel and rare populations of olfactory sensory neurons are reported as well (Elsaesser & Paysan 2007; Elsaesser et al. 2005). This further strengthen the hypothesis of existence of new olfactory sensory neurons in zebrafish. Crypt neurons appeared early in vertebrate evolution, are already present in cartilaginous fish (Ferrando et al. 2006), and have been described in many teleost fish as well (Hansen & Zeiske 1998). Crypt neurons exhibit a large globular soma and possess both cilia and microvilli, and the eponymous crypt of unknown significance. Electron microscopy study suggests the cilia (up to 7 in number, 9+2 pattern of microtubules) are submerged in the upper portion of the cell body and the microvilli are located on the apical rim of the crypt. In comparison to other known olfactory cell types, crypt neurons have relatively larger nucleus which covers 1/3rd of the cellular volume. Crypt neurons also contains larger size mitochondria and abundant ribosomes (Hansen & Zeiske 1998). Higher magnification in electron microscopy showed axons emanating from the crypt neurons, suggesting them to constitute functional neurons with projections to olfactory bulb. Each crypt neuron is in close contact to a specialized supporting cell, which is electron-lucent and bears microvilli (Hansen & Zeiske 1998; Hansen & Finger 2000). Furthermore, I have recently identified a novel, fourth olfactory sensory neuron population in zebrafish, which were named as kappe neurons for their characteristic shape (Ahuja et al. 2014).

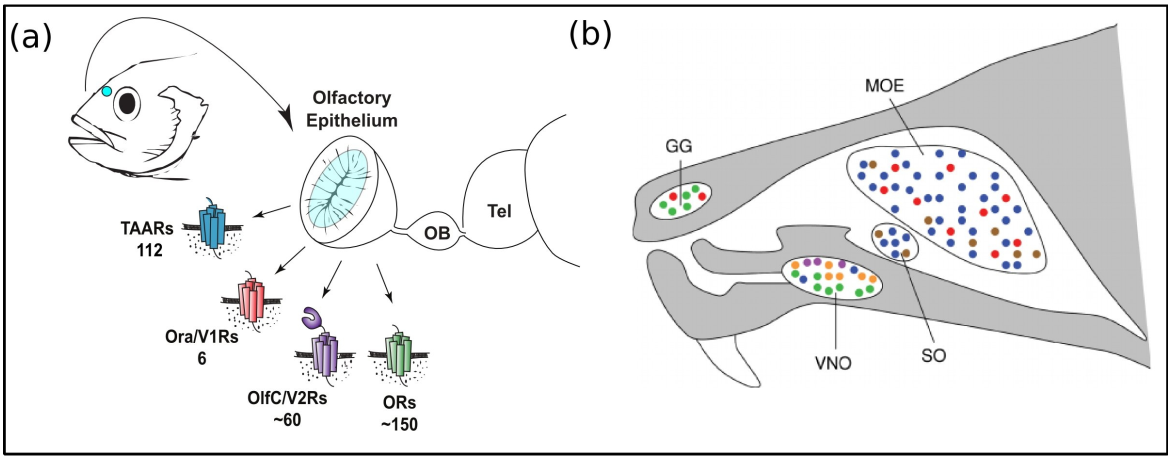

Figure 1: Schematic representation of the olfactory system of zebrafish (a) and mouse (b). (a) Cyan dot on the fish forehead is the representation of the olfactory epithelium. The sensory surface (cyan-colored) contains OSNs expressing olfactory receptors of 4 gene families. (b) Rodents olfactory architecture is characterized by segregation in several olfactory organs. The olfactory receptor types expressed in each of these organs are indicated by color: ORs in blue, V1Rs in orange, V2Rs in green, TAARs in red, FPRs in purple, GC-D in brown (a: modified from Luis Saraiva doctoral thesis (Saraiva & Korsching 2007); b: modified from (Fleischer et al. 2009)).

C. Principles of olfactory processing in vertebrates

Despite these obvious differences between the coarse structure of fish and mammalian olfactory organs, the logic of olfactory processing is remarkably similar. With very few exceptions (Sato et al. 2005), a receptor neuron selects a single receptor gene for expression out of the complete olfactory receptor repertoire. This feature is known as “one neuron–one receptor” rule. Thus individual OSN reflect the odor response spectrum of the particular olfactory receptor they express. However, a violation of this rule was observed in *Danio rerio*, where closely related receptors may be co-expressed (zOR103-1 with zOR103-2 and/or zOR103-5 (Sato et al. 2005).

Secondly, similar to mammals, fishes also obey principle of “convergence of like axons to target glomeruli” (Braubach et al. 2012). This principle suggest that the OSNs expressing a given olfactory receptor converge into a specific region in the olfactory bulb called glomeruli. This principle results in a receptotopic map on the olfactory bulb (Mori & Sakano 2011), however in comparison to rodents, a little is known about the receptotopic map in fishes (Friedrich & Korsching 1997; Friedrich & Korsching 1998).

D. All olfactory receptor gene families, except one are GPCRs

As mentioned in the initial remarks, the molecular identity of the olfactory receptors came to light in 1991, after the pioneer work of Linda Buck and Richard Axel which led to the discovery of a large and diverse family of G protein-coupled receptors (GPCRs), expressed in the rat olfactory epithelium that were proposed to function as odorant receptors (Buck & Axel 1991). The repertoire of olfactory receptor genes currently consists of 6 different gene families, the odorant receptors (*ors*), vomeronasal receptor genes (*v1rs and v2rs*), and trace amine-associated receptor genes (*taars*), membrane guanylate cyclase (GC-D) and the recently characterized formyl peptide-like receptors (*fprs*), for review see (Buck 2004; Fleischer et al. 2009) **(Figure 2).**

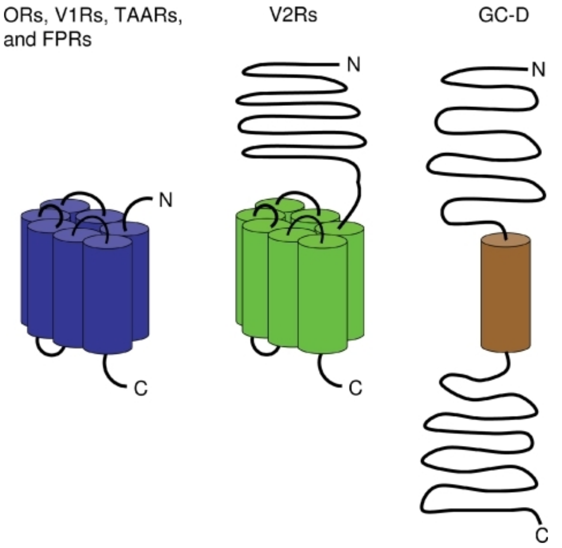

Figure 2: Schematic representation of the membrane topology of olfactory receptors. ORs, V1Rs, V2Rs, TAARs, and FPRs belong to the GPCRs which contains seven transmembrane domains (indicated by cylinders), guanylate cyclase GC-D comprises only one transmembrane domain. In all receptor types, the N-terminus is localized to the extracellular face of the cell membrane whereas the C-terminal end resides intracellularly. (modified from (Fleischer et al. 2009)).

1. ORA (v1r-related) olfactory receptors

Some mammalian species have over 100 *v1r* genes which are expressed in VNO (Fleischer et al. 2009; Ibarra-Soria et al. 2014). In contrast, the corresponding family in teleosts, the *v1r*-related ora gene family, is very small and comprises just 6 genes (Saraiva & Korsching 2007; Korsching 2009.). Like other olfactory receptors, ora genes are expressed in a sparse population within the sensory surface of fish olfactory epithelium (Saraiva & Korsching 2007; Pfister & Rodriguez 2005). In comparison with the other receptor gene families in teleosts, the *ora* gene family exhibits several peculiar properties i.e. orthologs of ora genes in other species are more closely related to each other than to their paralogs in the same species (Saraiva & Korsching 2007). In other words, the *ora* genes are evolutionary more ancient than the teleost species, and indeed their direct orthologs can be found in lineages as far as that of cartilaginous fishes (Saraiva & Korsching 2007). Consistent with this observation, an analysis of synonymous to nonsynonymous mutation rates revealed that *ora* genes are under strong selective pressure and evolve much slower than other olfactory receptor genes. Strikingly, the genomic arrangement of *ora* genes is also unlike other olfactory receptors which mostly exist in clusters, often in the same genomic orientation. In contrast, four out of the six *ora* genes are arranged in closely linked asymmetrical gene pairs across all species studied. Both head to head (*ora1/ora2*) and tail to tail (*ora3/ora4*) arrangements exist (Saraiva & Korsching 2007). Ligands for the mammalian *v1rs* were found among the low molecular weight steroids (Isogai et al. 2011; Punta et al. 2002; Boschat et al. 2002), whereas nothing is known about the ligands and their molecular identities of *v1r*-related *ora* genes. For this, Two research groups teamed up a while ago to attempt deorphanization of teleost *ora* receptors (ORA1), the Korsching lab in Cologne and the Meyerhof lab in Potsdam. They have identified that ORA1 detects p-hydroxy phenyl acetic acid (pHPAA) with high sensitivity and specificity. Furthermore, in order to elucidate the biological function of this compound, I have performed different behavioral experiments. Neither aversive nor attractive behavior was observed using the ligand, but interestingly I found that oviposition behavior could be elicited, when pairs of adult zebrafish were exposed even to low concentrations of this ligand (Behrens et al. 2014).

2. TAARs olfactory receptors

Trace amine-associated receptors (*taars*) are related to G-protein-coupled aminergic neurotransmitter receptors such as dopamine receptors. *Taar* genes have been found in several genomes including that of lower vertebrates (Gloriam et al. 2005). A detailed characterization of the teleost *taar* genes repertoire has been performed (Hashiguchi & Nishida 2007; Hussain et al. 2009). The latter analysis contradicts the former in that it suggests a late evolutionary origin of *taar* genes within the MRCA of cartilaginous fishes and bony fishes, since shark possesses *taar* genes with all signature motifs, whereas in lamprey only *taar*-like genes were found. Two of the three subclasses of teleost *taar* genes contain the amine binding motif and are expected to possess amine ligands (Hussain et al. 2009). Receptors from all three classes are expressed in sparse populations of OSNs, within the range of expression of *or* genes. Teleost *taar* families are generally larger that mammalian families, e.g. zebrafish possess 112 *taar* genes (Hussain et al. 2009), compared to only 14 *taar* genes for mouse. Mammalian TAARs are activated by amine ligands (Borowsky et al. 2001; Liberles 2009; Ferrero et al. 2011; Liberles & Buck 2006) . Some of these amines are present in mouse urine in gender- or stress-dependent concentrations, leading to speculations that TAARs might be involved in the detection of some 'urine-borne' pheromones (Liberles & Buck 2006). In the rodent MOE, TAARs are co-expressed with the Gαs- related G protein, Gαolf (Liberles & Buck 2006); in the grueneberg ganglion, however, TAARs are co-expressed with Gα i2 (Fleischer et al. 2009). A recent study suggests TAAR5 is activated by a sexually dimorphic mouse odor (Ferrero et al. 2012; Dewan et al. 2013). TAAR5 detects male mouse odor with exquisite sensitivity, and this response is both sex and age dependent. However, until very recently, no ligands for teleost TAAR receptors had been reported.

Recently, the first teleost TAAR receptor, TAAR13c was deorphanized in the Korsching lab (Hussain et al. 2013). In this publication it was shown that TAAR13c of zebrafish detects cadaverine with high sensitivity and specificity in an heterologous expression system. I have validated these findings *in vivo* by analyzing a neural activation marker (phospho-ERK) together with a TAAR13c antibody after exposure of zebrafish to different concentrations of cadaverine. Furthermore, I have also established a behavioral assay using a two-channel-choice paradigm that enables an accurate determination of the concentration dependence of the cadaverine-elicited aversive behavior reported in (Hussain et al. 2013). Together, my results show that at low concentrations of cadaverine TAAR13c constitutes the major receptor involved in the aversive response.

3. OlfC (V2R-related) olfactory receptors

The OlfC receptors are related to mammalian V2R receptors and like these belong to the class C of GPCRs. They contains a large N-terminal extracellular regions and also possess similarities to metabolic glutamate receptors (Alioto & Ngai 2006) **(Figure 2)**.

Unlike other olfactory receptors, they are not monophyletic. *OlfC* receptors repertoire size varies several-fold between teleost species, but are well within the range of mammalian *v2r* repertoires (Korsching 2009). Extreme species-specific specialization has led to the complete loss of the *v2r* family in several mammalian species. (Luu et al. 2004) performed modelling for OlfCa1 together with ligand analysis, and suggested amino acids as the key ligand for teleost OlfC receptors. Furthermore in 2013, another member of this family, Olfcc1, which exhibits a broad expression within the sensory surface of olfactory epithelium, was deorphanized. It recognizes polar, nonpolar, acidic, and basic amino acids as natural ligands (De Maria et al. 2013). This receptor co-expresses with other OlfC receptors and promotes their localization to the plasma membrane and therefore helps in intracellular trafficking of other olfactory receptors of the same family.

4. OR (Odorant receptors) olfactory receptors

OR (odorant receptors) have been subdivided into two classes: Class I which mainly contains fish specific *OR* genes, though it also contains some members of the mammalian ORs and Class II which solely contains members of mammalian *OR* genes (Buck & Axel 1991; Fleischer et al. 2009; Korsching 2009). Mammals have lost most of the teleost OR groups but large gene expansions in the two remaining groups increased the mammailan *OR* gene repertories severalfold as compared to the teleost fish (Korsching 2009). Within teleost fishes, zebrafish exhibit a severalfold larger *OR* repertoire than pufferfish (Korsching 2009). Similar to the genomic location of *or* genes in mammals, zebrafish *OR* genes are mainly present in gene clusters but some occur as isolated genes (Gaillard et al. 2004; Fleischer et al. 2009). Zebrafish *ORs* exhibit a slow rate of evolution in comparison with mammalian *OR* genes and thus do not show any sign of positive selection, in contrast to the latter (reviewed in (Korsching 2009)). In zebrafish as in mammals, each *OR* gene is expressed in a sparse population of OSNs within the sensory surface. An early study performed by (Weth et al. 1996), suggested restricted spatial expression patterns for different zebrafish *ORs*, so-called expression domains, within the adult olfactory epithelium.

5. FPR (formyl peptide receptors) olfactory receptors

About two decades ago a new class of GPCRs called formyl peptide receptors was discovered (Boulay et al. 1990). Interestingly, *fpr* genes are without introns and have known to be clustered on a single chromosome (mouse chromosome 17). FPRs were known to have a function in the immune system, but recently some rodent *fprs* have been shown to function as olfactory receptors (Rivière et al. 2009). Careful analysis revealed that seven murine *fpr* genes are expressed in about 1% of the VNO sensory neurons. FPR-expressing sensory neurons do not co-express other members of VNO-specific gene families i.e. V1Rs and V2Rs. Their coding sequences are intronless and their open reading frames encode proteins of about 350 amino acid residues (Gao et al. 1998; Wang & Ye 2002) with highly conserved transmembrane domains and more variable extracellular domains; the latter are supposed to be involved in ligand binding (Migeotte et al. 2006). **(Figure 2)**. Like the FPRs expressed in immune cells, FPRs expressed in VNO sensory neurons are activated by formylated peptides and other disease-related compounds, suggesting a potential function in detection of infected conspecifics or contaminated food.

6. Membrane Guanylate Cyclase (GC-D) olfactory receptors

A membrane bound GC-D was found to be expressed in a subset of OSNs in the MOE (Juilfs et al. 1997). These sensory neurons exhibit a different signaling pathway as compared to other sensory neurons of the mammalian MOE which mainly transduce *via* the canonical cAMP pathway (Liberles 2014). GC-D positive neurons are endowed with cGMP-dependent phosphodiesterase PDE2A and a cGMP sensitive cyclic nucleotide-gated ion channel (Juilfs et al. 1997; Meyer et al. 2000). Furthermore, a small subset of neurons in the septal organ also express GC-D receptors (Walz et al. 2007) . GC-D positive neurons project their axons to a discrete chain of glomeruli in the MOB (Juilfs et al. 1997; Leinders-Zufall et al. 2007; Walz et al. 2007). Higher magnification revealed the apical localization of GC-D receptor, co-localize with cilia and thus exhibits an ideal location for odor detection. Uroguanylin and guanylin were identified as a specific ligands to activate GC-D positive neurons, in a GC-D dependent manner (Leinders-Zufall et al. 2014; Leinders-Zufall et al. 2007). These findings were later supported in heterologous system expressing GC-D (Duda & Sharma 2008). Other findings indicate that GC-D may also be involved in the detection of carbon dioxide (CO_2), since GC-D neurons – in contrast to other OSNs – respond to low concentrations of CO_2 (Sun et al. 2009).

E. Expression of different receptor gene families is segregated to different OSN types

Consistent with the mammalian signal transduction pathway, zebrafish ciliated

OSNs express similar signal transduction machineries downstream of OR-type olfactory receptors, such as olfactory-specific GTP-binding protein subunit (*Golf*) and cyclic nucleotide-gated cation channel A2 subunit (*cnga2*) (Hansen et al. 2003; Sato et al. 2005) . Olfactory marker protein (*omp*) expression is restricted to ciliated OSNs, and is not found in the microvillous OSNs in zebrafish (Sato et al. 2005), different from the situation in mammals, where OMP is expressed in all the chemosensory neurons in both the MOE and VNO (Mombaerts 2006; Omura & Mombaerts 2014). The microvillous OSNs in zebrafish express transient receptor potential channel C2 (*trpc2*) (Sato et al. 2005; Oka et al. 2012), whose mouse ortholog plays a central role in the signal transduction cascade of vomeronasal sensory neurons for social and sexual behaviors (Ma 2012; Isogai et al. 2011). In addition to these two cell types known from mammals, fishes possess a third type of olfactory sensory neuron, crypt neurons. Recent studies in zebrafish suggest the expression of a single member of a highly conserved receptor gene family (the *v1r*-related *ora genes*) in crypt neurons (positive for S100-immunoreactivity) and suggests a ‘one cell type–one receptor’’ mode of expression (Oka et al. 2012). All three types of olfactory sensory neurons in fishes have been defined by the presence of characteristic molecular markers, *omp* for ciliated neurons, *trpc2* for microvillous neurons and S100-like immunoreactivity or TrkA-like immunoreactivity for crypt neurons (Germana et al. 2004; Catania et al. 2003).

F. Each OSN subtype expresses distinct signaling Gα proteins

The alpha subunits of the hetrotrimeric G proteins are mainly responsible for transducing signals and are well studied in mammalian systems. In mammals, OR and TAAR olfactory receptors signal via Golf (Belluscio et al. 1998; Liberles & Buck 2006), V1Rs and all FPRs except FPR-rs1 transduce via Gi2 and V2Rs and FPR-rs1 via Go (Berghard & Buck 1996; Rivière et al. 2009; Liberles 2009) .Recently a comprehensive evaluation of zebrafish G alpha proteins has shown the expression of Go1, Go2, Gi, and Golf in the olfactory epithelium (Oka & Korsching 2011). Thus, olfactory receptors in mammals and teleosts mostly have homologous signaling molecules but also show some molecular differences, possibly resulting from their adaptation to the respective environment. The fish-specific crypt neurons were shown to express a specific G alpha subunit, Gi1b and therefore suggest the sole identified receptor of crypt neurons, Ora4, may transduce via Gi1b in crypt neurons (Oka et al. 2012) **(Figure 3)**.

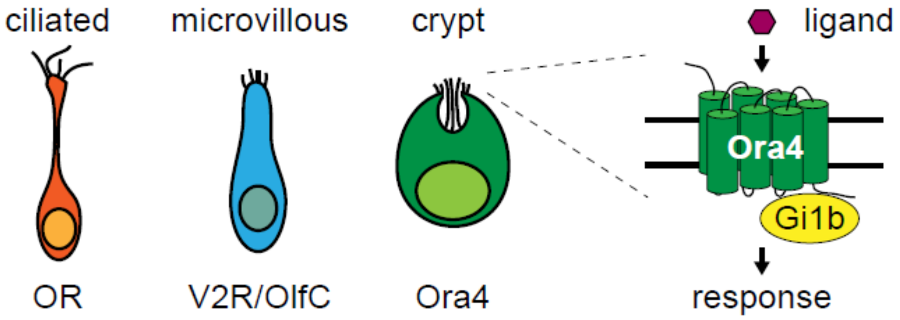

Figure 3: Schematic representation of all 3 olfactory sensory neuron types and corresponding olfactory receptors. Modified from (Oka et al. 2012).

G. Olfactory axon convergence to target glomeruli

Various studies in rodents suggest that axons originating from OSNs expressing a particular olfactory receptor projects to a specific pair of glomeruli with stereotypical position in the OB. This led to the idea of ¨one glomerulus-one receptor¨, and consequently suggested the presence of a receptotopic map in the olfactory bulb. Visualization of axonal projections of receptor-specific OSNs has been achieved by three different methods in mice. Firstly, OR-IRES-reporter knock-in mice have been employed to visualize the target glomeruli in the olfactory bulb (Mombaerts et al. 1996). Secondly, traces of OR receptor transcripts have been detected at the axon terminals by *in situ* hybridization (Vassar et al. 1994), and lastly, traces of the OR receptor protein have been detected at the axon terminals (Strotmann et al. 2004). In zebrafish the second and third methods failed to identify axonal convergence presumably due to lower abundance of mRNA and proteins in axonal terminals of OSNs. Therefore a transgenic approach was used to identify the target glomeruli for ciliated and microvillous neurons (Sato et al. 2005). Transgenic zebrafish with fluorescent reporter genes under promoter control of trpc2 and omp (Sato et al. 2005), showed mutually exclusive glomerular innervation in the olfactory bulb. All six glomeruli of the mediodorsal cluster in double transgenic fishes (Tg(OMP:lynRFP) and Tg(TRPC2:gap-Venus) were not labeled suggesting these glomeruli could belong to the third population of OSNs, crypt neurons (Sato et al. 2005). However, in two fish species, catfish and crucian carp, a ventral position of the crypt neuron target region has been suggested based on backtracing experiments (Hansen et al. 2003; Hamdani el & Doving 2006). Therefore it was unclear whether crypt neurons project to a single target glomerulus in the olfactory bulb in accordance with the rules found for mammalian olfactory receptors of the *OR* (Mombaerts et al. 1996) and *taar* (Johnson et al. 2012) families, or whether they might connect to several target regions like neurons expressing mammalian *v1rs* (Wagner et al. 2006).

I have used the crypt neuron marker TrkA-like immunoreactivity, backtracing and morphometry to identify the target region of crypt neurons as a single identified glomerulus of the mediodorsal cluster, mdg2 (Ahuja et al 2013). Thus the axonal convergence of neurons expressing the V1R-related ORA4 is unlike that observed for mammalian V1Rs, and corresponds to that observed for mammalian ORs and TAARs.

III. Aims of the study

Olfaction is a key sense by which organisms acquire information about the surrounding world. Basic features of olfactory information processing are conserved throughout the vertebrate phylum. Zebrafish has in recent years become a good vertebrate model system to study olfaction.

Olfactory sensory neurons come in different types, which constitute different subsystems with characteristic olfactory receptor repertoires, signal transduction machinery, neuronal circuits, and biological function. The two major types, ciliated and microvillous neurons, are well characterized, but a third type, crypt neurons, is not well understood. I have undertaken to identify the target region of crypt neuron axons in the olfactory bulb (Ahuja et al. 2013). In the course of these studies I have discovered a novel, fourth type of olfactory sensory neurons called *kappe* neurons, which constitute a fourth subsystem (Ahuja et al. 2014).

My second objective was the *in vivo* validation of ligands for zebrafish olfactory receptors that had been identified in heterologous expression systems. I have established phospho-ERK as a odor-induced neuronal activation marker in zebrafish, and used this marker together with a receptor antibody to assess, whether the receptor analyzed (TAAR13c) is the major receptor for its ligand (cadaverine). Moreover, I have established a two-choice behavioral assay to measure the cadaverine-induced aversion behavior at defined stimulus concentrations (Hussain et al. 2013). For another receptor/ligand pair, ORA1 and p-hydroxyphenylacetic acid, I have searched for a biological function, and have identified enhanced oviposition as olfactory-mediated response of zebrafish to p-hydroxyphenyl-acetic acid (Behrens et al. 2014; Ahuja & Korsching 2014).

IV. Publications of the Dissertation

Publication 1

Gaurav Ahuja, Ivan Ivandic, Mehmet Saltuerk, Yuichiro Oka, Walter Nadler & Sigrun I. Korsching. *Zebrafish crypt neurons project to a single, identified mediodorsal glomerulus.* Sci. Rep. 3, 2063; DOI:10.1038/srep02063 **(2013)**. http://www.nature.com/srep/2013/130624/srep02063/full/srep02063.html

SCIENTIFIC REPORTS

OPEN

SUBJECT AREAS:
OLFACTORY RECEPTORS
MOLECULAR BIOLOGY
CELL BIOLOGY
OLFACTORY BULB

Received
15 May 2013

Accepted
7 June 2013

Published
24 June 2013

Zebrafish crypt neurons project to a single, identified mediodorsal glomerulus

Gaurav Ahuja[1], Ivan Ivandić[1], Mehmet Saltürk[1], Yuichiro Oka[1]*, Walter Nadler[2] & Sigrun I. Korsching[1]

[1]Institute of Genetics, University at Cologne, D-50674 Cologne, Germany, [2]Institute for Advanced Simulation (IAS), Juelich Supercomputing Centre (JSC), Forschungszentrum Juelich, D-52425 Juelich, Germany.

Correspondence and requests for materials should be addressed to S.I.K. (sigrun.korsching@uni-koeln.de)

* Current address: Research Center for Child Mental Development, University of Fukui, 23-3 Matsuoka-shimoaizuki, Eiheiji, Fukui 910-1193, JAPAN.

Crypt neurons are a third type of olfactory receptor neurons with a highly unusual "one cell type - one receptor" mode of expression, the same receptor being expressed by the entire population of crypt neurons. Attempts to identify the target region(s) of crypt neurons have been inconclusive so far. We report that TrkA-like immunoreactivity specifically labeled somata, axons, and terminals of zebrafish crypt neurons and reveal a single glomerulus, mdg2 of the dorsomedial group, as target glomerulus of crypt neurons. Injection of a fluorescent tracing dye into the mdg2 glomerulus retrogradely labeled mostly crypt neurons, as assessed by quantitative morphometry, whereas no crypt neurons were found after injections in neighboring glomeruli. Our data provide strong evidence that crypt neurons converge onto a single glomerulus, and thus form a labeled line consisting of a single sensory cell type, a single olfactory receptor and a single target glomerulus.

Olfactory coding in vertebrates employs a receptotopic map in the target region of olfactory receptor neurons, the olfactory bulb[1,2]. The monogenic expression of large olfactory receptor gene families in ciliated olfactory receptor neurons engenders a correspondingly large repertoire of target modules (glomeruli) in the olfactory bulb, due to axonal convergence. Similarly, microvillous neurons, another type of olfactory receptor neurons, express large gene families and converge into many target glomeruli. Crypt neurons constitute a third type of olfactory receptor neurons[3]. They appeared early in vertebrate evolution, are already present in cartilaginous fish[4], and have been described in many teleost fish as well[5]. Crypt neurons have been originally identified by their conspicuous morphology, which includes a large globular soma, the presence of both cilia and microvilli, and the eponymous crypt of unknown significance. A single olfactory receptor, the V1R-related ORA4, was found to be expressed in zebrafish crypt neurons[6], but it is unclear whether crypt neurons project to a single target glomerulus in the olfactory bulb in accordance with the rules found for olfactory receptors of the OR[7] and TAAR[8] families, or whether they might connect to several target regions like neurons expressing mammalian V1Rs[9].

Crypt neurons constitute an intriguing cell population, and several attempts have been made to elucidate their function[10–13] and their target region in the olfactory bulb[14–18]. However, results have been partially incongruous, and progress has been hampered by the paucity of available markers, compounded by the absence of quantitative measures to identify crypt neurons. Germana et al (2004)[19] observed S100-like immunoreactivity in morphologically identified crypt cells, and this antibody was used in several subsequent studies, e.g[14–16]. These attempts to use S100-like immunoreactivity as marker for crypt neurons have led to the suggestion that crypt neuron terminals are located in the dorsomedial and lateral glomerular fields of the olfactory bulb[14]. However, anti S100 antibody requires very particular assay conditions to serve as specific marker for crypt neurons[6], which were not met in those studies, resulting in additional labeling of numerous receptor neurons with microvillous morphology and corresponding uncertainty about the true target glomeruli of crypt neurons. Oka et al, 2012[6] could show that the microvillous-like subpopulation labeled by the S100 antibody indeed expressed an *s100* gene, *s100z*[20], whereas the immunoreactivity in crypt neurons was caused by an unknown protein with better retention in the tissue, allowing to differentiate between these two cell populations by omitting the fixation step of the standard immunohistochemical procedure. However, this modification precludes the use of S100-like immunoreactivity in many procedures, including visualization of axonal terminal regions.

Another marker reported for crypt neurons, anti-trkA antibody[21], has not been investigated further so far. Using population-based quantitative analysis we report here that trkA-like immunoreactivity constitutes a robust and sensitive marker for crypt neurons that reliably labels only crypt neurons in a variety of experimental conditions. Using this marker we could identify a single mediodorsal glomerulus, mdg2, as target glomerulus for crypt neurons. Backtracing from this glomerulus with the fluorescent tracer DiI labeled mostly crypt neurons, in contrast to backtracing from neighboring glomeruli, confirming mdg2 as target glomerulus for crypt neurons. These results are consistent with a 'one olfactory receptor cell type – one target glomerulus' concept, a novel coding strategy in vertebrate olfaction.

Results

TrkA-like immunoreactivity is a robust and sensitive marker for crypt neurons. Crypt neurons are an intriguing olfactory receptor neuron population of so far unclear function. Here we have performed immunohistochemistry with TrkA antibody on cryostat sections of adult zebrafish olfactory epithelium to examine the suitability of TrkA-like immunoreactivity as a marker of crypt neurons under standard histological conditions, i.e. in fixed tissue. We identify crypt neurons in fixed tissue by a quantitative analysis of cell shape and position, using the corresponding values measured for an established crypt neuron marker[6] as reference.

In fresh frozen tissue sparse globose cells are co-labeled by S100 and TrkA antibody (Fig. 1d). In quantitative evaluation we find that TrkA-label completely overlaps with S100-label in unfixed tissue (Fig. 1e). In other words, TrkA replicates the S100 staining under conditions, in which S100-labeling is specific to crypt neurons, *cf.*[6].

Moreover, TrkA labeling also is restricted to sparse large globose cells under standard histological conditions (Fig. 1a–c, f, g), in which the S100 antibody labels many additional cells (Fig. 1c, e–g). As a measure of globosity we chose the ratio of vertical to horizontal diameter (SI Fig. 1a), *cf.*[6]. The distribution of values for this ratio is undistinguishable for cells labeled by S100 antibody in unfixed tissue and TrkA antibody-labeled cells in either fixed or unfixed tissue (Fig. 1f–g). Thus, TrkA-labeled cells in fixed tissue exhibit very similar cellular morphology to *bona fide* crypt neurons[6] (Fig. 1f, g). In contrast, values for the diameter ratio of S100-labeled cells in fixed tissue deviate drastically (Fig. 1f–g). Pairwise comparisons of the unbinned distributions by a Kolmogorov-Smirnov test[22] showed p values above 0.5 for the conditions 'TrkA in fixed tissue', 'TrkA in unfixed tissue', 'S100 in unfixed tissue', whereas all comparisons with 'S100 in fixed tissue' exhibited p values below 10^{-6} (SI Table 1). Thus, consistent with previous reports[6], statistical evaluation shows the population of cells labeled with S100 antibody in fixed tissue to be significantly different from the crypt neuron population, due to the presence of a large additional cell population with more elongated shapes. In contrast, TrkA-like immunoreactivity is a specific marker for crypt neurons, both in unfixed and in fixed tissue.

Furthermore, TrkA-labeled cells in fixed tissue exhibit an apical-centered distribution (Fig. 1a–b,h–i) characteristic for *bona fide* crypt neurons, *cf.*[6]. Again, the distribution for S100-labeled cells in fixed tissue (Fig. 1h–i) is significantly different ($p < 0.0002$), even though the S100-labeled non-crypt cells are rather apically located as well. Note that the Kolmogorov-Smirnov test detects small differences in position between different cell populations (*cf.* Fig. 1i), which are easily overlooked when relying on qualitative inspection or even the common histogram representation (Fig. 1h). We observe roughly 400 TrkA-labeled cells per olfactory epithelium, in good accordance with previously published values for frequency of crypt neurons[6]. Taken together, we conclude that TrkA-like immunoreactivity is a reliable, robust and specific marker for crypt neurons.

TrkA-like immunoreactivity is not caused by TrkA protein. To establish, whether TrkA-like immunoreactivity measures TrkA protein, we have compared the mRNA expression pattern of TrkA with the immunolabeling. An intron-spanning primer pair for TrkA was made within the region common to all predicted isoforms (*cf.* Ensembl gene ENSDARG00000004586) and expression was examined by RT-PCR with cDNA from different tissues. Brain, known to express both *trkA* and its ligand, NGF[23,24], gave a clear signal at the expected molecular weight, and nonneuronal tissues were negative as expected, but no band was detectable in olfactory epithelium (Fig. 2a).

We then performed *in situ* hybridization with a *trkA* probe on larval zebrafish whole mounts. As expected[25,26], the inner ear showed trkA expression, and the same structures were labeled by the trkA antibody (Fig. 2c,d,g,h), confirming the suitability of both probe and antibody. However, no *in situ* hybridization signal was observed in the olfactory epithelium (Fig. 2e, i), although the Trk antibody stained one to a few globose cells per larval nose (Fig. 2f, j), in accordance with expectations for the abundance of crypt neurons at that developmental stage[27].

Finally, we performed a Western blot with protein extracts from olfactory epithelium and brain (Fig. 2b) and observed a band with the characteristic fuzzy appearance of glycoproteins in brain samples at 133 kDa (Fig. 2b), which is very similar to the apparent molecular weight reported for glycosylated TrkA[28]. Such a band was absent from olfactory epithelium, which, however, showed several other bands not corresponding to TrkA (Fig. 2b). Taken together, these results suggest that in olfactory epithelium TrkA-like immunoreactivity is caused by a cross-reacting protein instead of TrkA itself. The molecular nature of this antigen is unknown.

A single mediodorsal glomerulus, mdg2, is labeled by TrkA antibody. The subcellular distribution of the TrkA antigen is rather homogenous, and even the initial axon segment of individual crypt neurons is visible at high magnification (Fig. 1b). Within the olfactory bulb axons are expected to converge into common fascicles and terminal structures, which should facilitate the detection of crypt neuron target glomeruli. Hence we used the TrkA antibody for immunohistochemical labeling of whole mounts of olfactory bulb in an attempt to identify the target region(s) of crypt neurons. We report that within each olfactory bulb a single terminal structure with the typical morphology of a glomerulus is labeled by the TrkA antibody (Fig. 3a–c, SI Fig. 1c). This glomerulus is bilaterally symmetrical for the left and right olfactory bulb, but there is no mirror glomerulus within each olfactory bulb, in contrast to such patterns in the rodent olfactory bulb[29]. This finding is consistent with the absence of a recognizable symmetry axis in the glomerular pattern within each olfactory bulb in zebrafish[30].

The TrkA-labeled glomerulus is situated extremely dorsal, as seen in cross sections (Fig. 3e), about one glomerular diameter away from the midline (Fig. 3a,d–f) and very far posterior, as seen in a dorsal view (Fig. 3a,d,f). This position was reproducibly found in ten glomeruli from five different animals, and the coordinates for the center of the glomerulus in dorsal view were quantified as 0.069 +/− 0.006, 0.27 +/− 0.02 (mean +/− SEM, n = 10; values represent normalized distance from the dorsal posterior end of the olfactory bulb and from the midline, respectively, see SI Fig. 1f,g for a graphical definition of coordinates). The shape of the glomerulus is oblong (major-to-minor diameter ratio 1.50 +/− 0.07, mean +/− SEM, n = 10), with the long axis parallel to the telencephalic surface and its dimensions (50 to 100 μm) are within the range reported for other glomeruli in zebrafish[30]. In the majority of cases two axon fascicles enter the TrkA-labeled glomerulus (Fig. 3a–c). Convergence of TrkA-labeled axons seems to occur well before they reach the target region proper, because the nerve bundles are visible for long distances (Fig. 3a,d,f) similar to observations made for genetically labeled glomeruli[7,9,31].

Zebrafish olfactory glomeruli form a stereotyped pattern and are interindividually recognizable[17,30]. We have performed double labeling of TrkA and SV2, a synaptic marker labeling the complete glomerular pattern, to identify the TrkA glomerulus (Fig. 3 a,d,f). We

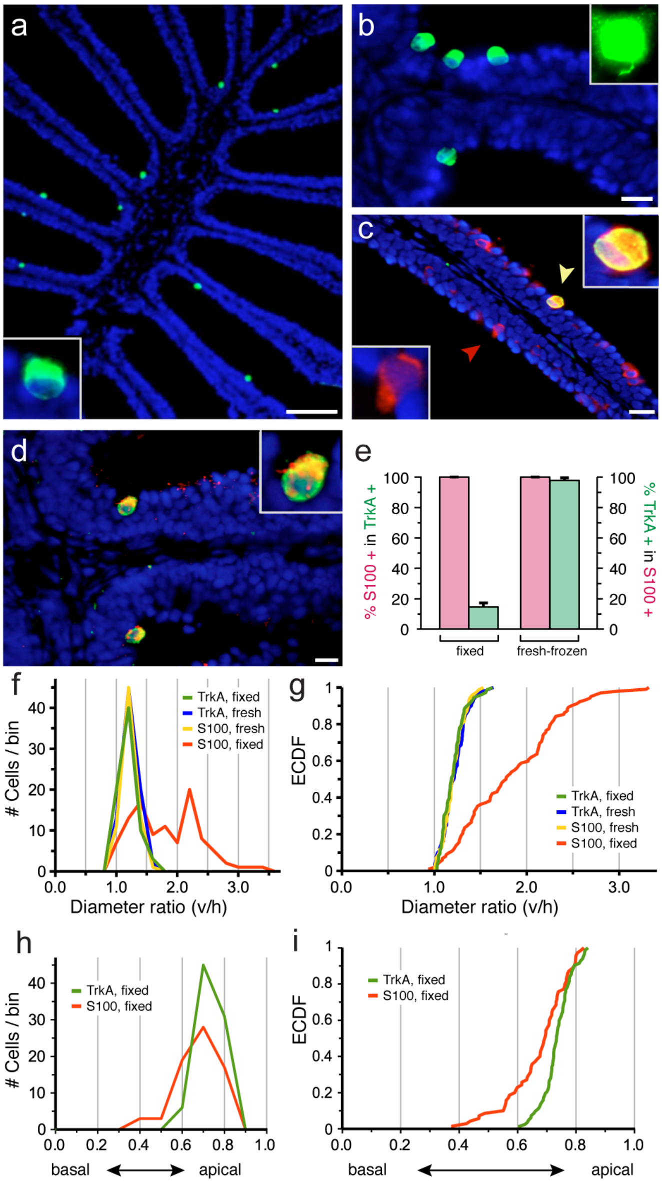

Figure 1 | **TrkA-like immunoreactivity co-localizes with S100-like immunoreactivity and crypt neuron morphology.** (a) TrkA-like immunoreactivity (green) is seen in a sparse population of ovoid cells in horizontal sections of olfactory epithelium (fixed); the inset shows another TrkA-labeled neuron at higher magnification. (b) Enlargement of several TrkA-labeled cells from another section showing the typical ovoid shape of crypt neurons; the inset shows another TrkA-labeled neuron at 1000× magnification, enabling visualization of the initial axon segment.
(c) Double labeling with anti-S100 antibody (red) and anti-TrkA antibody (green) in fixed tissue shows TrkA labeling restricted to a subset of cells with S100-like immunoreactivity. Note the difference in morphology between double-labelled cell (yellow) and TrkA-/S100+ cells (red). (d) In fresh-frozen tissue S100-like immunoreactivity and TrkA-like immunoreactivity label the same, sparse population of globose cells.
(e) Quantification of overlap between S100 and TrkA-staining, values given are mean +/− SEM. TrkA-positive cells show nearly complete overlap with S100-positive cells in fresh-frozen tissue ($p = 0.2$, Student's t-test, two-sided, unpaired), where S100 label is specific for crypt neurons[6], but constitute only a minority of S100-positive cells in fixed tissue ($p < 10^{-12}$, Student's t-test, two-sided, unpaired), in which S100 antibody labels many more cells besides crypt neurons[6]. (f, g) The ratio of vertical to horizontal diameter, 'diameter ratio (v/h)', was measured for TrkA- and S100-labeled cells under standard histological conditions ('fixed') and in fresh frozen tissue ('fresh'). (f) histogram, (g) empirical cumulative distribution function (ECDF) of the unbinned distributions. Note the extreme similarity of the distribution for TrkA in both conditions with the distribution for S100 in fresh-frozen tissue and the drastic difference ($p < 10^{-6}$, Kolmogorov-Smirnov test, *cf.* SI Table 1) to the distribution of S100-labeled cells under standard histological conditions ('fixed').
(h), (i) The relative height of labeled cells within the olfactory lamella was compared for TrkA- and S100-labeled cells under standard histological conditions, i.e. in fixed tissue. (h) histogram, (i) empirical cumulative distribution function (ECDF) of the unbinned distributions. The difference between distributions was highly significant (Kolmogorov-Smirnov test, $p < 0.0002$). Scale bars 80 μm for (a) and 10 μm for (b–d), respectively.

report that the TrkA-labeled glomerulus unambiguously maps to mdg2 (nomenclature after[17]), one of six glomeruli in the mediodorsal cluster. This assignment is based on nearly identical coordinates of the trkA-labeled glomerulus (*cf.* Fig. 3e, f, SI Fig. 1f,i) and mdg2 (SI Fig. 1f,g,j, *cf.*[17]) in all three dimensions (anterior-posterior, medial-lateral, and dorsal-ventral). All neighboring glomeruli show clearly different coordinates (SI Fig. 1g,i,j). Previously this mediodorsal cluster as well as a dorsolateral region had been suggested as target regions for crypt neurons, albeit based on S100 antibody staining in unspecific mode, e.g.[14]. We did not detect any trkA-positive fibers in the dorsolateral area (Fig. 3, SI Fig. 1c), suggesting that the S100 labeling observed in this area resulted from non-crypt neurons. Within the mediodorsal area we have identified the crypt neuron target as a single glomerulus, mdg2.

Backtracing with DiI from the mdg2 glomerulus labels nearly exclusively crypt neurons. We wished to verify mdg2 as crypt neuron target glomerulus by an independent method. To this end we backtraced olfactory receptor neurons connecting to this glomerulus by localized injection of DiI, an intensely fluorescent dye, into the mdg2 glomerulus. The injection site (Fig. 4e,i) was chosen in the unlabeled olfactory bulb according to the stereotyped position of mdg2, monitored during tracing by the emergence of fluorescent axon bundles, and its coordinates were determined in the whole mount after tracing. About half of the injections ($n = 12$) resulted in localized dye injections. We considered an injection localized, if the half-width of fluorescence intensity after tracing was 100–150 μm, at the lower range corresponding to about one glomerular diameter. Seven of these injections resulted in backtraced olfactory receptor neurons. Two of those injections (0.10, 0.26 and 0.12, 0.26; anterior-posterior, medial-lateral coordinates, respectively, *cf.* SI Fig. 1f) were centered at the position of the mdg2 glomerulus (0.07, 0.27, *cf.* SI Fig. 1i–j). As control we injected at a similar posterior level about one glomerular diameter further lateral (0.25, 0.52), a position where dlg1 and possibly dlg2 of the dorsolateral group are expected (SI Fig. 1i–j). The coordinates of another control injection, further anterior and very close to the midline (0.34, 0.06), suggest an injection into mdg3[17], the medially adjacent neighbor glomerulus of mdg2 (SI Fig. 1i–j).

After several weeks of tracing we analysed the labeled cell populations in cryostat sections of the olfactory epithelium. Between 10 and 130 cells were labeled per injection, at the upper range corresponding to a sizable fraction of neurons innervating a glomerulus[32,33]. Cells backtraced from mdg2 are mostly globose and exhibit an apical position within the olfactory lamellae (Fig. 4b,f,j, SI Fig. 1b,d,e,), both telltale signs of crypt neuron-like morphology[3,6]. In contrast, cells backtraced from the dlg1 injection site generally showed elongated shapes and more basal positions of the somata within the lamella (Fig. 4d,h,l, SI Fig. 1b,d,e). Furthermore, cells backtraced from mdg2 rarely exhibited any dendritic processes, as expected for crypt neurons, whereas cells backtraced from the more central injection site (dlg 1) mostly showed long dendritic processes, which are expected for ciliated olfactory receptor neurons (Fig. 4). Cells backtraced from

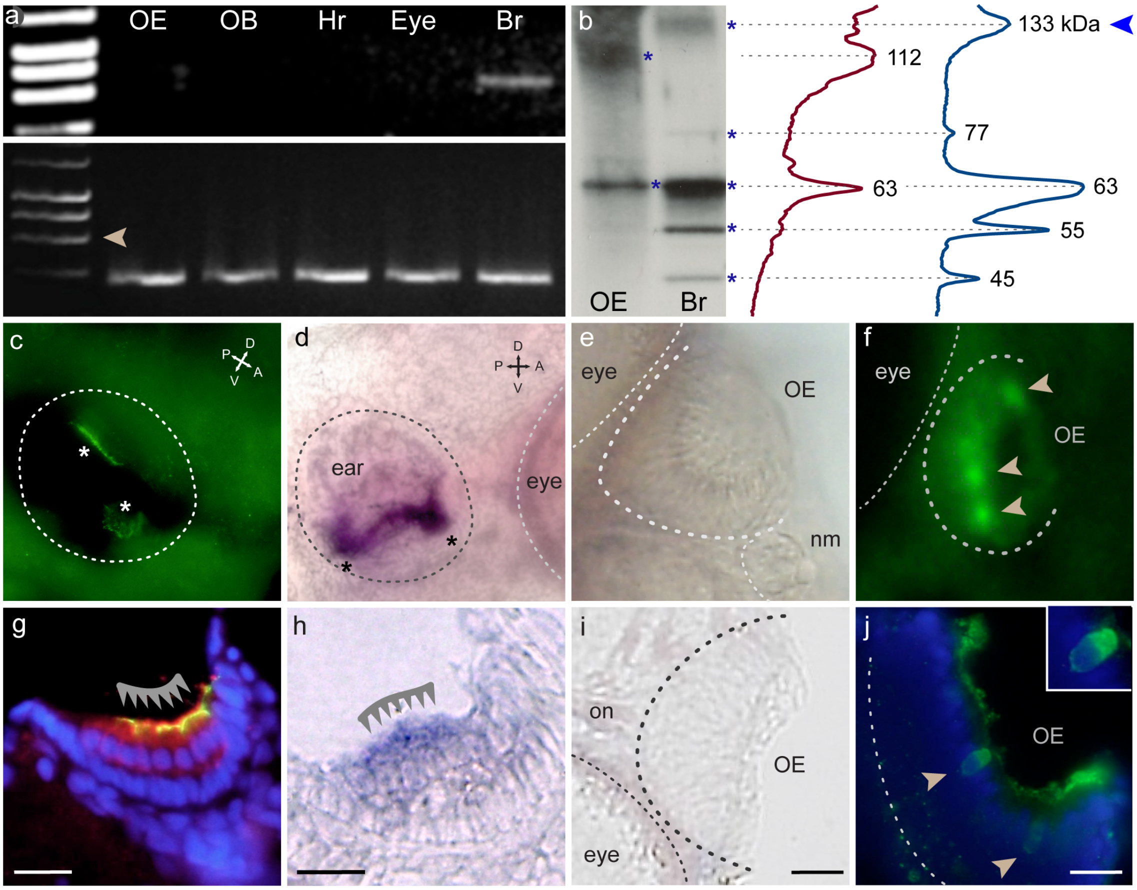

Figure 2 | TrkA-like immunoreactivity does not co-localize with TrkA expression in the olfactory epithelium. (a) RT-PCR shows TrkA expression (upper panel) in brain (Br), but not in olfactory epithelium (OE) nor olfactory bulb (OB), heart (Hr) and eye, all from adult animals. Beta actin signals (lower panel) are of similar intensity for all tissues. Arrowhead, position of amplification product from genomic DNA. (b) Left side, Western Blot with protein extracts from brain (Br) and olfactory epthelium (OE). Apparent molecular weight for several bands (asterisks) in brain and olfactory epithelium was determined from line scans (right side), only brain extracts show expected band (arrowhead). (c–f) Whole mounts of 5 dpf zebrafish larvae; (g–j), 8–10 μm sections from the whole mounts depicted above. Panels (c, f, g, j) show TrkA antibody staining, panels (d, e, h, i) depict in situ hybridization with TrkA probe. (c) TrkA antibody staining labels several structures in the inner ear of zebrafish larvae (asterisks). (d) TrkA probe labels similar structures in the inner ear (asterisks). (e) No signal is observed with the same TrkA probe in the olfactory epithelium of the same larvae. (f) However, TrkA antibody clearly labels several cells in the olfactory epithelium. (g) Specific labeling (barbed line) in hair cells of the macula (yellow due to complete overlap with HCS1 staining (red), a hair cell marker[51]. Blue, DAPI as nuclear counterstain. (h) The TrkA probe labels hair cells of the macula (barbed line). (i) No signal from TrkA probe detected in sections of the olfactory epithelium. (j) In contrast, TrkA antibody labels sparse cells in the OE with a globose morphology. Scale bars 20 μm for (g–j).

the mdg3 position exhibited an intermediate morphology (SI Fig. 1e), less elongated than those from the more central injection site and less globose than crypt neurons, consistent with a microvillous phenotype.

We evaluated the significance of these findings by quantification of morphological variables for cells backtraced from mdg2 glomerulus and comparing them with the values obtained for control injections in adjacent glomeruli. The most conspicuous feature of crypt cells is their globose shape. This shape will result in smaller values for the ratio of vertical to horizontal diameter, compared to those for other types of neurons. TrkA-labeling showed 1.7 as upper limit of diameter ratios for crypt neurons (Fig. 1g) and most non-crypt cells exhibit distinctly larger values (cf. Fig. 1g, SI Fig. 1e). We therefore selected 1.5 as a conservative cutoff criterion to assign a backtraced cell to either crypt or non-crypt neuron population.

The large majority of cells backtraced from the mdg2 glomerulus form a dense cluster in a scatter plot representation of vertical and horizontal cell diameter (Fig. 5a). All cells in the cluster exhibit diameter ratios below 1.5, in other words, crypt neuron morphology. The complete distribution of diameter ratios for cells backtraced from the mdg2 glomerulus is very similar to the distribution for TrkA-labeled crypt neurons, both in the traditional histogram representation (Fig. 5b) and, even more distinctly, in the unbinned representation as empirical cumulative distribution function (Fig. 5c). The distribution of cells backtraced from mdg2 deviates from the TrkA distribution only by the presence of a small shoulder towards larger diameter ratios, presumably reflecting the presence of a small population of non-crypt neurons in the backtraced cells, cf. (Fig. 5a). Another injection at mdg2 coordinates showed very similar results, albeit with a slightly larger shoulder towards larger diameter ratios (SI Fig. 1e), presumably due to the slightly less localized nature of this injection.

In contrast, cells backtraced from control injections into dlg1 and mdg3 glomeruli show without exception diameter ratios well above 1.5 (Fig. 5a, SI Fig. 1d,e), i.e. a drastically different distribution (Fig. 5b, c, SI Fig. 1e). Pairwise comparisons of the unbinned distributions by a Kolmogorov-Smirnov test[22] showed very significant differences between either control injection and TrkA-labeled crypt neurons ($p < 10^{-6}$, SI Table 1), whereas the mdg2 injection was not significantly different (SI Table 1). Furthermore, the distribution of

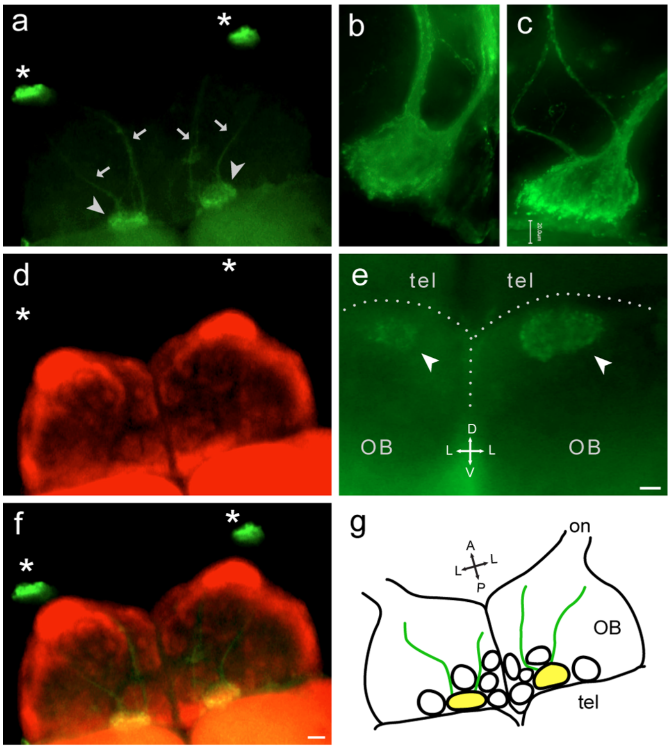

Figure 3 | TrkA antibody labels a single glomerulus in the olfactory bulb. (a), (d), (f) Whole mount of adult zebrafish olfactory bulb labeled with (a) TrkA antibody (green); (d) synaptic vesicle protein 2 (SV2, red); and (f) overlay of both labels. SV2 is a general synaptic marker, which visualizes all glomeruli. The olfactory nerves were cut at the entrance to the olfactory bulb (asterisks) before staining. Dorsal view, for orientation compare the schematic drawing (g). A single labeled glomerulus (arrowhead), very far posterior and 'not-quite-medial', is seen in each olfactory bulb, entered by two nerve fascicles (arrows). Yellow color in overlay (f) confirms the TrkA-labeled structure as glomerulus. (b), (c), higher magnification of two other TrkA-labeled glomeruli, each with two incoming nerve fascicles. (e) posterior vibratome cross section of olfactory bulbs shows the extremely dorsal position of the TrkA-labeled glomerulus. No other glomeruli are labeled by TrkA antibody in this or more anterior bulbar sections (Suppl. Fig. 1c). Scale bar 200 μm for (a,d,f) and 20 μm for (c,e).

cells backtraced from the mdg2 glomerulus was very significantly different from either of the two control injection sites ($p < 10^{-5}$, SI Table 1).

The highly segregated distributions for mdg2 and neighboring control injections show that dye uptake has been nearly completely localized to the mdg2 glomerulus or excluded from it in the case of control injections. Any sizable spillover of dye uptake should have resulted in considerable overlap of these distributions.

As an auxillary variable we also quantified the position of the cell somata with respect to the basal-to-apical dimension. Crypt neurons exhibit a very apical location, close to the lumen, with microvillous olfactory receptor neurons situated somewhat deeper and ciliated receptor neurons more basally located, closer to the basal lamina. We find that the basal-to-apical distribution of cells backtraced from the mdg2 glomerulus is very similar to that of TrkA-labeled crypt neurons (Fig. 5d, e). A small shoulder towards more basal values (Fig. 5d,e) in the former, but not the latter presumably reflects the presence of a small population of non-crypt neurons in the backtraced cells, *cf.* (Fig. 5a). In contrast, cells backtraced from the dlg1 control injection show a drastically different basal-to-apical distribution, both with respect to peak position and steepness of the distribution (Fig. 5d,e). Kolmogorov-Smirnov test showed this difference to be highly significant ($p < 10^{-6}$).

Taken together, a thorough quantitative analysis of cell morphology has shown that most cells backtraced from the mdg2 glomerulus are crypt neurons. Since we made a conservative estimate for the cutoff criterion for identification of crypt neurons, and since some diffusion of the dye outside the direct site of injection is unavoidable, resulting in a small fraction of backtraced cells that connect to adjacent glomeruli, these data support the assumption that mdg2 is innervated exclusively by crypt neurons.

Discussion

Crypt neurons have engendered considerable interest as a third type of olfactory receptor neurons with a peculiar morphology combining elements of the other two populations, ciliated and microvilllous receptor neurons[3]. Several attempts have been made to elucidate their neuronal circuits, beginning with studies that sought to identify their target regions in the olfactory bulb[14–18,34]. A cluster of mediodorsal glomeruli has been suggested as potential targets of crypt neurons, based on absence of fluorescence in some genetically labeled zebrafish lines and differential staining in others[16]. However, backtracing from the olfactory bulb pointed to broader target regions, as DiI injections in both dorsomedial and dorsolateral field resulted in labeled crypt neurons[14]. Similarly, attempts to use the crypt neuron marker S100-like immunoreactivity in the olfactory bulb clearly pointed to both dorsomedial and dorsolateral sites[17], although those authors chose to focus on only one of those sites. Taken together, all these attempts to localize the target glomerulus/glomeruli used unspecific antibodies[14,16,17] or diffusible backtracing dyes[14,15], both of which might overestimate the spatial extent of the target region.

Recently we reported that a single olfactory receptor, the V1R-like ora4 gene, is expressed in all crypt neurons[6] as defined by quantitative morphological assessment. This finding *per se* could suggest either several target glomeruli, *cf.* e.g.[9] or a single target glomerulus, *cf.* e.g.[8]. A clarification of the target region critically depends on the availability of a suitable marker for crypt neurons – as shown recently[6] and summarized here in the Introduction, S100-like immunoreactivity is not suitable for this purpose. Thus we set out to identify a robust and specific marker, which could be used to directly identify the crypt neuron target glomerulus/glomeruli.

We report here that a TrkA antibody previously shown to label cell somata with crypt neuron-like morphology in the olfactory epithelium[21] fulfills these criteria. We show that the TrkA antibody is fully specific under standard histological conditions that enable detection of axons and terminals, unlike the S100 antibody also suggested by the same group as crypt neuron marker[19]. Unfortunately, in crypt neurons the anti-TrkA antibody does not detect TrkA, but an unknown antigen, and consequently it is not straightforward to extend our results into development of a genetic marker for crypt neurons. Nevertheless we observe staining in all cellular compartments, somata, axons and axonal terminals, which allowed the unequivocal determination of the crypt cell target region.

Using this marker, we could show that crypt neurons project exclusively into a single glomerulus of the mediodorsal field, the mdg2 glomerulus. The glomerulus is named according to[17] and is identical to the mdpG2 glomerulus in the original study showing stereotyped interindividually invariant glomeruli in the zebrafish olfactory bulb[30]. Crypt neuron termini were neither detected in the remaining glomeruli of the mediodorsal group nor in any other glomerulus. Backtracing with DiI confirmed this conclusion, since the large majority of neurons backtraced from the mdg2 glomerulus showed crypt neuron-specific morphology, whereas no such cells were labeled by backtracing from neighboring glomeruli. Our backtracing results are partially consistent with experiments by Gayoso et al, 2012[15], who showed labeling of crypt neurons after application of DiI to the mediodorsal glomerular field (mdg1–6), although in those studies no attempt was made to narrow down the target structure(s).

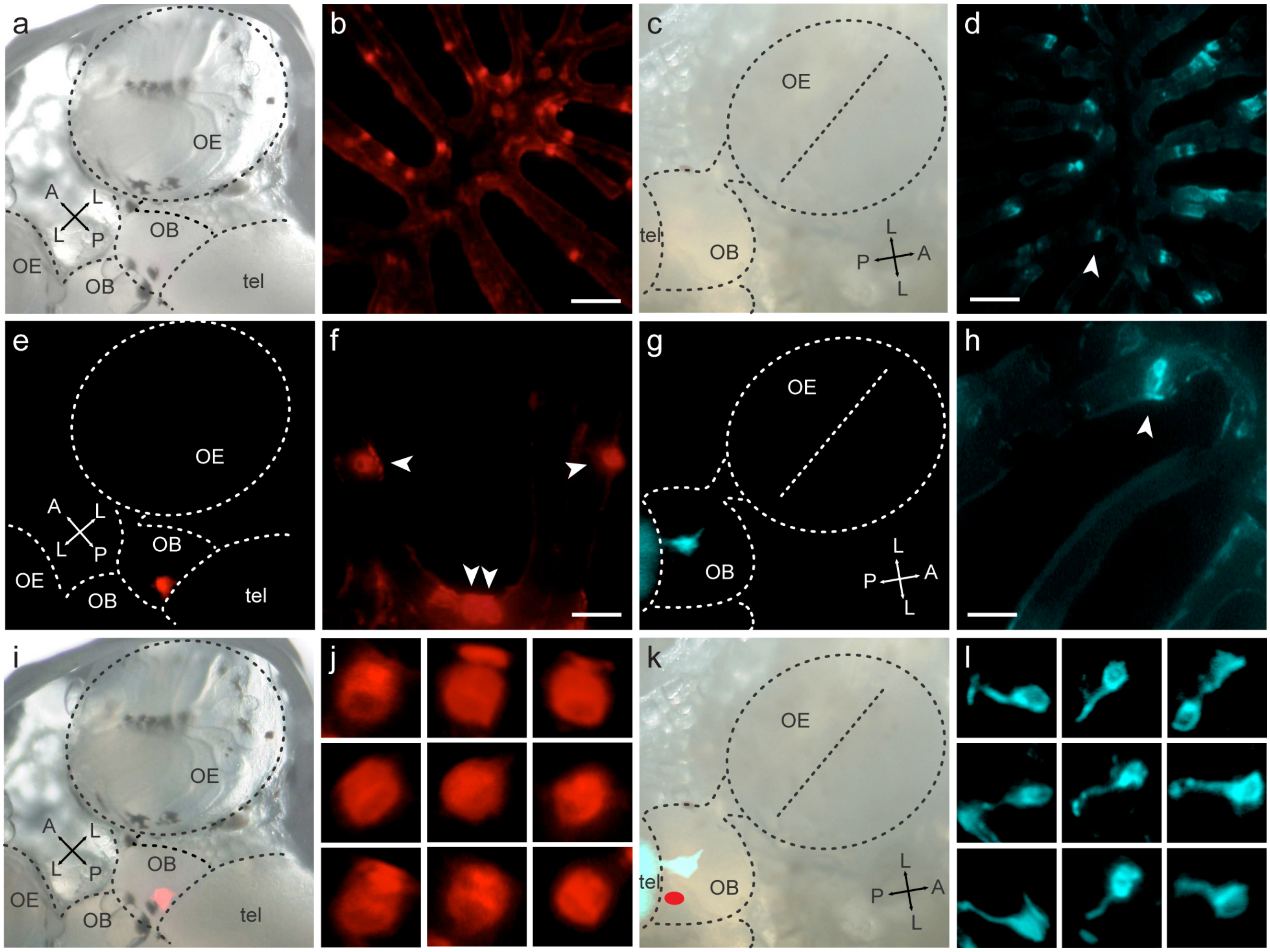

Figure 4 | **DiI injection in mdg2 glomerulus labels crypt neurons, in contrast to injection in neighboring glomeruli.** Localized injections of DiI were placed at the approximate position of mdg2 and dlg1 glomerulus and verified after tracing ((e), (i) and (g), (k), respectively). False color is used to distinguish mdg2 injections (red) and dlg1 injections (blue) in all panels. Results shown are from one animal each for mdg2 and dlg1 position. (a), (c), brightfield micrographs show olfactory epithelium, olfactory bulb and anterior telencephalon. (e), (g), fluorescent images of the same area show the injection sites after the tracing period. (i), (k), overlay of brightfield and fluorescent images above shows the position of injection sites. Red oval in k) represents the site of injection into mdg2. Second (mdg2 injection) and fourth (dlg1 injection) column show tracing results in cryostat sections of the olfactory epithelium. (b), (d), several cells are labeled within a section; (f), (h), enlargements from another (f) or the same section (h). (J) nine representative cells backtraced from mgd2 position from several different sections are shown at high magnification; (l). likewise for dlg1 position. Note the clear difference in morphology between cells backtraced from mdg2 and the adjacent dlg1 position. Scale bars, b,d (80 µm) and (f,h) (10 µm) respectively.

However,[15] also reported backtracing of crypt neurons after DiI injections into the dorsolateral field (dlg glomeruli), in contrast to results from our injection into the dlg1 glomerulus. We assume that this result[15] might be explainable by subtle differences in dye application leading to increased diffusion of the dye compared to our experiments. Taking into account that the more restricted pattern of backtraced cells is more likely to accurately reflect the true condition we conclude that crypt neurons in zebrafish possess a single dorsomedial target glomerulus, named mdg2 according to[17].

The presence of a single target glomerulus for crypt neurons is consistent with expectations for the target size of crypt neurons, since both the sparse spatial pattern of crypt neurons[3,6] and the absolute numbers of neurons labeled by either of the crypt neuron markers (TrkA, this study; ORA4, S100 in specific labeling conditions[6]) are well within the range of corresponding values for individual olfactory receptor genes[31,33,35].

The very homogenous labeling of glomerular structures by the TrkA antibody would seem to argue against the small number of backtraced cells without explicit crypt neuron morphology reflecting an additional innervation to the mdg2 glomerulus. We consider it much more likely that some diffusion of DiI from the injection site into neighboring glomeruli, e.g. the very closely appositioned mdg3 glomerulus, results in labeling of some non-crypt neurons. Generally it has not been possible to restrict such dye injections to a single glomerulus[14,34]. Even though our injections do show glomerular resolution, a small minority of cells backtraced from adjacent glomeruli is to be expected.

Our characterisation of a second immunohistochemical marker for crypt neurons (TrkA-like immunoreactivity), independent from a previously characterized marker (S100-like immunoreactivity[6]), and nevertheless completely overlapping, strengthens the concept resulting from a preceding study[6] that crypt neurons show a novel 'one cell type – one receptor' mode of expression, distinct from the 'one neuron – one receptor' mode of expression established for ciliated olfactory receptor neurons[31,36]. Furthermore, here we extend this observation to a 'one cell type – one receptor – one glomerulus'

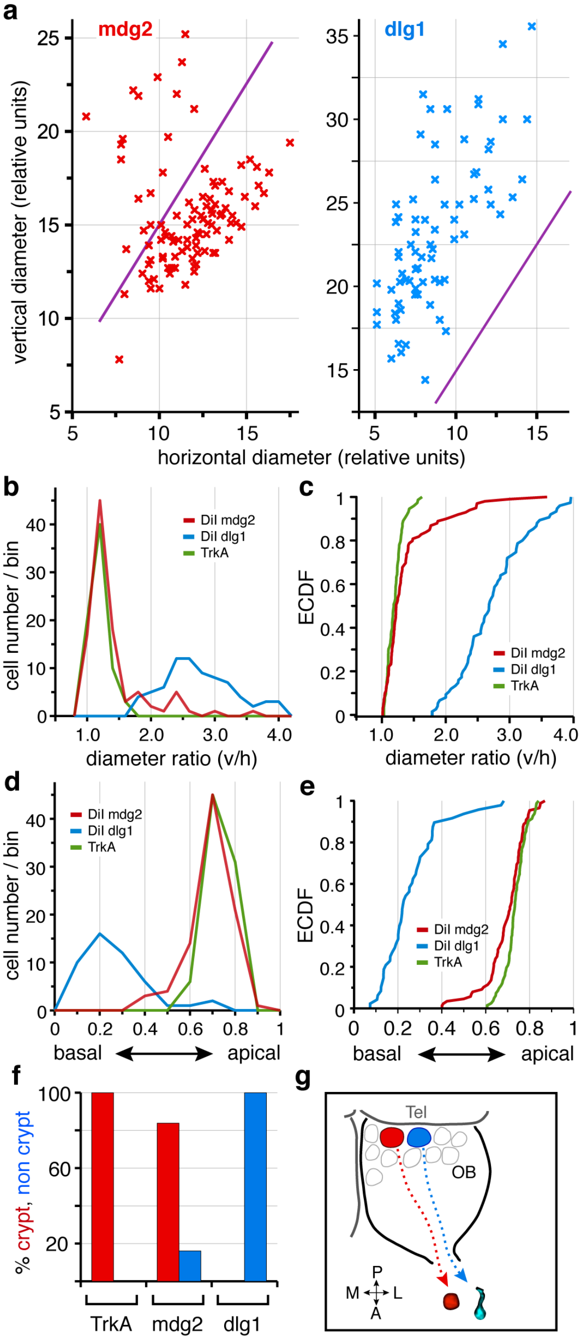

Figure 5 | Quantitative analysis of tracing results shows specific crypt neuron labeling for mdg2 injection sites. (a) Scatter plot of vertical *vs.* horizontal diameter for injections into mdg2 (left panel) and dlg1 (right panel), each cross represents a single cell, data are from the same injections depicted in Fig. 4. Cells are considered to have crypt-like morphology, if the ratio vertical to horizontal diameter is equal or less than 1.5 (cutoff visualized by the magenta line). Note the dense cluster of crypt neurons in the mdg2 injection and the absence of crypt neurons for injections into the dlg position. (b) histogram and (c) CDF of the diameter ratios for mdg2 (red) and dlg1 (blue) injections and trkA-labeled cells (green, same values as shown in Fig. 1f). Note that distributions for mgd2 injections and TrkA, the crypt neuron marker, are indistinguishable, whereas the distribution for dlg1 sharply diverges. (d) histogram and (e) CDF of the basal-to-apical position for mdg2 (red) and dlg1 (blue) injections and trkA-labeled cells (green), same conclusion as in (b–c). (f) Percentage of cells with crypt-like diameter ratios in TrkA-labeled cells, cells backtraced from the mdg2 injection and the dlg1 injection. (g) schematic representation of the backtracing results.

concept, which is reminescent of the specialized subsystems used in insect pheromone detection[37] but to the best of our knowledge represents a novel coding strategy in vertebrate olfaction.

It should be noted that this interpretation rests on the assumption that the entire crypt neuron population is labeled by TrkA-like immunoreactivity. Since it is not possible to quantify crypt neuron numbers at the EM level with any degree of accuracy, *cf.*[38], one could posit the existence of a 'cryptic' cell population with crypt neuron morphology, but invisible in either TrkA- or S100-antibody labeling. In particular the neighboring mediodorsal glomeruli[17] could be considered candidate targets for such a 'cryptic' population, since they, like mdg2, are not labeled in zebrafish transgenic for markers of the other two known cell populations, ciliated and microvillous receptor neurons[16]. While we can not rule out this hypothetical possibility altogether, several observations provide contrary evidence.

Firstly, a control injection of DiI at the approximate coordinates of the mdg3 glomerulus labeled elongated cells resembling microvillous neurons, i.e. with non-crypt morphology. Secondly, G_o-like immunoreactivity is a specific marker for another mediodorsal glomerulus, mdg5[17], and labels cells with non-crypt morphology in the olfactory epithelium[17]. Thirdly, the mere existence of a small and variable proportion of non-crypt neurons in addition to the crypt neurons backtraced from injections into the mdg2 glomerulus argues against crypt neurons innervating all adjacent glomeruli, since these non-crypt (and non-ciliated) neurons presumably result from dye diffusion into the adjacent mediodorsal glomeruli.

The receptor genes expressed by neurons innervating the other five glomeruli of the mediodorsal group[17] are not known. It is noteworthy that there are six genes in the V1R-like *ora* gene family of zebrafish[39], and six glomeruli in the mediodorsal group. Here we have paired one of these genes (*ora4*) with one of these glomeruli (mdg2). It remains to be seen, whether this finding might be generalizable to the entire ORA family and entire mediodorsal glomerular group.

Interestingly, for two other fish species, catfish and crucian carp, a ventral position of the crypt neuron target region has been suggested based on backtracing experiments[34,40] similar to those performed here. A distinctly different position of the target glomerulus of crypt neurons could entail differences in the subsequent circuits and thus possibly differences in function of crypt neurons between species. The relatively medial position of the zebrafish crypt neuron glomerulus is consistent with the axons of downstream projection neurons joining the medial olfactory tract, *cf.*[41] for the topology of the projection neurons. In several species the medial olfactory tract is assumed to convey pheromone detection[42–44] as well as alarm response[11], and conceivably either pheromones or alarm substance might act as activators of crypt neurons. However, different ligands have been reported to activate crypt neurons[12,13] and their downstream projection neurons in different species[34]. So far it is not known whether this reflects a difference in receptor gene expression between species or, alternatively, species-specific alterations of the ORA4 receptor. Additionally, species differences in G alpha gene expression have been reported[6,40,45], which also may implicate different functions for crypt neurons of different species.

Taken together, we have identified the target region for zebrafish crypt neurons as a single glomerulus, situated dorsally and rather medially in the olfactory bulb. This extends the previous hypothesis of 'one cell type – one receptor' for crypt neurons into a 'one olfactory receptor cell type – one target glomerulus' concept, a novel coding strategy in vertebrate olfaction.

Methods

Antibodies, tissue and animal handling. Primary antibodies used were anti-S100 antibody (rabbit IgG; 1 : 1000; catalog no. Z0311, Dako), anti-TrkA (763) antibody (rabbit IgG; 1 : 100; sc-118, Santa Cruz Biotechnology), anti-HCS1 monoclonal and anti-SV2 monoclonal mouse IgG1 (supernatant 1 : 250 and 1 : 50, respectively, Developmental Studies Hybridoma Bank, University of Iowa, Iowa City, IA).

Secondary antibodies used were donkey anti-rabbit IgG conjugated to Alexa Fluor 488 (A21206, Invitrogen), goat anti-rabbit IgG conjugated to Alexa Fluor 594 (A11012, Invitrogen) and goat anti-mouse conjugated to Alexa Fluor 594 (A11005, Invitrogen).

Adult wild type zebrafish (Ab/Tü strain, 8–12 months old) were maintained at 28°C on 14/10-hour light/dark cycle. Progeny was raised in a nursery incubator under the same conditions.

Adult fish were sacrificed by decapitation during anesthesia with MS-222 (ethyl 3-aminobenzoate, Sigma). Animal handling was covered by Animal Use Record 20.10.217 (issued by the State Agency for Nature, Environment and Consumer Protection NRW, LANUV).

Tissues were embedded in 5% low melting agarose and sectioned by vibratome (Pelco 101) or embedded in TissueTek O.C.T. compound (Sakura), and cut by cryostat (Leica CM1900) at −20°C. Fluorescence was analysed using wide field fluorescence microscopes (Keyence BZ-8100E and BZ-9000) for sections and a Nikon CoolPix 950 digital camera attached to a Nikon SMZ-U binocular for whole mounts.

Whole mount olfactory bulb immunohistochemistry. The dorsal cranium was removed, exposed brains were fixed by immersion in 4% paraformaldehyde (PFA, pH 7.4) in phosphate-buffered saline (PBS, pH 7.5) overnight at 4°C and olfactory bulbs still connected to telencephalon were dissected out. Staining was performed according to[17], with minor modifications. After blocking, samples were incubated with primary antibodies anti-TrkA and anti-synaptic vesicle protein 2 (SV2) at 4°C for 20 to 25 days on a vertical rotator (5 sec/round), followed by several washes over a period of 3 hrs at room temperature. Subsequently, the olfactory bulbs were incubated with secondary antibodies for 7 days at 4°C, followed by several washes at room temperature. Tissue was cleared as described[17]. Both primary and secondary antibodies were used at a final dilution of 1 : 100 in blocking reagent. For detailed examination 100 µm vibratome sections were analysed.

Whole mount larvae immunohistochemistry. 10–20 5dpf embryos were fixed overnight in 4% PFA in PBS, washed in PBS and permeabilized overnight with 1.5% Triton-X 100 in 1× PBS at 4°C, followed by 2 hrs blocking at room temperature in BDP (0.1% DMSO, 1% BSA in 1× PBS) containing 5% NGS (Normal goat serum). The larvae were incubated with a cocktail of primary antibodies in BDP overnight at 4°C, followed by multiple washes in BDP at room temperature. Larvae were incubated with secondary antibodies (1 : 250 dilution) in BDP overnight at 4°C, followed by extensive washes with BDP over a period of several hours with multiple changes; subsequently the BDP was exchanged with 1× PBS. The success of the staining was confirmed using a fluorescent microscope, subsequently cryosections of 8 µM thickness were prepared. Slides were mounted with VectaShield containing DAPI (Vector).

Immunohistochemistry on cryosections. Heads were either pre-incubated before dissection overnight at 4°C in freshly prepared 4% PFA in 1× PBS (pre-fixed tissue) or dissected directly (fresh-frozen tissue). Horizontal cryosections (8 µm) of the olfactory epithelia were thaw-mounted onto Superfrost Plus slide glasses (Thermo), incubated in acetone at −20°C for 15 mins, washed several times in PBST, and blocked in 5% normal goat serum in PBST (blocking solution) for 1 hr at room temperature. In order to overcome the limitations arising from same species antibodies in double labeling, the Fc portion of the anti-S100 antibody was covalently conjugated with fluorescein (Thermo Scientific, 53029) as described[46]. For double labeling, the slides were overnight incubated at 4°C with anti-TrkA antibody (1 : 200 dilution in blocking solution), washed 3 times in PBST to remove unbound anti-TrKA and incubated for 2 hrs at room temperature with the first of the two secondary antibodies (anti-rabbit alexa fluor 488). Slides were further washed 3 times in PBST, incubated for 1 hr in blocking solution, followed by overnight incubation at 4°C with flu-labeled anti-S100 (second primary antibody), washed 3 times for 10 min each and incubated for 2 hrs at room temperature with alkaline phosphatase (AP) conjugated anti-fluorescein (the second of the two secondary antibodies). S100-labeled cells were visualized by enzymatic reaction of AP with HNPP Fluorescent Detection Set (Roche). The slides were washed in PBS and mounted with VectaShield containing DAPI (Vector).

Western blot analysis. Olfactory epithelium and telencephalon from six fishes were dissected and immediately transferred to RIPA lysis buffer (Sigma, R0278), followed by mechanical homogenization and 10 min sonication. The samples were centrifuged for 10 mins at 4°C and the protein concentration in the supernatant was determined by Bradford. Protein samples were separated by SDS-PAGE and transferred onto PVDF membrane by electrophoretic transfer (100 V, 90 min). Afterwards, the membrane was washed 3 times with PBS containing 0.1% Tween 20 for 5 minutes each and blocked using 5% milk powder (BIO-RAD, 170-6404) dissolved in PBST for 1 hour at room temperature. Primary antibody was prepared in 5% skim milk (DNA grade, BioRad) in PBST and added to the membrane followed by incubation at 4°C overnight. After 3 washes for 5 minutes each in PBST, the membrane was incubated in secondary antibody, prepared in 5% skim milk in PBST for 1 hour at room temperature. After three rinses in PBST, ECL reagent plus Western Blotting Detection Reagents (RPN2132) was used for developing. Western blots were analysed using ImageJ (http://rsbweb.nih.gov/ij/).

RT-PCR. Total RNA samples were prepared from adult zebrafish tissues of the wild-type Ab/Tübingen strain with the RNeasy kit (QIAGEN). After digestion with DNase I, 100 ng RNA for each tissue were subjected to the first-strand cDNA synthesis with RevertAid MmLV reverse transcriptase (Fermentas), using oligo(dT)$_{15}$ primer. Subsequent PCR was performed using Red Taq mix (Bioline) with gene-specific primers for Dr_actin and Dr_TrkA (forward: CCCCATTGAGCACGGTATT, reverse: TCATGGAAGTCCACATGGCAGAAG, and forward: ACTTTGAAAATAGCCAATGAGTCC, reverse: TGATGACCAACCTTTGCTGT, respectively).

The following conditions were used: 10 min at 95°C, followed by 35 cycles of 45 sec at 95°C, 45 sec at 55°C, and 60 sec at 72°C, and a final extension of 10 min at 72°C.

Whole mount in situ hybridization. Digoxigenin (DIG) RNA probes were synthesized according to the DIG RNA labeling kit supplier protocol (Roche Molecular Biochemicals) using the Dr_TrkA primers.

FW 5′- AAGGTACC GGCTGAATGTGCCAATCTCT -3′ and RV 5′- AAGAGCTCTCCCCGATCTTCACTACCAG -3′. In situ hybridization was carried out according to[47]. Hybridizations were performed on 5 dpf old larvae overnight at 65°C and stringent washes were done in 0.2× SSC at 65°C. Anti-DIG primary antibody coupled to alkaline phosphatase (Roche Molecular Biochemicals) and NBT-BCIP (Roche Molecular Biochemicals) were used for signal detection.

DiI tracing. The fluorescent carbocyanine dye 1,1′-dioctadecyl 3,3,3′,3′-tetramethylindocarbocyanine perchlorate (DiI; Molecular Probes) was used for retrograde tracing of olfactory receptor neurons as described by[32]. Briefly, zebrafish heads were pre-fixed in freshly prepared 4% PFA overnight. Afterwards, the dorsal side of the olfactory bulbs was exposed and a small DiI crystal was placed with the help of a glass micro-needle for 5–10 seconds. Tracing was allowed to proceed in 4% PFA in PBS at 37°C for 2–3 weeks. The fixative was changed every 2–3 days. After tracing, olfactory epithelia, and olfactory bulbs plus telencephalon were dissected. Cryosections of olfactory epithelia were immediately analyzed. The olfactory bulb was documented as whole mount, and afterwards sectioned by vibratome (Pelco 101; 100 µm transverse sections). Sections were mounted on Superfrost Plus slide glasses.

Measurement and analysis of spatial coordinates. Spatial coordinates were measured in arbitrary units and normalized. For olfactory bulb coordinates whole mounts of olfactory bulb, with telencephalon attached, were viewed from dorsal. An axis cross was put at the center of the glomerulus or injection site and maximal values were determined for medial-to-lateral and anterior-to-posterior direction as the corresponding line segments (see SI Fig. 1f). Thus possible values range from 0/0 (medial most/posterior-most) to 1/1 (lateral-most/anterior-most). Vertical cell diameter was determined as maximal cell length perpendicular to the basal lamina (soma and dendrite, if any) and horizontal diameter as maximal cell width, i.e. parallel to the basal lamina (see SI Fig. 1a). For apical-to-basal position in the olfactory epithelium the shortest distance between center of the cell soma and basal border of the epithelial layer was normalized to the shortest distance between basal and apical border of the epithelial layer at the position of the cell to be measured (see SI Fig. 1b). Thus the range of values is between 0 (most basal) and 1 (most apical).

Unbinned distributions were represented as the corresponding empirical cumulative distribution function (ECDF)[48,49]. To estimate, whether two spatial distributions were significantly different, we performed Kolmogorov-Smirnov tests on the unbinned distributions as described in[22]. This test is particularly suitable for continuous distributions and makes no assumptions about the nature of the distributions investigated. This is essential since the skewness of some observed distributions showed that these are not Gaussian. Due to the sensitive nature of the test on large distributions ($n > 100$) we selected $p < 0.01$ as cutoff criterion for significant difference. Results of the Kolmogorov-Smirnov test were confirmed by permutation analysis[50] without exception.

1. Mori, K. & Sakano, H. How is the olfactory map formed and interpreted in the mammalian brain? *Annual review of neuroscience* **34**, 467–499 (2011).
2. Mombaerts, P. Axonal wiring in the mouse olfactory system. *Annual review of cell and developmental biology* **22**, 713–737 (2006).
3. Hansen, A. & Zeiske, E. The peripheral olfactory organ of the zebrafish, Danio rerio: an ultrastructural study. *Chemical senses* **23**, 39–48 (1998).
4. Ferrando, S. *et al.* Observations of crypt neuron-like cells in the olfactory epithelium of a cartilaginous fish. *Neuroscience letters* **403**, 280–282 (2006).
5. Hansen, A. & Finger, T. E. Phyletic distribution of crypt-type olfactory receptor neurons in fishes. *Brain, behavior and evolution* **55**, 100–110 (2000).
6. Oka, Y., Saraiva, L. R. & Korsching, S. I. Crypt neurons express a single V1R-related ora gene. *Chemical senses* **37**, 219–227 (2012).
7. Mombaerts, P. *et al.* Visualizing an olfactory sensory map. *Cell* **87**, 675–686 (1996).
8. Johnson, M. A. *et al.* Neurons expressing trace amine-associated receptors project to discrete glomeruli and constitute an olfactory subsystem. *Proceedings of the National Academy of Sciences of the United States of America* **109**, 13410–13415 (2012).
9. Wagner, S., Gresser, A. L., Torello, A. T. & Dulac, C. A multireceptor genetic approach uncovers an ordered integration of VNO sensory inputs in the accessory olfactory bulb. *Neuron* **50**, 697-709 (2006).
10. Hamdani el, H., Lastein, S., Gregersen, F. & Doving, K. B. Seasonal variations in olfactory sensory neurons--fish sensitivity to sex pheromones explained? *Chemical senses* **33**, 119–123 (2008).

11. Mathuru, A. S. *et al.* Chondroitin fragments are odorants that trigger fear behavior in fish. *Current biology: CB* **22**, 538–544 (2012).
12. Vielma, A., Ardiles, A., Delgado, L. & Schmachtenberg, O. The elusive crypt olfactory receptor neuron: evidence for its stimulation by amino acids and cAMP pathway agonists. *The Journal of experimental biology* **211**, 2417–2422 (2008).
13. Bazaes, A. & Schmachtenberg, O. Odorant tuning of olfactory crypt cells from juvenile and adult rainbow trout. *The Journal of experimental biology* **215**, 1740–1748 (2012).
14. Gayoso, J. A., Castro, A., Anadon, R. & Manso, M. J. Differential bulbar and extrabulbar projections of diverse olfactory receptor neuron populations in the adult zebrafish (Danio rerio). *The Journal of comparative neurology* **519**, 247–276 (2011).
15. Gayoso, J., Castro, A., Anadon, R. & Manso, M. J. Crypt cells of the zebrafish Danio rerio mainly project to the dorsomedial glomerular field of the olfactory bulb. *Chemical senses* **37**, 357–369 (2012).
16. Sato, Y., Miyasaka, N. & Yoshihara, Y. Mutually exclusive glomerular innervation by two distinct types of olfactory sensory neurons revealed in transgenic zebrafish. *The Journal of neuroscience: the official journal of the Society for Neuroscience* **25**, 4889–4897 (2005).
17. Braubach, O. R., Fine, A. & Croll, R. P. Distribution and functional organization of glomeruli in the olfactory bulbs of zebrafish (Danio rerio). *The Journal of comparative neurology* **520**,2317–2339, Spc2311 (2012).
18. Koide, T. *et al.* Olfactory neural circuitry for attraction to amino acids revealed by transposon-mediated gene trap approach in zebrafish. *Proceedings of the National Academy of Sciences of the United States of America* **106**, 9884–9889 (2009).
19. Germana, A. *et al.* S100 protein-like immunoreactivity in the crypt olfactory neurons of the adult zebrafish. *Neuroscience letters* **371**, 196–198 (2004).
20. Kraemer, A. M., Saraiva, L. R. & Korsching, S. I. Structural and functional diversification in the teleost S100 family of calcium-binding proteins. *BMC evolutionary biology* **8**, 48 (2008).
21. Catania, S. *et al.* The crypt neurons in the olfactory epithelium of the adult zebrafish express TrkA-like immunoreactivity. *Neuroscience letters* **350**, 5–8 (2003).
22. Press, W. H. T. S., Vetterling, W. T. & Flannery, B. P. *Numerical recipes in C: The art of scientific computing.* Vol. second (1992).
23. Martin, S. C., Marazzi, G., Sandell, J. H. & Heinrich, G. Five Trk receptors in the zebrafish. *Developmental biology* **169**, 745–758 (1995).
24. Korsching, S., Auburger, G., Heumann, R., Scott, J. & Thoenen, H. Levels of nerve growth factor and its mRNA in the central nervous system of the rat correlate with cholinergic innervation. *The EMBO journal* **4**, 1389–1393 (1985).
25. Schimmang, T. *et al.* Survival of inner ear sensory neurons in trk mutant mice. *Mechanisms of development* **64**, 77–85 (1997).
26. Catania, S. *et al.* Neurotrophin and Trk neurotrophin receptors in the inner ear of Salmo salar and Salmo trutta. *Journal of anatomy* **210**, 78–88 (2007).
27. Sandulescu, C. M., Teow, R. Y., Hale, M. E. & Zhang, C. Onset and dynamic expression of S100 proteins in the olfactory organ and the lateral line system in zebrafish development. *Brain research* **1383**, 120–127 (2011).
28. Germana, A. *et al.* Neurotrophin receptors in taste buds of adult zebrafish (Danio rerio). *Neuroscience letters* **354**, 189–192 (2004).
29. Nagao, H., Yoshihara, Y., Mitsui, S., Fujisawa, H. & Mori, K. Two mirror-image sensory maps with domain organization in the mouse main olfactory bulb. *Neuroreport* **11**, 3023–3027 (2000).
30. Baier, H. & Korsching, S. Olfactory glomeruli in the zebrafish form an invariant pattern and are identifiable across animals. *The Journal of neuroscience: the official journal of the Society for Neuroscience* **14**, 219–230 (1994).
31. Sato, Y., Miyasaka, N. & Yoshihara, Y. Hierarchical regulation of odorant receptor gene choice and subsequent axonal projection of olfactory sensory neurons in zebrafish. *The Journal of neuroscience: the official journal of the Society for Neuroscience* **27**, 1606–1615 (2007).
32. Baier, H., Rotter, S. & Korsching, S. Connectional topography in the zebrafish olfactory system: random positions but regular spacing of sensory neurons projecting to an individual glomerulus. *Proceedings of the National Academy of Sciences of the United States of America* **91**, 11646–11650 (1994).
33. Weth, F., Nadler, W. & Korsching, S. Nested expression domains for odorant receptors in zebrafish olfactory epithelium. *Proceedings of the National Academy of Sciences of the United States of America* **93**, 13321–13326 (1996).
34. Hamdani el, H. & Doving, K. B. Specific projection of the sensory crypt cells in the olfactory system in crucian carp, Carassius carassius. *Chemical senses* **31**, 63–67 (2006).
35. Hussain, A., Saraiva, L. R. & Korsching, S. I. Positive Darwinian selection and the birth of an olfactory receptor clade in teleosts. *Proceedings of the National Academy of Sciences of the United States of America* **106**, 4313–4318 (2009).
36. Barth, A. L., Dugas, J. C. & Ngai, J. Noncoordinate expression of odorant receptor genes tightly linked in the zebrafish genome. *Neuron* **19**, 359–369 (1997).
37. Hildebrand, J. G. Analysis of chemical signals by nervous systems. *Proceedings of the National Academy of Sciences of the United States of America* **92**, 67–74 (1995).
38. Hansen, A. & Zielinski, B. S. Diversity in the olfactory epithelium of bony fishes: development, lamellar arrangement, sensory neuron cell types and transduction components. *Journal of neurocytology* **34**, 183–208 (2005).
39. Saraiva, L. R. & Korsching, S. I. A novel olfactory receptor gene family in teleost fish. *Genome research* **17**, 1448–1457 (2007).
40. Hansen, A. *et al.* Correlation between olfactory receptor cell type and function in the channel catfish. *The Journal of neuroscience: the official journal of the Society for Neuroscience* **23**, 9328–9339 (2003).
41. Miyasaka, N. *et al.* From the olfactory bulb to higher brain centers: genetic visualization of secondary olfactory pathways in zebrafish. *The Journal of neuroscience: the official journal of the Society for Neuroscience* **29**, 4756–4767 (2009).
42. Doving, K. B. & Selset, R. Behavior patterns in cod released by electrical stimulation of olfactory tract bundlets. *Science (New York, N.Y.)* **207**, 559–560 (1980).
43. Sorensen, P. W., Hara, T. J. & Stacey, N. E. Sex pheromones selectively stimulate the medial olfactory tracts of male goldfish. *Brain research* **558**, 343–347 (1991).
44. Friedrich, R. W. & Korsching, S. I. Chemotopic, combinatorial, and noncombinatorial odorant representations in the olfactory bulb revealed using a voltage-sensitive axon tracer. *The Journal of neuroscience: the official journal of the Society for Neuroscience* **18**, 9977–9988 (1998).
45. Hansen, A., Anderson, K. T. & Finger, T. E. Differential distribution of olfactory receptor neurons in goldfish: structural and molecular correlates. *The Journal of comparative neurology* **477**, 347–359 (2004).
46. Korsching, S. & Thoenen, H. Two-site enzyme immunoassay for nerve growth factor. *Methods in enzymology* **147**, 167–185 (1987).
47. Oka, Y., Saraiva, L. R., Kwan, Y. Y. & Korsching, S. I. The fifth class of Galpha proteins. *Proceedings of the National Academy of Sciences of the United States of America* **106**, 1484–1489 (2009).
48. Wilk, M. B. & Gnanadesikan, R. Probability plotting methods for the analysis of data. *Biometrika* **55**, 1–17 (1968).
49. Feller, W. *An introduction to Probability Theory and its Applications.* Vol. II chap I.12 (Wiley, 1966).
50. Manly, B. *Randomization, bootstrap and Monte Carlo methods in biology* (Chapman and Hall/CRC, London, 1997).
51. Goodyear, R. J. *et al.* Identification of the hair cell soma-1 antigen, HCS-1, as otoferlin. *Journal of the Association for Research in Otolaryngology: JARO* **11**, 573–586 (2010).

Acknowledgements

We thank Vladimir Shiriagin for providing initial larval TrkA stainings. We gratefully acknowledge financial support from the German Science foundation (grant KO 1046/7-1 to S.I.K.) and the International Graduate School IGSDHD (G.A.).

Author contributions

The experiments were designed by S.I.K., G.A. and Y.O. and performed by G.A., I.I., M.S., Y.O. and S.I.K., S.I.K., I.I. and G.A. drafted the illustrations. Data analysis was done by S.I.K., W.N. and G.A., S.I.K. wrote the paper.

Additional information

Supplementary information accompanies this paper at http://www.nature.com/scientificreports

Competing financial interests: The authors declare no competing financial interests.

How to cite this article: Ahuja, G. *et al.* Zebrafish crypt neurons project to a single, identified mediodorsal glomerulus. *Sci. Rep.* **3**, 2063; DOI:10.1038/srep02063 (2013).

This work is licensed under a Creative Commons Attribution-NonCommercial-NoDerivs 3.0 Unported license. To view a copy of this license, visit http://creativecommons.org/licenses/by-nc-nd/3.0

Supplementary Information

Title: Zebrafish crypt neurons project to a single, identified mediodorsal glomerulus

Authors: Gaurav Ahuja, Ivan Ivandić, Mehmet Saltürk, Yuichiro Oka,
Walter Nadler, Sigrun I. Korsching

SI Figure 1 Korsching

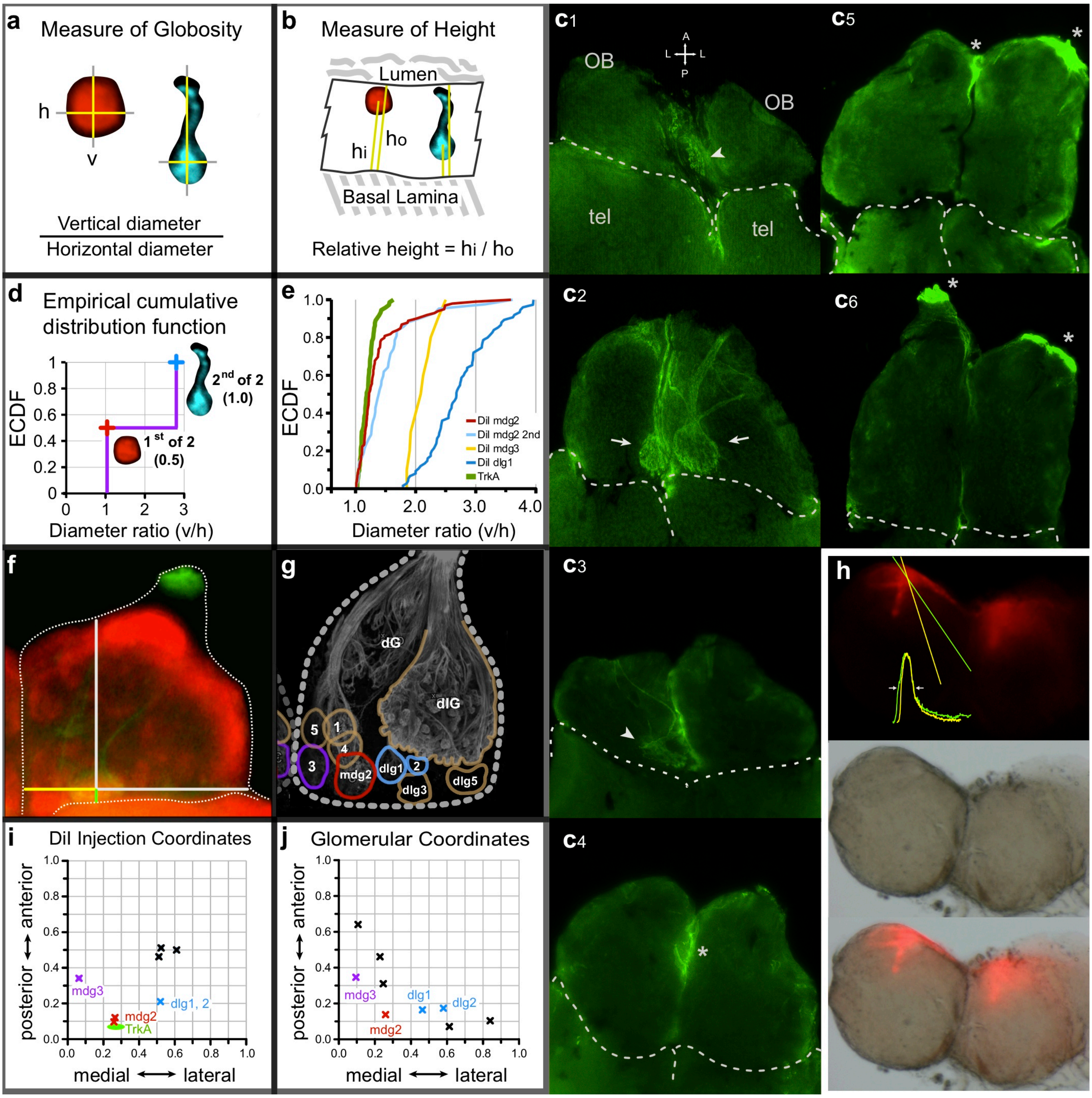
a
Measure of Globosity
h
v
Vertical diameter
Horizontal diameter
b
Measure of Height
Lumen
hi
ho
Basal Lamina
Relative height = hi / ho
c1
A
L
L
P
OB
OB
tel
tel
c5
*
*
d
Empirical cumulative distribution function
ECDF
1
0.8
0.6
0.4
0.2
0
0
1
2
3
Diameter ratio (v/h)
2nd of 2 (1.0)
1st of 2 (0.5)
e
ECDF
1.0
0.8
0.6
0.4
0.2
0.0
1.0
2.0
3.0
4.0
Diameter ratio (v/h)
DiI mdg2
DiI mdg2 2nd
DiI mdg3
DiI dlg1
TrkA
c2
c6
*
*
f
g
dG
dlG
5
1
4
3
mdg2
dlg1
2
dlg3
dlg5
c3
h
i
DiI Injection Coordinates
posterior ⟷ anterior
1.0
0.8
0.6
0.4
0.2
0.0
0.0
0.2
0.4
0.6
0.8
1.0
medial ⟷ lateral
mdg3
mdg2
TrkA
dlg1, 2
j
Glomerular Coordinates
posterior ⟷ anterior
1.0
0.8
0.6
0.4
0.2
0.0
0.0
0.2
0.4
0.6
0.8
1.0
medial ⟷ lateral
mdg3
mdg2
dlg1
dlg2
c4
*

SI Figure 1 Quantification of shape and position

a) Diameter ratio for cells is measured as ratio of maximal vertical length to maximal horizontal diameter. Vertical diameter is measured perpendicular to lumen border and basal lamina border of the olfactory lamella. b) Height of the cell within the olfactory lamella (h_i, value for center of soma) is normalized to maximal height of the lamella (h_o) at the position of the cell to account for the rather variable thickness of the olfactory lamellae. c) TrkA-like immunoreactivity after whole mount staining of the olfactory bulb in a complete series of 50 µm thick horizontal cryosections. Z Stack images (0.5 µm optical section) were taken at 40x magnification, maximal projection is shown. Dorsal to ventral, from top to down; arrows, a single labeled glomerulus per olfactory bulb is seen in section C_2; arrowheads, peripheral segments of the glomerulus are visible in the directly adjoining sections; asterisks, background signal at the tissue surface; dashed line, telencephalic border; tel, telencephalon; OB, olfactory bulb. d) Visualization of the empirical cumulative distribution function (ECDF) for the diameter ratio of the two cells depicted in a). While this is a fictive example, distributions with as few as ten measurements can be examined for coarse features, and high resolution is obtained above 50-100 measurements, which makes the (unbinned) cumulative distribution function much more sensitive than the commonly used histogram representation of binned values. e) Diameter ratios for olfactory receptor neurons backtraced from DiI injections in mdg2 (red, data shown in main text; cyan, another injection), mdg3 (yellow) and dlg1 (blue, data shown in main text). Values for trkA-labeled crypt neurons (green) are shown for comparison. Data are shown as empirical cumulative distribution function (CDF) as described in d). f) Coordinates of trkA glomeruli and injection site centers in the olfactory bulb are normalized to maximal bulbar length and width visible in dorsal view with telencephalon still attached at that position. Anterior-posterior length is measured from posterior (0) to anterior (1), parallel to the midline; medial-lateral length is measured from medial, perpendicular to the anterior-posterior axis. g) Outline of mediodorsal and dorsolateral glomeruli traced onto a cropout of Fig. 3b of Braubach et al.[1]. This orientation of the olfactory bulb is most similar to that of our experiments. h) Minimal DiI diffusion after tracing is seen in a vibrotome cross section obtained after tracing. Fluorescence (top panel), brightfield (middle panel) and the overlay of both (third panel). Line scans through the center of the left injection site (yellow, green, top panel) show minimal spread of the dye. Half width of fluorescence intensity is indicated by the arrows. i) Coordinates of injection sites in the olfactory bulb, measured as described in f). Colors and labels represent the nearest glomerular position. The centroid of the coordinates for the TrkA-labeled glomerulus is given for comparison (green oval, mean+/-SD, n=10) . j) Coordinates of glomeruli outlined in g), measured as described in f). Colors and labels represent glomeruli examined in this paper.

1 Braubach OR, Fine A, Croll RP. Distribution and functional organization of glomeruli in the olfactory bulbs of zebrafish (Danio rerio). *The Journal of comparative neurology* 2012, **520**(11)**:** 2317-2339, Spc2311.

Table S1 Pairwise comparison of distributions for Diameter ratio using the *Kolmogorov-Smirnov* test

Diameter ratio (vertical / horizontal)		
cell label 1 *vs.*	cell label 2	p-value
S100 'fresh'	S100 'fixed'	$p<0.000001$
S100 'fresh'	TrkA 'fresh'	$p=0.72$
S100 'fresh'	TrkA 'fixed'	$p=0.69$
S100 'fixed'	TrkA 'fixed'	$p<0.000001$
TrkA 'fresh'	TrkA 'fixed'	$p=0.55$
TrkA 'fixed'	Mdg2	$p=0.027$
TrkA 'fixed'	Mdg3	$p<0.000001$
TrkA 'fixed'	Dlg1	$p<0.000001$
Mdg2	Mdg3	$p=0.000001$
Mdg2	Dlg1	$p<0.000001$
Mdg3	Dlg1	$p=0.00066$

The Kolmogorov-Smirnov test [1], a measure of distribution differences, makes no assumption about the nature of the distributions. This is essential because distributions analysed here are non-Gaussian. As cutoff for significance we chose $p<0.01$ due to the sensitive nature of this test for large distributions. S100 'fresh', S100-like immunoreactivity in unfixed tissue; S100 'fixed', S100-like immunoreactivity in fixed tissue; TrkA 'fresh', TrkA-like immunoreactivity in unfixed tissue; TrkA 'fixed', TrkA-like immunoreactivity in fixed tissue; Mdg2, DiI injection into mdg2; Mdg3, DiI injection into mdg3; Dlg1, DiI injection into dlg1.

1 Press WH TS, Vetterling WT, Flannery BP. *Numerical recipes in C: The art of scientific computing*, vol. second, 1992.

Publication 2

Gaurav Ahuja, Shahrzad Bozorg Nia, Veronika Zapilko, Vladimir Shiriagin, Daniel Kowatschew, Yuichiro Oka & Sigrun I. Korsching. *Kappe neurons, a novel population of olfactory sensory neurons*. Sci. Rep. 4, 4037; DOI:10.1038/srep04037 **(2014)**.

http://www.nature.com/srep/2014/140210/srep04037/full/srep04037.html

SCIENTIFIC REPORTS

OPEN

SUBJECT AREAS:
OLFACTORY SYSTEM
PERIPHERAL NERVOUS SYSTEM

Received
19 December 2013

Accepted
13 January 2014

Published
10 February 2014

Kappe neurons, a novel population of olfactory sensory neurons

Gaurav Ahuja, Shahrzad Bozorg Nia*, Veronika Zapilko*, Vladimir Shiriagin, Daniel Kowatschew, Yuichiro Oka† & Sigrun I. Korsching

Institut für Genetik, Universität zu Köln, Zülpicher Str. 47a, 50674 Köln, Germany.

Correspondence and requests for materials should be addressed to S.I.K. (sigrun.korsching@uni-koeln.de)

* These authors contributed equally to this work.

† Current address: Anatomy and Neuroscience, Graduate School of Medicine, Osaka University, 2-2 Yamadaoka, Suita, Osaka, Japan.

Perception of olfactory stimuli is mediated by distinct populations of olfactory sensory neurons, each with a characteristic set of morphological as well as functional parameters. Beyond two large populations of ciliated and microvillous neurons, a third population, crypt neurons, has been identified in teleost and cartilaginous fishes. We report here a novel, fourth olfactory sensory neuron population in zebrafish, which we named *kappe* neurons for their characteristic shape. Kappe neurons are identified by their G_o-like immunoreactivity, and show a distinct spatial distribution within the olfactory epithelium, similar to, but significantly different from that of crypt neurons. Furthermore, kappe neurons project to a single identified target glomerulus within the olfactory bulb, mdg5 of the mediodorsal cluster, whereas crypt neurons are known to project exclusively to the mdg2 glomerulus. Kappe neurons are negative for established markers of ciliated, microvillous and crypt neurons, but appear to have microvilli. Kappe neurons constitute the fourth type of olfactory sensory neurons reported in teleost fishes and their existence suggests that encoding of olfactory stimuli may require a higher complexity than hitherto assumed already in the peripheral olfactory system.

Two main types of olfactory sensory neurons are employed by the vertebrate olfactory system for detection of odors, ciliated neurons that express olfactory receptors of the OR and TAAR gene families, and microvillous neurons that express V1R and V2R genes[1–3]. Both types are present in tetrapods as well as teleost fish[4]. Additionally, fish employ a third type of olfactory sensory neuron, the crypt neurons, named for their conspicuous shape, and possessing cilia and microvilli within the same cell[4]. The three cell types are intermingled within a single sensory surface in fishes, but can be distinguished by their characteristic shape and spatial position: a slender dendrite and a basal soma for ciliated neurons, a plump cell body and an intermediate soma position for microvillous neurons, and a large globose soma with an apical position for crypt neurons[5,6]. Moreover, all three types have been defined by the presence of characteristic molecular markers, OMP for ciliated neurons[7], TRPC2 for microvillous neurons[7] and TrkA- as well as S100-like immunoreactivity (TrkA-ir, S100-ir) for crypt neurons[8,9], see[5,6] for clarification. Crypt neurons have recently been shown to express a single olfactory receptor, ORA4[5], and to project to a single target glomerulus in the olfactory bulb, mdg2 of the mediodorsal cluster[6]. On the other side, a recent report has suggested that some of the neurons innervating another glomerulus of the mediodorsal cluster, mdg5, and identified by G_o-ir, show crypt neuron-like morphology[10]. This was an intriguing suggestion because it implied that neurons innervating a single glomerulus could be morphologically and presumably functionally heterogenous – a violation of the well-established rule of axonal convergence of same receptor-expressing neurons into a homogenous glomerulus[11]. The question remained unanswered, though, because neither quantitative assessment of shape and spatial position nor double labeling with a crypt neuron marker had been reported. Here we performed a thorough quantitative analysis of several morphological parameters, together with double-labeling experiments for established molecular markers of ciliated, microvillous and crypt neurons. We find that the neuronal population identified by G_o-ir does not overlap with crypt, ciliated and microvillous neurons, using established molecular markers for the latter three types of olfactory sensory neurons. Furthermore, cell shape and spatial position are unique for G_o-ir-positive neurons, and significantly different from either crypt, ciliated or microvillous neurons. We conclude that G_o-ir-positive neurons constitute a novel, fourth type of olfactory sensory neurons. This suggests a higher complexity than so far assumed already in the peripheral olfactory system.

Results

A homogenous population of olfactory sensory neurons with characteristic shape and spatial position is labeled by G_o antibody. G_o-ir-positive neurons have been described as a morphologically heterogenous population including cells with the globose shape typical of crypt neurons[10]. We suspected that at least part of this heterogeneity might be due to different sectioning angles[5] of the labelled cells. Therefore we engaged in analysis of distributions for different cell shape and position parameters, as opposed to focusing on single cell properties. In our experience the former approach is much more powerful, and allows to distinguish homogenous from heterogenous cell populations with high sensitivity and accuracy[5,6,12].

We report here that G_o-ir labels a sparse population of pear- or bottle-shaped cells with a characteristic cap of intense G_o-ir at the apical end of the cells (Fig. 1a, b, c). We have used the ratio of horizontal to vertical diameter of these cells as measure of their shape *cf.*[5,6]. A value of 1 would correspond to a perfectly circular shape, with decreasing values pointing to increasingly elongated shapes. We find a median value of 0.66 for G_o-ir-positive neurons, distinctly lower than that of crypt neurons[5] and see below, but also much larger than that of ciliated neurons[6] and see below. The distribution of diameter ratios is narrow (Fig. 1f), consistent with a homogenous population. Importantly, the empirical cumulative distribution function (ECDF) of the diameter ratio is a single sigmoid curve (Fig. 1g), indicative of a homogenous population (a mix of different populations would result in either a step or quasi-linear function, *cf.*[6].

Beyond a characteristic shape, G_o-ir-positive neurons also have a very conspicuous position within the olfactory epithelium. It is known that such restricted spatial distributions are characteristic parameters for particular subpopulations, e.g. olfactory sensory neurons expressing a particular receptor[6,13,14]. Across a lamella, G_o-ir-positive neurons tend to lie very apical, close to the lumen and far away from the basal lamina. We quantified this parameter as relative height ($h_{rel} = h_{soma\ center}$/thickness of sensory layer; 0, basal; 1, apical). The histogram shows a rather narrow peak and the ECDF exhibits a sigmoidal shape, indicative of a homogenous population (Fig. 1f, g).

Within a lamella, the distance of G_o-ir-positive cells to the median raphe, the center of the epithelium, is generally rather small, compared to the full extent of the sensory epithelium. We quantified this coordinate as relative radius ($r_{rel} = r_{soma\ center}$/length of the lamella; 0, innermost; 1, outermost, *cf.*[13]. The histogram of radial distance values shows a steep and narrow peak, and the corresponding ECDF exhibits a sigmoidal shape consistent with a homogenous population (Fig. 1f, g). Within the epithelium, a third axis is defined by the series of horizontal sections. Here, the majority of G_o-ir-positive cells were concentrated in a few sections close to the opening of the cup-shaped epithelium, and far away from the basal region containing the olfactory nerve bundles (Fig. 1f, g).

Taken together, we have quantified four different morphological and spatial parameters for G_o-ir-positive cells. All four distributions are consistent with the presence of a single, homogenous cell population. G_o-ir-positive cells are also labeled by zns2-immunostaining, a general marker for sensory neurons, and in high magnification initial axon segments are visible, suggesting that G_o-ir-positive cells are indeed neurons (Fig. 1a).

Furthermore, whole mount immunohistochemistry of the olfactory bulb using G_o antibody results in the labeling of a single, bilateral symmetric glomerulus (Fig. 1 d, e), confirming that these cells are sensory neurons that convey information to the brain. Comparison with zns2-immunostaining, which labels the entire glomerular pattern, allows to identify the G_o-ir-positive glomerulus as mdg5, consistent with a previous report[10]. Between 200 to 500 G_o-ir-positive neurons are present in a single olfactory epithelium, which is well within the range expected to innervate a single glomerulus, *cf.*[11].

G_o-ir-positive neurons are different from crypt neurons. The apical laminar position of G_o-ir-positive neurons is roughly similar to that of crypt neurons[6], even though their shape is generally somewhat more slender than that of crypt neurons *cf.*[5,6]. However, cells with morphology similar to that of crypt neurons have been reported in the G_o-ir-positive cell population[10]. Therefore we have used the G_o antibody in parallel with an established crypt neuron marker, S100-ir, to examine a potential overlap between these two markers. We report here that G_o-ir and S100-ir label mutually exclusive cell populations (Fig. 2a–c, f). Also, as shown above, G_o-ir-positive neuron terminals in the olfactory bulb innervate a different glomerulus, mdg5, compared to mdg2, the crypt neuron glomerulus[6].

Furthermore, we have examined the shape and spatial distribution of G_o-ir-positive and crypt neurons identified by a second marker, TrkA-ir, in alternating sections to obtain a stringent comparison of the properties of both cell populations. We find subtle, but highly significant ($p < 10^{-6}$) differences in relative height and relative radius between the two populations (Fig. 2e, g). G_o-ir-positive neurons are even more apically situated within the lamella than TrkA-ir-positive neurons (maximal difference between the distributions 25%), and they are found closer to the median raphe than crypt neurons (maximal difference between the distributions 22%). Within the entire olfactory epithelium, G_o-ir-positive neurons are found in more apical sections closer to the opening of the cup-shaped olfactory organ, compared to TrkA-ir-positive neurons (Fig. 2h). Finally the comparison of cell shapes shows the largest difference between both populations (54%), with G_o-ir-positive neurons significantly ($p < 10^{-6}$) less globose than crypt neurons (Fig. 2d).

Taken together, G_o-ir-positive neurons differ significantly in all morphological parameters analysed from crypt neurons. Next, we examined, whether G_o-ir-positive neurons might belong to either microvillous or ciliated neuron populations.

G_o-ir-positive neurons are different from ciliated and microvillous neurons. Ciliated neurons in teleosts specifically express the olfactory marker protein (OMP), and a transgenic line is available, in which the OMP promoter faithfully drives expression of a red fluorescent protein (RFP), *Tg(OMP:lynRFP)*[7]. We performed G_o immunostaining with transgenic epithelia, and report here that almost all G_o-ir-positive neurons (98%) are negative for RFP (Fig. 3a, f). This suggests that G_o-ir-positive neurons do not belong to the population of ciliated neurons.

Moreover, a comparison of cell shape and preferred laminar position within the lamella shows highly significant differences between G_o-ir-positive and OMP-positive neurons. Ciliated neurons tend to have a very slender shape, and rather basal cell bodies, whereas G_o-ir-positive neurons are mostly pear-shaped and are found at extreme apical positions within the lamella, even more apical than crypt neurons (Fig. 3e, g, h). Only 1–2% overlap are observed between G_o-ir and OMP distributions (Fig. 3h).

Next, we investigated, whether G_o-ir-positive neurons might express the microvillous neuronal marker TRPC2[7]. First, we employed a transgenic line, which largely reproduces the endogenous TRPC2 pattern, *Tg(TRPC2:gap-Venus)*[7]. We report that G_o-ir-positive cells were negative for Venus fluorescence (Fig. 3b, f). Secondly, we also performed direct double labeling in wildtype zebrafish, detecting G_o-ir by immunostaining and TRPC2 by *in situ* hybridization. Again, almost all G_o-ir-positive cells (>98%) were negative for TRPC2 signals (Fig. 3c, f), suggesting that G_o-ir-positive neurons are different from microvillous neurons.

Furthermore, a comparison of cell shape and preferred laminar position within the lamella shows highly significant differences between G_o-ir-positive and TRPC2-positive neurons ($p < 10^{-6}$). Microvillous neurons are somewhat slender in shape, and their cell bodies are preferentially located more basal than crypt neuron somata, whereas G_o-ir-positive neurons are mostly pear-shaped and are found at extreme apical positions within the lamella, more apical than crypt neurons (Fig. 3c, e, g, h).

Finally we have examined a potential overlap of G_o-ir-positive neurons with the calretinin-positive population of olfactory sensory neurons. Calretinin appears to label subpopulations of ciliated and

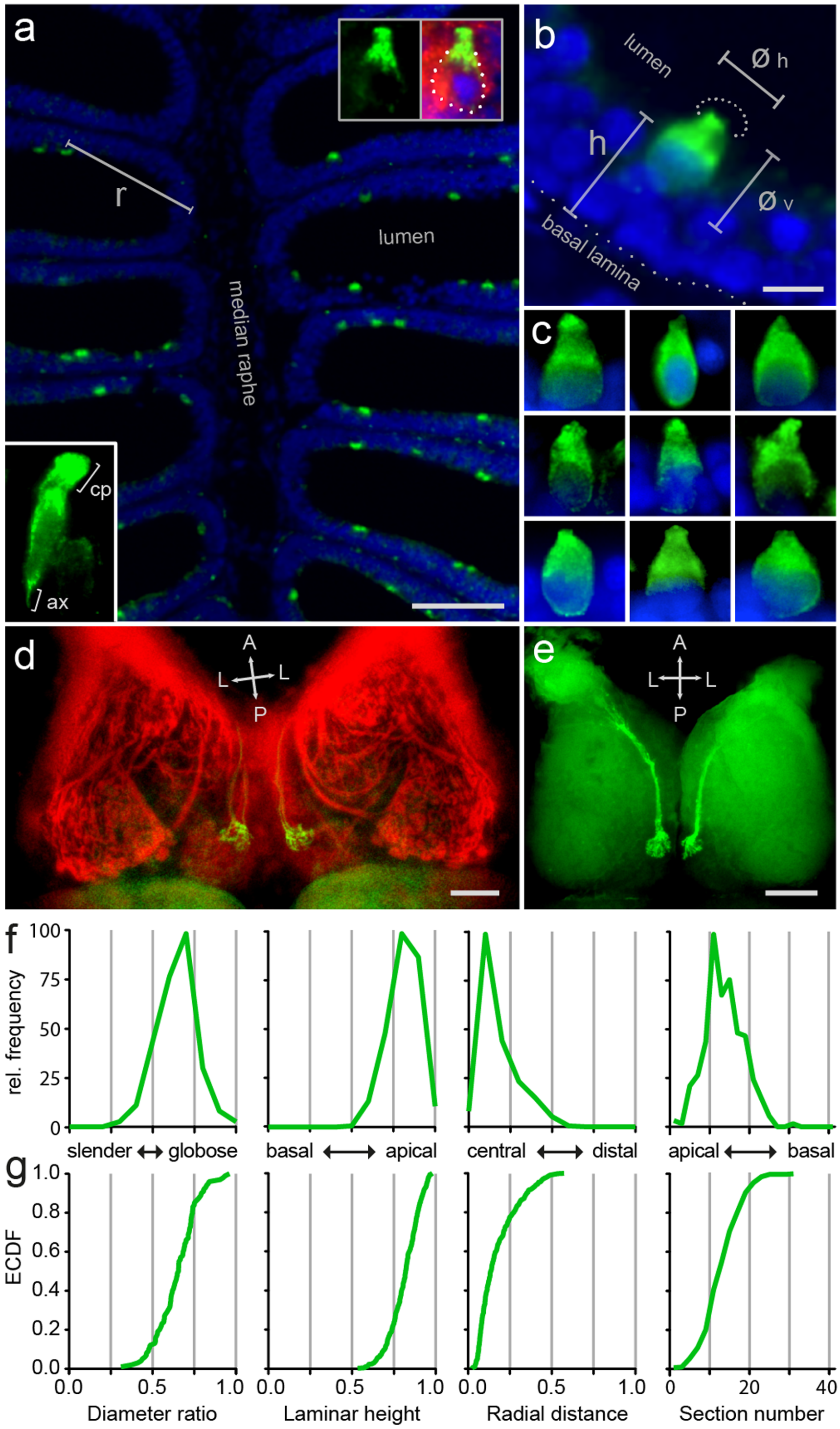
a
r
lumen
median raphe
cp
ax
b
lumen
Ø h
h
Ø v
basal lamina
c
d
A
L
L
P
e
A
L
L
P
f
100
75
50
25
0
rel. frequency
slender ↔ globose
basal ⟷ apical
central ⟷ distal
apical ⟷ basal
g
1.0
0.8
0.6
0.4
0.2
0.0
ECDF
0.0
0.5
1.0
Diameter ratio
0.0
0.5
1.0
Laminar height
0.0
0.5
1.0
Radial distance
0
20
40
Section number

Figure 1 | G_o-like immunoreactivity reveals a distinct population of sparse, pear-shaped sensory neurons in zebrafish olfactory epithelium. (a) G_o-ir (green) is seen in a sparse population of pear-shaped cells in horizontal sections of the olfactory epithelium (short-fixed), using DAPI as counter-stain (blue); r, radial distance. Top right inset at higher magnification shows a G_o-ir-positive cell (green), co-labeled with zns2 (red), and visible nucleus (DAPI, blue). Bottom left inset at higher magnification shows a G_o-ir-positive cell with initial axon segment (ax) and cap (cp). (b) At higher magnification the apical position of G_o-ir-positive cells (green) is clearly visible. $\o_v$, vertical cell diameter; $\o_h$, horizontal cell diameter; h, laminar height; dotted half-circle, the apical dendritic part of G_o-ir-positive olfactory sensory neurons resembles a cap. (c) Nine G_o-ir-positive cells show the typical range of morphologies for these neurons. (d) Whole mount of adult zebrafish olfactory bulb double-labeled with anti- G_o and anti-zns2 antibodies, dorsal view. Zns2 labels all glomeruli, whereas G_o-ir labels a single medial glomerulus (yellow).The olfactory nerves were cut at the entrance to the olfactory bulb before staining. (e) Horizontal vibrotome cross-section (100 μm) reveals the extremely dorsal position of the Go-immunoreactive glomerulus in each olfactory bulb. A single, thick axon bundle is seen entering the glomerulus. (f,g) One shape parameter and three spatial parameters were quantified for the G_o-ir-positive cell population, and shown as histogram (f) and empirical cumulative distribution function, ECDF (g). From left to right: ratio of horizontal to vertical diameter, laminar height (normalized to maximal height), radial distance (normalized to maximal radius), and number of cells per 10 μm horizontal cross section of the olfactory epithelium; x axis units and labels are valid for both (f) and (g). Scale bars correspond to 50 μm (a), 5 μm (b), and 100 μm (d, e).

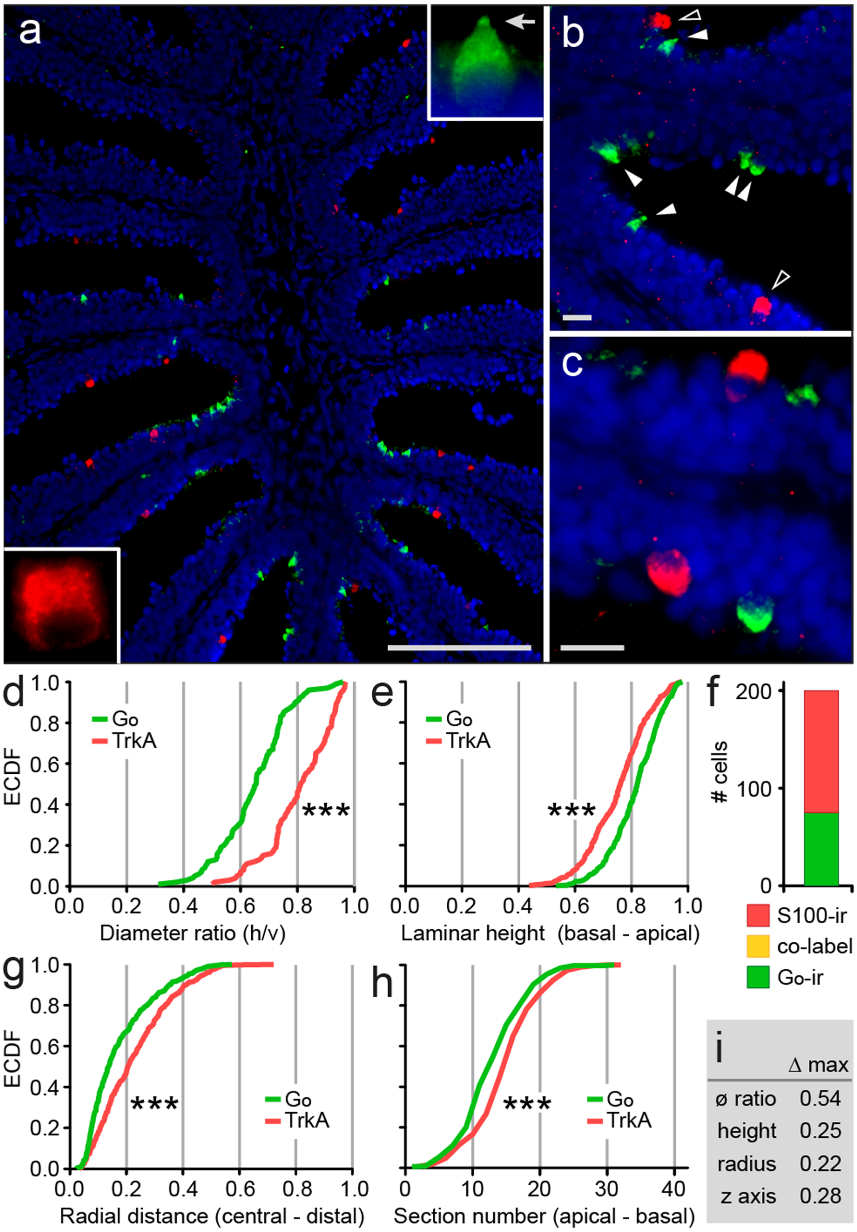

Figure 2 | G_o-ir-positive neuron population is different from crypt neurons. (a) Double labeling with anti-G_o antibody (green) and anti-S100 antibody (red, marker for crypt neurons) in cryostat sections of short-fixed olfactory epithelium reveals two mutually exclusive sensory neuron populations. Insets, single neurons at higher magnifications. Note the differences in morphology of these two cell populations; arrow in top right insert, the cap-like structure typical for G_o-ir-positive neurons. (b–c) Higher magnifications show the typical shapes of G_o-ir-positive neurons (pear-shaped) and crypt neurons (globose), indicated by filled arrow heads and open arrow heads, respectively. (d–e, g–h) One shape parameter and three spatial parameters (see Fig. 1b for graphical explanation) were quantified for the TrkA-ir-positive cell population and the corresponding empirical cumulative distribution function, ECDF, was compared with that of G_o-ir-positive neurons; ***, distributions of TrkA-ir and G_o-ir cells are significantly different ($p < 10^{-6}$), as assessed by Kolmogorov-Smirnov test of the unbinned distributions. (d), ratio of horizontal to vertical diameter [diameter ratio ($ø_h/ø_v$)], (e), laminar height normalized to maximal height is shown. (f), Absence of co-label for G_o-ir and TrkA-ir cell populations. (g) Relative radial distance of labeled cells is shown. (h) Number of cells per 10 μm horizontal cross section of the olfactory epithelium was analysed for G_o-ir and TrkA-ir-positive neurons. (i) Maximal vertical distance (Δ max) of distributions as indicated; ø ratio, diameter ratio; height, normalized laminar height; radius, normalized radial distance; z axis, section number (ordinal). Vertical distance can range between 0 (identical curves) and 1 (no overlap of x value range). Scale bars correspond to 100 μm (a) and 10 μm (b, c).

microvillous neurons[10,15,16]. Again we observe no co-localisation for G_o-ir and calretinin (<1%, Fig. 3d, f), confirming the results for ciliated and microvillous neuron markers (OMP and TRPC2, respectively). We note that both cell shape and laminar height distribution of calretinin-positive neurons are identical to the respective distributions of OMP-positive neurons, which itself show nearly no overlap with those of TRPC2-positive neurons (Fig. 3e, g, h). These results are consistent with calretinin-positive neurons being ciliated neurons, *cf.*[10]. In summary, G_o-ir-positive neurons exhibit a conspicuous distinct shape and preferred laminar position, significantly different from the morphology and location observed for the three known populations of olfactory sensory neurons. Moreover, molecular markers for ciliated, microvillous and crypt neurons are absent in G_o-ir-positive neurons. We conclude that G_o-ir-positive neurons do

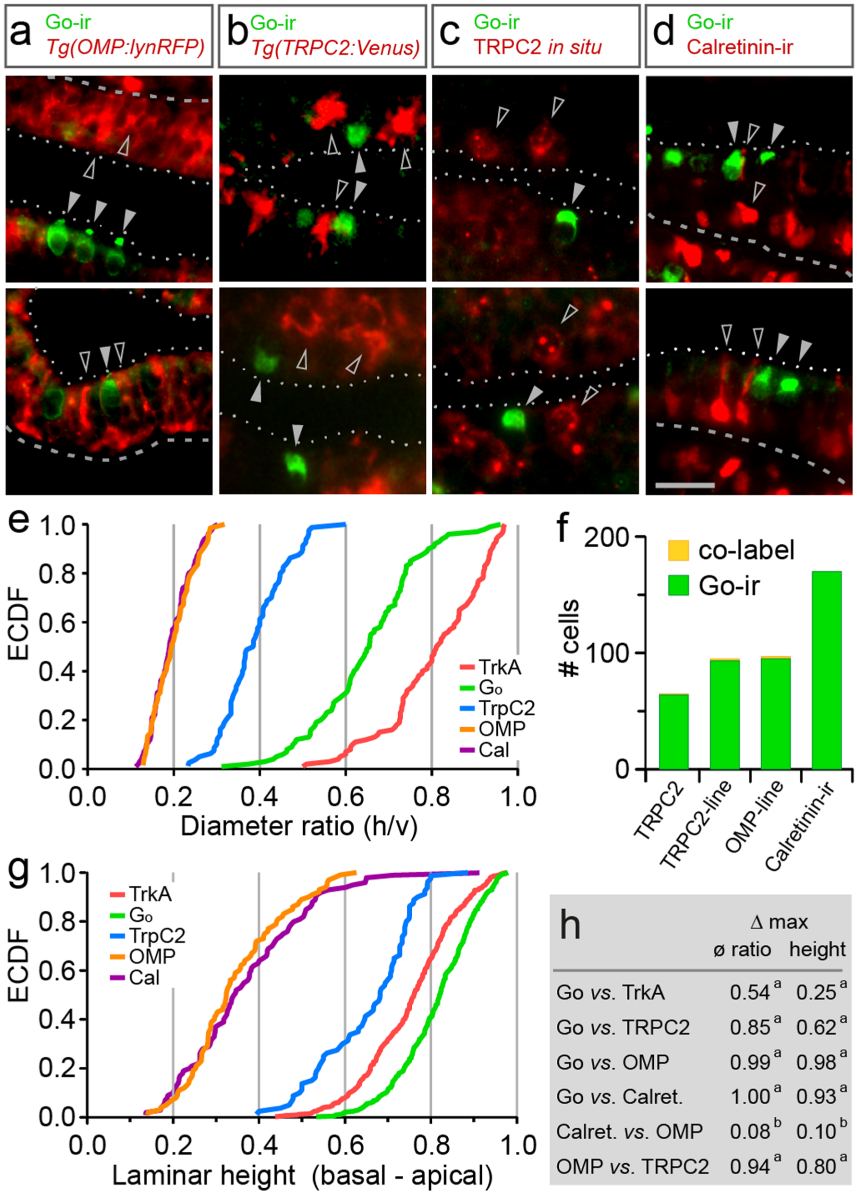

	Δ max ø ratio	height
Go *vs.* TrkA	0.54[a]	0.25[a]
Go *vs.* TRPC2	0.85[a]	0.62[a]
Go *vs.* OMP	0.99[a]	0.98[a]
Go *vs.* Calret.	1.00[a]	0.93[a]
Calret. *vs.* OMP	0.08[b]	0.10[b]
OMP *vs.* TRPC2	0.94[a]	0.80[a]

Figure 3 | G_o-ir-positive neurons do not co-localize with established markers for ciliated and microvillous neurons. (a–d), Double labeling of G_o-ir-positive cells with different markers is analysed in horizontal cryostat sections of olfactory epithelia; dashed line, basal border; dotted line, apical border of the sensory layer; scale bar, 20 µm. (a) Double fluorescent labeling of anti-Go antibody (green) with RFP (red) expressed in ciliated neurons in *Tg(OMP:lyn-mRFP)* shows absence of co-localization; filled grey arrowhead, G_o-ir-positive cell; open arrowhead, RFP-positive cell. (b) Double fluorescent labeling of anti-G_o antibody with Venus expressed in microvillous neurons in *Tg(TRPC2:Venus)* line shows absence of co-localization. G_o-ir signal is set to green, Venus signal is set to red; filled arrowhead, G_o -ir-positive cell; open arrowhead, Venus-positive cell. (c) Double fluorescent labeling of anti- G_o antibody (green) with *in situ* hybridisation signal from TRPC2 probe[5] shows absence of co-localization; filled grey arrowhead, G_o-ir-positive cell; open arrowhead, TRPC2-positive cell. (d) Double fluorescent labeling of anti-G_o antibody (green) with anti-calretinin antibody (red) shows absence of co-localization; filled grey arrowhead, G_o-ir-positive cell; open arrowhead, calretinin-positive cell. (e) The empirical cumulative distribution function (ECDF) for a cell shape parameter (diameter ratio) shows distributions for TRPC2 and OMP-positive cells to be different from each other as well as from G_o-ir and TrkA-ir, shown for comparison here. (f) Quantification of co-label for G_o-ir and markers for microvillous, ciliated and crypt neurons (as indicated) shows 0 to 2% co-label (yellow) in G_o-ir-positive neurons. Such small percentages amount to a handful of cells in an entire olfactory epithelium, and are likely to accrue from the dense packing of cells, dendrites, cilia and microvilli, at the limit of light-microscopic resolution. (g) The empirical cumulative distribution function (ECDF) for a cell localisation parameter (laminar height) shows distributions for TRPC2 and OMP-positive cells to be different from each other as well as from G_o-ir and TrkA-ir-positive cells, shown for comparison here. (h) Maximal vertical distance (Δ max) of distributions as indicated; ø ratio, diameter ratio; height, normalized laminar height. Significance of distribution differences is assessed by Kolmogorov-Smirnov test of the unbinned distributions; a, $p < 10^{-6}$; b, $p > 0.6$.

not belong to the three known populations, but constitute a fourth type of olfactory sensory neuron. Due to their conspicuous 'cap' (German: Kappe) we suggest to name this novel population *kappe* neurons.

Kappe neurons are tubulin-negative and actin-positive. We performed immunostaining with anti-tubulin and anti-actin antibodies together with G_o antibody to further characterize kappe neurons. We report that tubulin staining mostly does not overlap with G_o-ir

(Fig. 4a, c). Rare cases of overlap may be due to technical reasons, since tubulin-positive cilia of ciliated neurons are densely packed in the apical layer, *cf.* (Fig. 4a). Since tubulin is an essential component of cilia[17] we conclude that kappe neurons do not possess cilia. Microvilli, on the other hand, require actin as essential component[18]. We observe nearly complete co-labeling of G_o-ir and actin (Fig. 4c), with the actin antibody consistently labeling a small apical spot within the cap of kappe neurons (Fig. 4b). Although immuno-EM studies will be required to draw a firm conclusion, these results suggest that kappe neurons may possess microvilli.

Discussion

Three different types of olfactory sensory neurons are known in the vertebrate sense of smell, ciliated, microvillous and crypt neurons[4]. Here we report the presence of a fourth type of olfactory sensory neurons, kappe neurons, identified by the presence of G_o-ir[10], which do not express the molecular markers commonly accepted as defining ciliated, microvillous, and crypt neurons. We used a population-based quantitative approach to characterize kappe neurons, and show them to be highly significantly different in shape and spatial location from each of the three previously known populations of olfactory sensory neurons. Kappe neurons are a rare cell population with a few hundred cells per olfactory organ, consistent with the expression of only one or very few olfactory receptor genes in this type of sensory neurons. Thus, it is conceivable that additional such populations of olfactory sensory neurons might exist, *cf.*[19,20], but they would presumably only come into view after identification of a molecular marker specific for such a population.

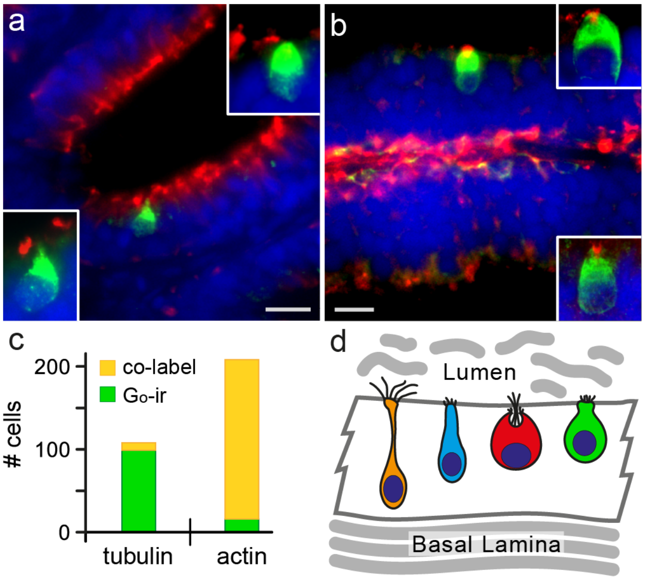

Figure 4 | Kappe neurons are tubulin-negative and actin-positive. Double labeling of G_o-ir-positive cells with anti-tubulin or anti-actin antibody is analysed in horizontal cryostat sections of olfactory epithelia. (a) Double fluorescent labeling of G_o-ir (green) and tubulin (red) shows absence of co-localization; scale bar 10 μm. The insets represent magnified images of single neurons taken at 100× magnification, 0.1 μm optical sections. (b) Double fluorescent labeling of G_o-ir (green) and actin (red) shows co-localization: G_o-ir positive neurons exhibit highly localized actin staining at the apical surface of their cell bodies, the expected position for microvilli. Scale bar 10 μm. The insets show single neurons, images taken at 100× magnification, 0.1 μm optical sections. (c) Quantification of co-label for G_o-ir and actin or tubulin, respectively, shows over 90% co-label (yellow) for actin, but less than 10% co-label for tubulin. The small number of G_o-ir/tubulin co-labeled cells is likely to result from the dense packing of cells, dendrites, cilia and microvilli, at the limit of light-microscopic resolution. (d) Schematic representation of four types of olfactory sensory neurons with their laminar position. Ciliated neurons (orange) have round somata and slender dendrites that terminate in bundles of cilia on the epithelial surface. They constitue the most basal layer of olfactory sensory neuron. Microvillous neurons (blue) have bundles of microvilli on their apical surface. Crypt neurons (red) are globular-shaped and carry both microvilli and cilia on their apical surface. They are located more apical than microvillous neurons. G_o-ir-positive kappe neurons (green) are pear-shaped with an apical appendage resembling a cap (German: Kappe), have no cilia, and are located even more apical than crypt neurons. Kappe neurons (green) constitute a novel olfactory sensory neuron population.

It is not clear, whether G_o-ir labels the same type of kappe neurons in other teleost fish species. Different patterns of G_o immunoreactivity have been reported for different fish species, both for sparse neuron populations described as crypt-like neurons[21–23] and for frequent neuron populations of undefined[16] or microvillous[21,24] phenotype. It is conceivable that in the absence of knowledge about kappe neurons, some may have been mistaken as crypt neurons in those earlier studies, since kappe neurons are more similar to crypt neurons than to the other two populations, ciliated and microvillous neurons. In any case, the observed species differences preclude the use of G_o-ir as a defining criterion of kappe neurons in other fish species.

Kappe neurons project to a single glomerulus in the mediodorsal cluster, mdg5 (this manuscript, see also[10]). With the identification of kappe neurons two of the six glomeruli in this cluster have been shown to be innervated by distinct populations of olfactory neurons, mdg5 by kappe neurons and mdg2 by crypt neurons. It will be interesting to see, whether this observation will be generalizable to the remaining four glomeruli in this cluster. Indeed, all six mediodorsal glomeruli are negative for ciliated and microvillous markers[7] in the double transgenic line also used here.

The presence of G_o-like immunoreactivity in kappe neurons could suggest G_o as a possible signal transduction molecule for these neurons. However, the subcellular distribution of G_o-ir in dendrite, cytoplasm, axon and axon terminals is unexpectedly broad. Additionally, *in situ* hybridization with G_o shows a large and broadly distributed cell population[25], inconsistent with the small and spatially restricted population of G_o-ir-positive neurons. Thus, we cannot exclude that G_o-ir in kappe neurons might be caused by a cross-reacting antigen, reminescent of the situation for standard molecular markers of crypt neurons, S100-ir[5] and TrkA-ir[6].

Kappe neurons feature a dot of intense actin signal somewhat recessed on their apical cap, suggesting the presence of microvilli in these neurons. However, in all other aspects investigated (shape, location, molecular markers), kappe neurons are highly significantly different from microvillous neurons, and in particular they do not express TRPC2, the accepted molecular marker and signal transduction molecule of microvillous neurons.

The functional role of kappe neurons is not known so far, but their sheer existence shows an astonishing complexity of odor representation already in the periphery of the olfactory system.

Methods

Antibodies, tissue and animal handling. Primary antibodies used were anti-S100 antibody (rabbit IgG; 1 : 500; catalog no. Z0311, Dako), anti- G_o (K-20) antibody (rabbit IgG; 1 : 50; sc-387, Santa Cruz Biotechnology), anti-TrkA (763) antibody (rabbit IgG; 1 : 100; sc-118, Santa Cruz Biotechnology), anti-zns2 (monoclonal mouse IgG1;1 : 50; supernatant, Developmental Studies Hybridoma Bank, University of Iowa, Iowa City, IA), anti-calretinin (mouse IgG; 1 : 200; Swant (Bellinzona, Switzerland), anti-tubulin (mouse monoclonal antibody IgG, 1 : 300; G712, Promega) and beta-actin (mouse monoclonal antibody; A5441; 1 : 300; Sigma). Secondary antibodies used were donkey anti-rabbit IgG conjugated to Alexa Fluor 488 (A21206, Invitrogen), goat anti-rabbit IgG conjugated to Alexa Fluor 594 (A11012, Invitrogen) and goat anti-mouse conjugated to Alexa Fluor 594 (A11005, Invitrogen).

Adult wild type zebrafish (Ab/Tü strain, 8–12 months old) were maintained at 28°C on 14/10-hour light/dark cycle. Adult fish were sacrificed by decapitation during anesthesia with MS-222 (ethyl 3-aminobenzoate, Sigma). Those experiments were approved by the governmental animal care and use office (Landesamt für Natur, Umwelt und Verbraucherschutz Nordrhein- Westfalen, Recklinghausen, Germany, Protocol No. 8.87-51.05.20.10.217) and were in accordance with the German Animal Welfare Act as well as with the General Administrative Directive for the Execution of the Protection of Animals Act. Tissues were embedded in 5% low melting agarose and sectioned by vibratome (Pelco 101) or embedded in TissueTek O.C.T. compound (Sakura), and cut by cryostat (Leica CM1900) at -20°C. Fluorescence was analysed using a wide field fluorescence microscope (Keyence BZ-9000) for sections and whole mounts. Transgenic zebrafish lines for ciliated neurons, *Tg(OMP:lyn-mRFP-S)*, and microvillous neurons, *Tg(TRPC2:gap-Venus)*, were used in this study.

Whole mount olfactory bulb immunohistochemistry. The dorsal cranium was removed, exposed brains were fixed by immersion in 4% paraformaldehyde (PFA, pH 7.4) in phosphate-buffered saline (PBS, pH 7.5) overnight at 4°C and olfactory bulbs were dissected out, keeping their connection to the telencephalon intact. Staining was performed according to[6]. After blocking, samples were incubated with primary antibodies anti-G_o and anti-zns2 either single or in mixture at 4°C for 20 to 25 days on a vertical rotator (5 sec/round), followed by several washes over a period of 3 hours at room temperature. Subsequently, the olfactory bulbs were incubated with secondary antibodies for 7 days at 4°C, followed by several washes at room temperature. Tissue was cleared as described[6]. Both primary and secondary antibodies were used at a final dilution of 1 : 100 in blocking reagent. For detailed examination 100 μm vibratome sections were analysed.

Immunohistochemistry on cryosections. Heads were either pre-incubated before dissection in cold freshly prepared 4% PFA in PBS for 5 min (pre-fixed tissue) or dissected directly (fresh-frozen tissue). We found that a short fixation step of 5 min does not impair the specificity of the S100 antibody for crypt neurons, in contrast to long fixation times, *cf.*[5]. Horizontal cryosections (8 μm) of the olfactory epithelia were thaw-mounted onto Superfrost Plus slide glasses (Thermo), incubated in acetone at -20°C for 15 min, washed several times in PBST, and blocked in 5% normal goat serum in PBST (blocking solution) for 1 hour at room temperature.

In order to overcome the limitations arising from same species antibodies in double labeling, the Fc portion of the anti-S100 antibody was covalently conjugated with fluorescein (Thermo Scientific, 53029) as described[26]. For double labeling, the slides were overnight incubated at 4°C with anti-G_o antibody (1 : 50 dilution in blocking solution), washed 3 times in PBST to remove unbound anti-G_o antibody and incubated for 2 hours at room temperature with the first of the two secondary antibodies (anti-rabbit alexa fluor 488). Slides were further washed 3 times in PBST, incubated for 1 hour in blocking solution, followed by overnight incubation at 4°C with flu-labeled anti-S100 (second primary antibody), washed 3 times for 10 min each and incubated for 2 hours at room temperature with alkaline phosphatase (AP) conjugated anti-fluorescein (the second of the two secondary antibodies). S100-labeled cells were visualized by enzymatic reaction of AP with HNPP Fluorescent Detection Set (Roche). The slides were washed in PBS and mounted with VectaShield containing DAPI (Vector).

Immunohistochemistry combined with in situ hybridization. TRPC2 cRNA riboprobe was prepared as described[5]. Pretreatment of sections, probe hybridization, and stringent washing were performed as described previously[13], except that Proteinase K treatment was omitted. For high stringency conditions the final washes were performed at 65°C in 0.2× SSC. Afterward, sections were blocked in 1% blocking reagent (Roche) in PBS for 1 h. The slides were then incubated with sheep anti-DIG Fab fragments conjugated with alkaline phosphatase (AP, Roche; 1 : 200) together with rabbit anti-G_o antibody (1 : 50) in the blocking solution at 4°C overnight. After washing three times in PBS, sections were treated with the secondary antibody (1 : 200) in PBS for 2 h at room temperature. Hybridized probes were visualized by enzymatic reaction of AP with HNPP Fluorescent Detection Set (Roche). After evaluating the success of the staining, slides were washed in PBS, mounted with VectaShield with DAPI (Vector), and observed and photographed with a fluorescent microscope (BZ-9000, Keyence).

Quantification and statistical evaluation. Spatial coordinates were measured in arbitrary units and normalized. Horizontal cell diameter was determined as maximal cell width, i.e. parallel to the basal lamina, and vertical diameter was determined as maximal cell length perpendicular to the basal lamina (soma and dendrite, if any), see Fig. 1b. For laminar height in the olfactory epithelium the distance between center of the cell soma and basal border of the epithelial layer (see Fig. 1b) was normalized to the distance between basal and apical border of the epithelial layer at the position of the cell to be measured. Thus the range of values is between 0 (most basal) and 1 (most apical). Radial distance was measured from the apex of the lamellar 'curve', i.e. closest to the median raphe, to the cell soma center (see Fig. 1b), and normalized to the distance between the central position and the border of the epithelial section. Finally, the cardinal number of sections served as z axis coordinate. One hundred to several hundred cells were measured for each marker and spatial coordinate.

Distributions are depicted as histograms or as the corresponding empirical cumulative distribution function (ECDF) of the unbinned distributions[27,28].

To estimate whether two spatial or shape distributions were significantly different, we performed Kolmogorov-Smirnov tests on the unbinned distributions as described[29]. This test is particularly suitable for continuous distributions and makes no assumptions about the nature of the distributions investigated, which is essential because the skewness of the observed distributions shows that these are not Gaussian. Due to the sensitive nature of the test on large distributions ($n > 100$), we selected $P < 0.01$ as cutoff criterion for significant difference. Results of the Kolmogorov-Smirnov test were confirmed by permutation analysis[30] without exception.

1. Mombaerts, P. *et al*. Visualizing an olfactory sensory map. *Cell* **87**, 675–86 (1996).
2. Johnson, M. A. *et al*. Neurons expressing trace amine-associated receptors project to discrete glomeruli and constitute an olfactory subsystem. *Proc Natl Acad Sci U S A* **109**, 13410–5 (2012).
3. Wagner, S., Gresser, A. L., Torello, A. T. & Dulac, C. A multireceptor genetic approach uncovers an ordered integration of vno sensory inputs in the accessory olfactory bulb. *Neuron* **50**, 697–709 (2006).
4. Hansen, A. & Zeiske, E. The peripheral olfactory organ of the zebrafish, danio rerio: An ultrastructural study. *Chem Senses* **23**, 39–48 (1998).
5. Oka, Y., Saraiva, L. R. & Korsching, S. I. Crypt neurons express a single v1r-related ora gene. *Chem Senses* **37**, 219–27 (2012).
6. Ahuja, G. *et al*. Zebrafish crypt neurons project to a single, identified mediodorsal glomerulus. *Sci Rep* **3**, 2063 (2013).
7. Sato, Y., Miyasaka, N. & Yoshihara, Y. Mutually exclusive glomerular innervation by two distinct types of olfactory sensory neurons revealed in transgenic zebrafish. *J Neurosci* **25**, 4889–97 (2005).
8. Germana, A. *et al*. S100 protein-like immunoreactivity in the crypt olfactory neurons of the adult zebrafish. *Neurosci Lett* **371**, 196–8 (2004).
9. Catania, S. *et al*. The crypt neurons in the olfactory epithelium of the adult zebrafish express trka-like immunoreactivity. *Neurosci Lett* **350**, 5–8 (2003).
10. Braubach, O. R., Fine, A. & Croll, R. P. Distribution and functional organization of glomeruli in the olfactory bulbs of zebrafish (danio rerio). *J Comp Neurol* **520**, 2317–39, Spc1 (2012).
11. Mombaerts, P. Axonal wiring in the mouse olfactory system. *Annu Rev Cell Dev Biol* **22**, 713–37 (2006).
12. Syed, A. S., Sansone, A., Nadler, W., Manzini, I. & Korsching, S. I. Ancestral amphibian v2rs are expressed in the main olfactory epithelium. *Proc Natl Acad Sci U S A* **110**, 7714–9 (2013).
13. Weth, F., Nadler, W. & Korsching, S. Nested expression domains for odorant receptors in zebrafish olfactory epithelium. *Proc Natl Acad Sci U S A* **93**, 13321–6 (1996).
14. Conzelmann, S. *et al*. A novel brain receptor is expressed in a distinct population of olfactory sensory neurons. *Eur J Neurosci* **12**, 3926–34 (2000).
15. DeMaria, S. *et al*. Role of a ubiquitously expressed receptor in the vertebrate olfactory system. *J Neurosci* **33**, 15235–47 (2013).
16. Gayoso, J. A., Castro, A., Anadon, R. & Manso, M. J. Differential bulbar and extrabulbar projections of diverse olfactory receptor neuron populations in the adult zebrafish (danio rerio). *J Comp Neurol* **519**, 247–76 (2011).
17. Arikawa, K. & Williams, D. S. Acetylated alpha-tubulin in the connecting cilium of developing rat photoreceptors. *Invest Ophthalmol Vis Sci* **34**, 2145–9 (1993).
18. Arikawa, K., Hicks, J. L. & Williams, D. S. Identification of actin filaments in the rhabdomeral microvilli of drosophila photoreceptors. *J Cell Biol* **110**, 1993–8 (1990).
19. Brechbuhl, J., Klaey, M. & Broillet, M. C. Grueneberg ganglion cells mediate alarm pheromone detection in mice. *Science* **321**, 1092–5 (2008).
20. Elsaesser, R. & Paysan, J. The sense of smell, its signalling pathways, and the dichotomy of cilia and microvilli in olfactory sensory cells. *BMC Neurosci* **8 Suppl 3**, S1 (2007).
21. Hansen, A. & Zielinski, B. S. Diversity in the olfactory epithelium of bony fishes: Development, lamellar arrangement, sensory neuron cell types and transduction components. *J Neurocytol* **34**, 183–208 (2005).
22. Hansen, A. *et al*. Correlation between olfactory receptor cell type and function in the channel catfish. *J Neurosci* **23**, 9328–39 (2003).
23. Hansen, A., Anderson, K. T. & Finger, T. E. Differential distribution of olfactory receptor neurons in goldfish: Structural and molecular correlates. *J Comp Neurol* **477**, 347–59 (2004).
24. Ferrando, S. *et al*. Immunolocalization of g protein alpha subunits in the olfactory system of polypterus senegalus (cladistia, actinopterygii). *Neurosci Lett* **499**, 127–31 (2011).
25. Oka, Y. & Korsching, S. I. Shared and unique g alpha proteins in the zebrafish versus mammalian senses of taste and smell. *Chem Senses* **36**, 357–65 (2011).
26. Korsching, S. & Thoenen, H. Two-site enzyme immunoassay for nerve growth factor. *Methods Enzymol* **147**, 167–85 (1987).
27. Wilk, M. B. & Gnanadesikan, R. Probability plotting methods for the analysis of data. *Biometrika* **55**, 1–17 (1968).
28. Feller, W. *An introduction to probability theory and its applications*. (Vol. II., New York: Wiley, 1966).
29. Press, W. H., Teukolsky, S. A., Vetterling, W. T. & Flannery, B. P. *Numerical recipes in c: The art of scientific computing*. (Cambridge university press, cambridge. Vol. Second, 1992).
30. Manly, B. F. J. *Randomization, bootstrap and monte carlo methods in biology*, (London: Chapman and Hall/CRC, London, 1997).

Acknowledgments

We thank Walter Nadler for implementing the Kolmogorov-Smirnov test and the permutation analysis, Priyanka Maiti for technical help, and Mehmet Saltürk for taking good care of the zebrafish. We gratefully acknowledge financial support from the German Science foundation (grant KO 1046/7-1 to S.I.K.) and the International Graduate School IGSDHD (G.A., V.S.).

Author contributions

The experiments were designed by S.I.K. and G.A., and performed by G.A., V.S., D.K. and Y.O. Illustrations were drafted by V.Z., G.A. and S.I.K. Data analysis was done by S.I.K., S.B. and G.A. S.I.K. wrote the paper.

Additional information

Competing financial interests: The authors declare no competing financial interests.

How to cite this article: Ahuja, G. *et al.* Kappe neurons, a novel population of olfactory sensory neurons. *Sci. Rep.* **4**, 4037; DOI:10.1038/srep04037 (2014).

This work is licensed under a Creative Commons Attribution-NonCommercial-NoDerivs 3.0 Unported license. To view a copy of this license, visit http://creativecommons.org/licenses/by-nc-nd/3.0

Publication 3

Ashiq Hussain*, Luis R. Saraiva*, David M. Ferrero*, **Gaurav Ahuja***, Venkatesh S. Krishna, Stephen D. Liberles, and Sigrun I. Korsching. *High-affinity olfactory receptor for the death-associated odor cadaverine*; PNAS, doi/10.1073/ pnas. 1318596110 (**2013**). *** Equal contribution**

http://www.pnas.org/content/110/48/19579.abstract

High-affinity olfactory receptor for the death-associated odor cadaverine

Ashiq Hussain[a,1,2], Luis R. Saraiva[a,2,3], David M. Ferrero[b,2], Gaurav Ahuja[a,2], Venkatesh S. Krishna[a], Stephen D. Liberles[b,4], and Sigrun I. Korsching[a,4]

[a]Institut für Genetik, Universität zu Köln, 50674 Cologne, Germany; and [b]Department of Cell Biology, Harvard University, Boston, MA 02115

Edited* by Cornelia I. Bargmann, The Rockefeller University, New York, NY, and approved October 18, 2013 (received for review October 2, 2013)

Carrion smell is strongly repugnant to humans and triggers distinct innate behaviors in many other species. This smell is mainly carried by two small aliphatic diamines, putrescine and cadaverine, which are generated by bacterial decarboxylation of the basic amino acids ornithine and lysine. Depending on the species, these diamines may also serve as feeding attractants, oviposition attractants, or social cues. Behavioral responses to diamines have not been investigated in zebrafish, a powerful model system for studying vertebrate olfaction. Furthermore, olfactory receptors that detect cadaverine and putrescine have not been identified in any species so far. Here, we show robust olfactory-mediated avoidance behavior of zebrafish to cadaverine and related diamines, and concomitant activation of sparse olfactory sensory neurons by these diamines. The large majority of neurons activated by low concentrations of cadaverine expresses a particular olfactory receptor, trace amine-associated receptor 13c (TAAR13c). Structure-activity analysis indicates TAAR13c to be a general diamine sensor, with pronounced selectivity for odd chains of medium length. This receptor can also be activated by decaying fish extracts, a physiologically relevant source of diamines. The identification of a sensitive zebrafish olfactory receptor for these diamines provides a molecular basis for studying neural circuits connecting sensation, perception, and innate behavior.

Danio rerio | aversion | heterologous expression | polyamines

Cadaverine, putrescine, and other biogenic diamines are strongly repulsive odors to humans, for whom these odors presumably signal bacterial contamination. It may be expected that animal species feeding on carcasses attribute a more positive valence to diamines, and indeed both putrescine and cadaverine have been reported to be feeding attractants for rats (1) as well as goldfish (2). Similarly, insects depositing their eggs in carcasses or other proteineacous materials are attracted by these diamines (3). Beyond signaling danger or food, putrescine and cadaverine also serve as social cues in several vertebrate species, both for marking of territories—for example, in feline species (4)—and for burial of conspecifics (5).

Very little is known about the molecular and cellular basis of cadaverine-driven behaviors. Cadaverine and putrescine evoke electrophysiological responses in the olfactory epithelium of two fish species (2, 6) and cadaverine-responsive olfactory sensory neurons and glomeruli have been identified in the mouse (7, 8). However, chemosensory receptors that detect cadaverine or related diamines are unknown in any species, and could provide valuable tools to study how the olfactory system mediates innate aversion or attraction.

Here, we show that cadaverine is a major product of zebrafish tissue decay, activates a zebrafish olfactory receptor (trace amine-associated receptor 13c, TAAR13c) with high affinity, and elicits a strong, low-threshold, and olfactory-mediated avoidance response in zebrafish. In vivo measurements indicate that high affinity cadaverine responses occur primarily in TAAR13c-expressing olfactory sensory neurons. These findings provide an important foundation for understanding the molecular basis of a powerful odor-driven behavior.

Results

Zebrafish Avoid a Cadaverine Odor Source. The zebrafish has in recent years emerged as an important model system for understanding olfaction in vertebrates because of a remarkable similarity in the basic principles of olfactory representation (9) and some technical advantages over the mammalian system (10). However, behavioral responses of zebrafish to diamines have not been described. We report here that zebrafish, like humans, show pronounced innate aversion behavior for cadaverine (Fig. 1).

We developed a valence assay to measure behavioral responses of zebrafish to olfactory cues. Zebrafish were habituated to a rectangular tank, and the position of each fish was recorded before and after odor delivery. Shifts in average position toward or away from the odor source were recorded as attraction and avoidance, respectively. Food odor, an attractant for zebrafish, caused a mean displacement of 0.25 tank lengths (TLs, $P < 0.01$) toward the odor source (Fig. 1*B*), but tank water alone had no effect (Fig. 1*C* and Table S1). In contrast, cadaverine caused a mean displacement of 0.28 TLs ($P < 0.01$) away from the odor source, and was thus aversive (Fig. 1 *A* and *C*, and Table S1). Furthermore, the fish spent severalfold less time in close approach (distances < 0.05 TL) to the stimulus application site ($P < 0.0001$), although this area was not completely avoided ($P < 0.03$) (Fig. 1*A* and Table S1), suggesting that the zebrafish did for short periods of time investigate the area, where stimulus was given. Mean velocity or total distance traveled was not altered during avoidance behavior (Table S1). Thus, the displacement observed is not caused by changes in motility but may result from an assessment of odor valence by the fish.

Next, we analyzed whether related diamines were similarly aversive. We tested diamines with different carbon chain lengths, ranging from C3 (diaminopropane) to C10 (diaminodecane). Avoidance behavior was observed (Fig. 1*C*) to putrescine (C4), cadaverine (C5), diaminohexane (C6), diaminoheptane (C7),

Significance

Cadaverine and putrescine, two diamines emanating from decaying flesh, are strongly repulsive odors to humans but serve as innate attractive or social cues in other species. Here we show that zebrafish, a vertebrate model system, exhibit powerful and innate avoidance behavior to both diamines, and identify a high-affinity olfactory receptor for cadaverine.

Author contributions: S.D.L. and S.I.K. designed research; A.H., L.R.S., D.M.F., G.A., and V.S.K. performed research; A.H., S.D.L., and S.I.K. analyzed data; and A.H., L.R.S., G.A., S.D.L., and S.I.K. wrote the paper.

The authors declare no conflict of interest.

*This Direct Submission article had a prearranged editor.

[1] Present address: Department of Molecules, Signaling, and Development, Max-Planck-Institut für Neurobiologie, 82152 Martinsried, Germany.

[2] A.H., L.R.S., D.M.F., and G.A. contributed equally to this work.

[3] Present address: European Molecular Biology Laboratory–European Bioinformatics Institute (EMBL–EBI) and Wellcome Trust Sanger Institute, Wellcome Trust Genome Campus, Hinxton-Cambridge CB10 1SD, United Kingdom.

[4] To whom correspondence may be addressed. E-mail: stephen_liberles@hms.harvard.edu or sigrun.korsching@uni-koeln.de.

This article contains supporting information online at www.pnas.org/lookup/suppl/doi:10.1073/pnas.1318596110/-/DCSupplemental.

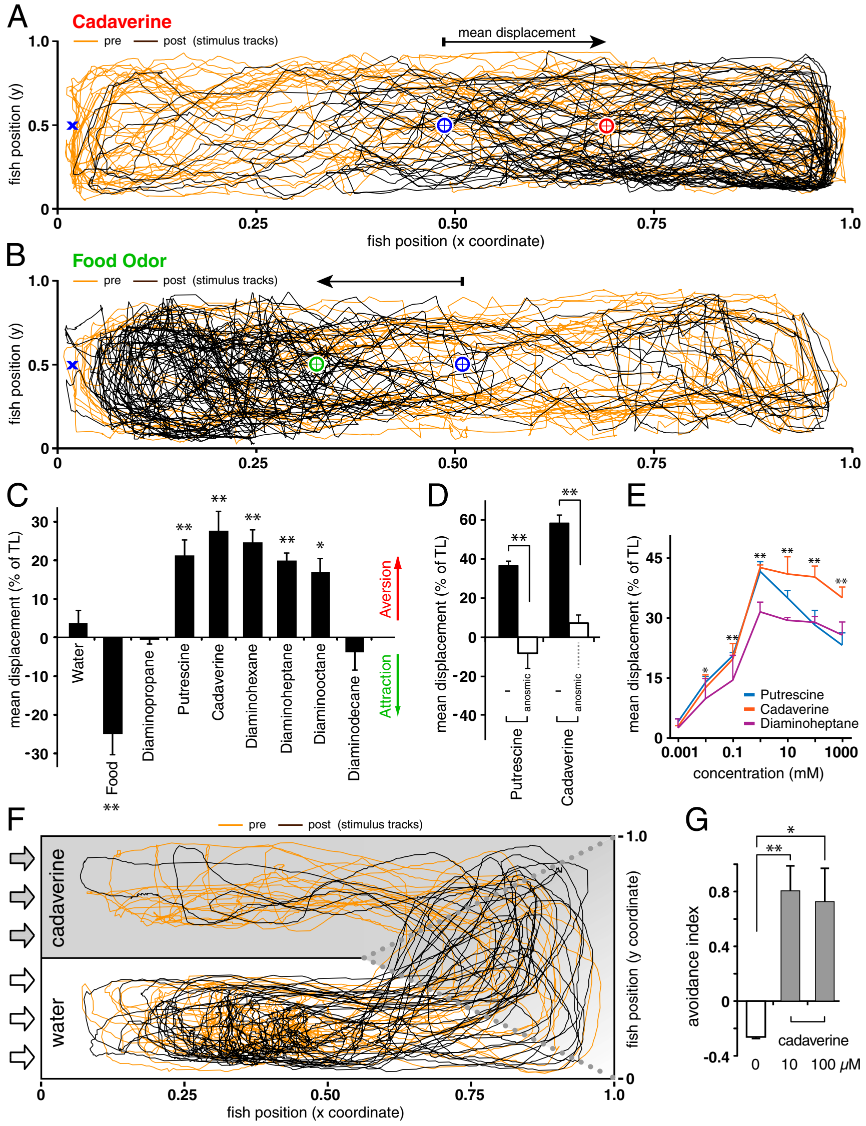

Fig. 1. Aversive behavioral response of zebrafish to diamines. (*A* and *B*) Cadaverine-evoked aversion and food odor-evoked attraction of individual zebrafish as visualized by movement patterns before (orange tracks) and after (brown tracks) stimulus addition (1 mM, 180 μL). The position of stimulus deposition (blue X), as well as the mean location before (blue circle) and after (red, green circles) stimulus addition are indicated. The axes represent tank dimensions. (*C*) Mean displacement was expressed as a percentage of tank length ($n = 6 \pm$ SEM). Addition of tank water alone had no significant effect, whereas food odor elicited strong attraction. Similar avoidance behavior was observed in male and female fish. Significance was evaluated by Student *t* test, $^*P < 0.05$, $^{**}P < 0.01$. (*D*) Aversion behavior requires olfactory input. Nostril closure of zebrafish eliminates aversion to 1 mM cadaverine or putrescine. Black bars, no treatment; white bars, nostril closure; $^{**}P < 0.01$, $n = 3 \pm$ SEM. (*E*) Avoidance behavior to diamines was dose-dependent. Responses to cadaverine and diaminoheptane were measured over a broad concentration range (1 μM to 1 M, $n = 3 \pm$ SEM). The behavior is clearly saturable at 1-mM stimulus concentration. Significance was evaluated by Student *t* test, asterisks refer to cadaverine, $^*P < 0.05$, $^{**}P < 0.01$. The slight decrease at higher concentrations is not significant except for putrescine ($P < 0.05$). (*F*) Cadaverine-evoked aversion of an individual zebrafish in a flow-through two-channel set-up (11) as visualized by movement patterns before (orange tracks) and after (brown tracks) change of the upper channel to a chronic concentration of 10 μM cadaverine. The arrows indicate direction of flow (cadaverine, gray; water, white). Dotted gray lines enclose the mixing zone not included in analysis of preference. The axes represent tank dimensions. (*G*) Aversion behavior of zebrafish in the two-channel preference test is maximal at 10 μM cadaverine. The avoidance index shows similar avoidance of the cadaverine channel for 10 and 100 μM cadaverine (gray bars). Significance in comparison with water was evaluated by Student *t* test, $^*P < 0.05$, $^{**}P < 0.01$.

and diaminooctane (C8), but not to diaminopropane (C3) or diaminodecane (C10). Time spent in close approach to the stimulus application site did not differ significantly from prestimulus values for diaminopropane and diaminodecane, but was reduced to one-third or less for the other diamines ($P < 0.0001$) (Table S1). Only cadaverine and putrescine are naturally abundant in carrion (see below); other diamines not found ecologically may be aversive because they function as agonists for cadaverine and putrescine-activated receptors.

Avoidance behavior to cadaverine and putrescine was abolished ($P < 0.01$) in fish, whose nostrils were closed by tissue glue, showing the avoidance to be mediated by olfaction and not other sensory modalities (Fig. 1*D*). Avoidance responses to cadaverine, putrescine, and diaminoheptane exhibited similar dose-dependence (Fig. 1*E*), with complete saturation at 1 mM diamine in the stimulus, half-maximal values at 100 μM, and about one-third of maximal values at 10 μM (Fig. 1*E*). The actual concentrations encountered by the zebrafish at the time of decision-making are expected to be much lower than these values because of dilution of a small stimulus volume (180 μL) into a large tank volume (9 L). To obtain a more stringent estimate of behavioral sensitivity, we have therefore used a two-channel preference assay (11), with a constant cadaverine concentration in one of the two streams during the stimulus period. Cadaverine evoked robust avoidance responses in this paradigm, with similar levels of avoidance observed at 10 μM (avoidance index 0.81 ± 0.18 SEM, $n = 4$, $P < 0.01$) and 100 μM (avoidance index 0.73 ± 0.24 SEM, $n = 4$, $P < 0.05$). Such sensitive detection suggests the existence of specialized olfactory receptors for diamines.

Cadaverine and Other Diamines Activate Sparse Olfactory Sensory Neurons. We observed diamine-evoked increases in c-Fos expression and pERK levels in sparse olfactory sensory neurons. ERK phosphorylation and c-Fos expression are induced by neuronal activity, and are widely used reporters for neuron responsiveness, including in the olfactory system (12, 13). Olfactory tissue was obtained from zebrafish ($n = 102$) exposed to diamines or control stimuli and stained using standard immunohistochemical (IHC) techniques. c-Fos expression was similarly and robustly induced by food odor, cadaverine, and other diamines (~6.0 cells per lamella) but not tank water alone (<0.5 cells per lamella), with low background levels likely resulting from residual odors in tank water (Fig. 2 *A* and *B*, and Fig. S1). The frequency of pERK-containing cells was similar to that of c-Fos–expressing cells for food odor, cadaverine, and diaminohexane. Some differences in c-Fos induction and ERK phosphorylation were observed for other diamines, and could reflect differences in reporter sensitivity for lower affinity ligands or the much longer exposure time

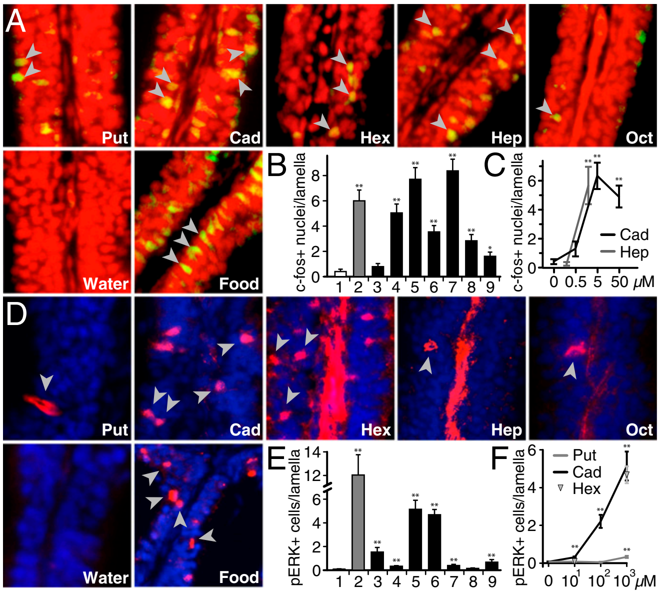

Fig. 2. Diamines elicit c-Fos and pERK increase in olfactory sensory neurons. (*A*) Zebrafish (n = 21) were exposed to stimuli indicated (2 or 5 mM). c-Fos IHC (green) and nuclear staining (propidium iodide, red), enabled visualization of c-Fos$^+$ nuclei (yellow), some emphasized by gray arrow heads. (*B* and *C*) Quantification of c-Fos$^+$ nuclei/lamella as a function of diamine chain length (*B*) or concentration (*C*). Results from one representative experiment each are shown. Counting was done on randomized micrographs, values given represent mean ± SEM. Significance in comparison with water was evaluated by Student *t* test, $^*P < 0.05$, $^{**}P < 0.01$. (*B*) 1, water; 2, food extract; 3–8, numbers reflect carbon chain length of diamines; 9, diaminodecane. (*D*) Zebrafish (n = 14) were exposed to stimuli indicated (1 mM). Some pERK-labeled cells (red) are emphasized by gray arrowheads; nuclear counterstain (DAPI, blue). Red central stripes in some panels, unspecific label in the basal lamina outside the sensory region. (*E* and *F*) Quantification of pERK$^+$ cells/lamella as function of chain length (*E*) or concentration (*F*). Values given represent mean ± SEM. Significance in comparison with water was evaluated by Student *t* test, $^{**}P < 0.01$. (*E*) Results from two experiments are shown; 1, water; 2, food extract; 3–8, numbers reflect carbon chain length of diamines; 9, diaminodecane. (*F*) Evaluation was partly on randomized data, no difference was seen between randomized and nonrandomized evaluation.

required for c-Fos expression. Dose-dependent analysis indicated threshold c-Fos responses to cadaverine and diaminoheptane at 2 and 5 μM, respectively (Fig. 2*C*). Low concentrations of cadaverine and putrescine resulted in very low frequencies of pERK-labeled cells (Fig. 2*F*), consistent with detection by a single olfactory receptor (cf. refs. 14 and 15). The range of diamine chain lengths (C3 to C10) that stimulate either c-Fos expression or ERK phosphorylation in olfactory tissue includes all diamines that promote aversive behavior (C4 to C8), consistent with this behavior being mediated by olfaction. However, olfactory receptors that detect cadaverine in zebrafish or any species have not been identified so far.

TAAR13c Is an Olfactory Receptor for Cadaverine and Other Diamines. As in mammals (16), zebrafish TAARs function as olfactory receptors (17). We reasoned that a zebrafish TAAR could mediate the cadaverine avoidance behavior because several rodent TAARs detect biogenic amines, including some highly aversive odors (16, 18–20). As a result of numerous gene-duplication events, the zebrafish TAAR family is large, with 112 receptors encoded by the zebrafish genome (17). So far, ligands have not been identified for any zebrafish TAAR, and identification of such ligands would be a key step toward understanding their physiological roles.

The dynamic evolution of the teleost *Taar* gene family led to widespread loss (17) of an amine-binding motif found in biogenic amine receptors (21). However, most class I and class II teleost TAARs retain this amine-binding motif (17), making them good candidates for contributing to amine perception by the fish olfactory system.

We initiated a chemical screen to identify agonists for zebrafish TAARs and selected representatives from each of the five TAAR subfamilies retaining the amine-binding motif and three TAARs without it (see Fig. 3*D* for phylogenetic position of genes analyzed). We previously developed a reporter gene system to measure ligand-induced TAAR activation (16, 19); here, we used this system to identify zebrafish TAAR agonists among 93 test odorants, including a large number of amines, diamines, polyamines, and amino acids.

One receptor tested, zebrafish TAAR13c, gave robust responses to cadaverine (1,5-diaminopentane) and related aliphatic diamines (Fig. 3 *A* and *C*). Cadaverine activated HEK293 cells expressing TAAR13c, but not control cells lacking TAAR13c, with a half-maximal response (EC_{50}) occurring at 23 ± 3 μM (mean ± SD) and a threshold response occurring at 3 μM (Fig. 3*E*). Cadaverine variants, in which one amino group is replaced with a hydroxyl group, methyl group, or hydrogen, did not activate TAAR13c (Fig. 3*B*). Furthermore, 47 different aliphatic and aromatic monoamines with varying chain lengths, degrees of substitution, and functional groups, did not activate TAAR13c (Fig. 3*A*). This structure–activity analysis suggests that TAAR13c contains two remote cation recognition sites, both of which require occupancy for receptor activation.

TAAR13c Preferentially Detects Odd-Chained Diamines. We next measured TAAR13c responses to diamines ranging from C3 to C10 across several concentrations (Fig. 3*E*) and found cadaverine (C5) and diaminoheptane (C7) to activate TAAR13c with highest affinity (EC_{50} = 23 ± 3 μM and 30 ± 2 μM, respectively). Diaminohexane (C6) had ~fivefold reduced affinity, whereas putrescine (C4) and diaminooctane (C8) had >10-fold reduced affinity. Diaminopropane (C3) and diaminodecane (C10) did not activate TAAR13c at any concentration tested. Furthermore, other dibasic ligands, including cystamine, agmatine, and histamine, activated TAAR13c with reduced affinity (Fig. S1). Although TAAR13c detected numerous primary amines, it showed reduced activity for the tertiary amine derived from putrescine, tetramethyl-1,4-diaminobutane (Fig. 3*A*). Indeed, TAAR13c is phylogenetically closer to those mammalian TAARs that detect primary amines than to those preferring tertiary amines (Fig. 3*D*) (cf. ref. 18).

Interestingly, both fish avoidance behavior and sensory neuron responses showed no distinct preference for odd-chained diamines, suggesting the existence of other receptors tuned to even-chained diamines. This finding is consistent with electrophysiological studies indicating limited cross-adaptation of olfactory responses to cadaverine and putrescine (2). Here, we identified TAAR13c as a highly sensitive detector of odd-chained diamines that include the repulsive odor cadaverine.

A Physiological Source of Cadaverine Activates TAAR13c. A physiologically relevant source of diamine odors is decomposing carcasses, whose presence may signal danger. In these circumstances, cadaverine will be present in a complex mixture together with other potentially odorous chemicals that also result from tissue decay. Thus far we have examined TAAR13c responses to pure chemicals; next we asked whether TAAR13c could detect cadaverine produced during the natural process of tissue decomposition.

We prepared fish extracts by placing a killed zebrafish in PBS for 0 min ("fresh") or 1 wk ("rotten"). PBS solutions were homogenized and centrifuged to remove debris, and resulting supernatants used as "extracts." We found that rotten fish extracts provided a potent stimulus for TAAR13c, but that fresh extracts had no activity (Fig. 4*A*). Next, we analyzed the concentration dependence of fresh and rotten fish extracts. We observed a half-maximal response to rotten fish extracts diluted ~1,000-fold from the initial preparation (Fig. 4*B*). In contrast, fresh fish extracts

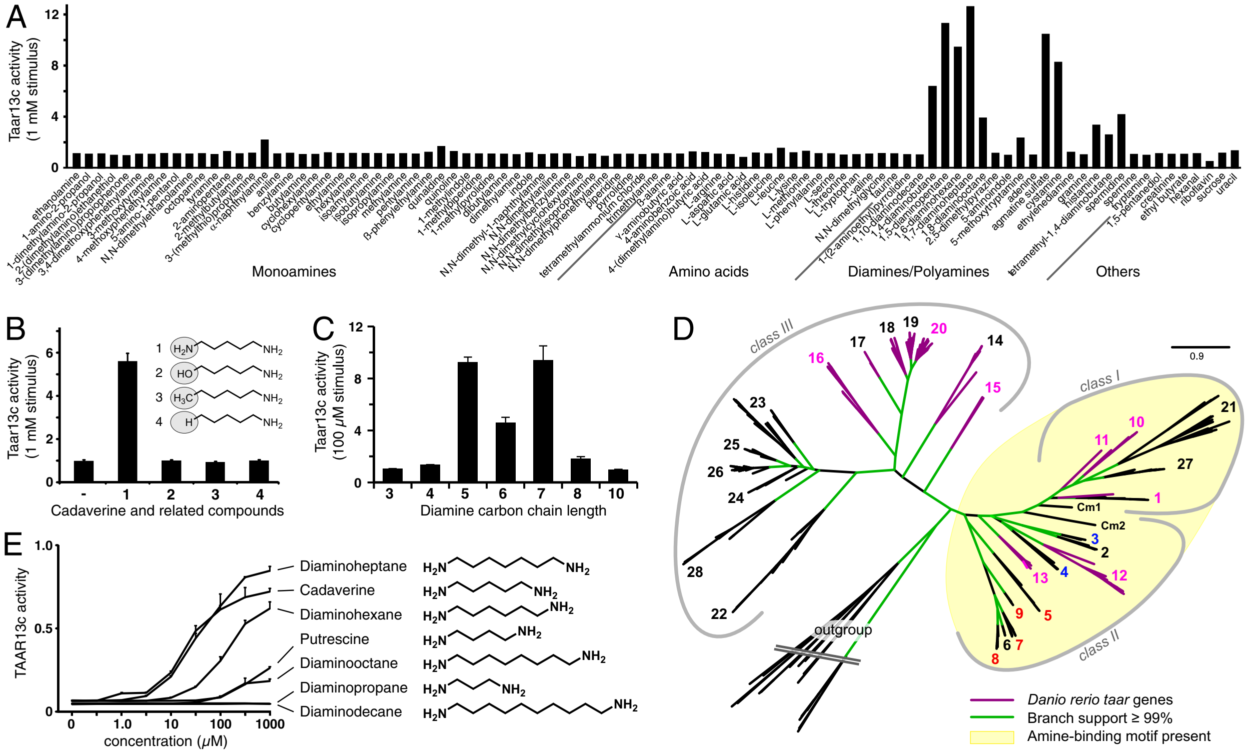

Fig. 3. TAAR13c is a sensitive diamine detector. (*A*) HEK293 cells were transfected with TAAR13c plasmid and a reporter gene, incubated with 93 different test chemicals (1 mM), and assayed for reporter gene activity. TAAR13c activity is reported after normalization to responses from control stimuli (media alone). Only aliphatic and mixed aliphatic/aromatic diamines and polyamines activate TAAR13c. No responses to diamines were observed in cells transfected with reporter gene alone. (*B*) TAAR13c activation requires a divalent ligand with two amino groups. TAAR13c responses ($n = 3 \pm$ SEM, 1-mM stimuli) were measured for: 1, cadaverine; 2, 5-amino-1-pentanol; 3, hexylamine; 4, pentylamine; or "–" no ligand. (*C*) TAAR13c prefers odd-chained diamines. Responses of TAAR13c ($n = 3 \pm$ SEM) were measured to diamines of carbon chain length 3–10 (100 μM). (*D*) Phylogenetic tree for *taar* genes, gene set as described previously (17), but only three mammalian species included (mouse, rat, human). Class I and II TAARs retain the amine-binding motif (yellow shade). Numbers indicate TAAR subfamilies, including mammalian TAARs that detect primary (blue) or tertiary (red) amines, as well as zebrafish TAARs analyzed here (purple). TAAR13c terminal branch, light purple; Cm1, Cm2, elephant shark *taar* genes. (*E*) Dose-dependent activation of TAAR13c by aliphatic diamines; values are in relative units. A representative experiment is shown ($n = 3 \pm$ SEM). No responses to diamines were observed in cells transfected with reporter gene alone. Higher affinity is seen for odd-chained diamines.

did not activate TAAR13c at any concentration tested, up to a 10-fold dilution (Fig. 4*B*). These results indicate that TAAR13c is able to detect diamines in a complex and physiologically relevant mixture.

Cadaverine Is the Principal TAAR13c Activator in Decayed Fish. To determine the most relevant TAAR13c ligands in rotten fish extracts, we quantified the levels of diamines using liquid chromatography and tandem mass spectrometry (LC/MS). The number of ion counts with the mass-charge ratio (*m*/*z*) corresponding to nine different diamines (putrescine, cadaverine, diaminohexane, diaminoheptane, diaminooctane, agmatine, cystamine, histamine, and cysteamine) were separately graphed over time. The retention time and integrated area of observed peaks were compared with standards for chemical assignment and quantification. None of these nine amines were detected in fresh fish extracts, and only cadaverine, putrescine, and histamine were detected in rotten fish extract (Fig. 4*C*). Cadaverine was the most abundant diamine detected, and levels of cadaverine, but not putrescine or histamine, were sufficient to explain the striking sensitivity of TAAR13c for decomposed tissue (Fig. 4*D*).

High-Affinity Cadaverine Responses Occur Primarily in TAAR13c-Expressing Neurons. We next sought to determine whether high-affinity cadaverine responses occurred primarily in TAAR13$^+$ or TAAR13c$^-$ olfactory sensory neurons. We generated a polyclonal antibody that recognizes a highly divergent region of the TAAR13c sequence that is not conserved in closely related TAAR13 family members (Fig. S1). This antibody labeled a 55-kDa protein in olfactory epithelium, but not other tissues by Western blot analysis, and an extremely sparse population of olfactory sensory neurons (0.3 cells per lamella) (Fig. S1) by IHC analysis. Two-color analysis indicated colabeling of olfactory sensory neurons with TAAR13c antibody and *Taar13c* cRNA riboprobe, with *Taar13c* riboprobe labeling three- to sixfold more cells, likely because of cross-hybridization to the four other *Taar13c* family members. Neurons labeled by TAAR13c antibody showed a ciliary morphology (Fig. S1) and occurred at a frequency similar to that predicted for expression of individual olfactory receptor genes (15).

Next, we asked whether cells labeled by the TAAR13c antibody responded to diamines using two-color IHC analysis for pERK and TAAR13c. We found that cadaverine-responsive neurons could be classified as low or high affinity based on response sensitivity. High-affinity (10 μM) cadaverine responses occurred primarily (~90%) in TAAR13c-expressing cells (Fig. 5), whereas increasing cadaverine concentration 10-fold resulted in increased numbers of responsive neurons, suggesting recruitment of additional low-affinity receptors (Fig. 5). TAAR13c cells were distinct from those activated by low concentrations (10 μM) of putrescine (Fig. 5), consistent with our findings that TAAR13c prefers odd-chained diamines. Taken together, these results are consistent with TAAR13c being a major component in high-affinity cadaverine recognition by zebrafish.

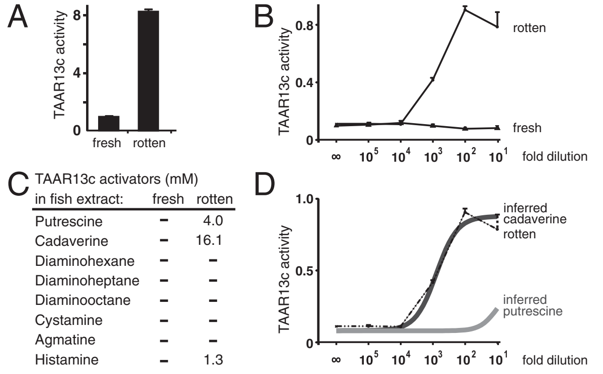

TAAR13c activators (mM) in fish extract:	fresh	rotten
Putrescine	–	4.0
Cadaverine	–	16.1
Diaminohexane	–	–
Diaminoheptane	–	–
Diaminooctane	–	–
Cystamine	–	–
Agmatine	–	–
Histamine	–	1.3

Fig. 4. TAAR13c is activated by a biological source of diamines. (*A*) TAAR13c detects rotten but not fresh fish extracts diluted 100-fold. Values are given as signal-to-blank ratios. (*B*) Rotten fish extract activates TAAR13c in a dose-dependent manner, whereas fresh extract shows no activity at any concentration. (*C*) LC/MS analysis showed that rotten but not fresh fish extracts contain cadaverine, putrescine, and histamine at concentrations indicated. No other TAAR13c activators were detected ("–", below detection limit of 0.5 mM). (*D*) TAAR13c activation by rotten fish extract can be explained by cadaverine content. Gray solid curves indicate inferred TAAR13c activation by cadaverine and putrescine present in the various dilutions of rotten fish extract and are superimposed on a curve (dashed lines) reporting measured dose-dependent TAAR13c activation by rotten fish extract (see *B*).

Discussion

Cadaverine and putrescine are death-associated odors produced by microbe-mediated decarboxylation of basic amino acids (22). Chemosensory receptors that detect these odors are unknown in any species and could provide valuable tools to study how the olfactory system mediates innate aversion or attraction (cf. ref. 23).

Here, we show that zebrafish TAAR13c detects cadaverine with high sensitivity and specificity. This study is unique in reporting a ligand for any of the 112 zebrafish TAARs, and following identification of two amino acid-activated receptors from the V2R-related receptor family (24, 25), constitutes the third deorphanization of any fish olfactory receptor. TAAR13c is strongly activated by primary amines and indeed is phylogenetically closer to those rodent TAARs that prefer primary over tertiary amines (18). Moreover, TAAR13c has distinct molecular recognition properties compared with many biogenic amine-activated G protein-coupled receptors in that it is selective for diamines compared with monoamines. Structure activity analysis indicates an unusual divalent ligand binding pocket requiring two remote positive charges for activation. A conserved aspartic acid in biogenic amine receptors that forms a salt bridge with the ligand amino group is retained in TAAR13c (Asp$^{3.32}$), but residues important for recognition of the second amine are not known. Nevertheless, the existence of a second amine contact site raises the possibility for a unique inverted mode of monoamine recognition by G protein-coupled receptors that lose the conserved Asp$^{3.32}$ but retain the second recognition site.

TAAR13c is a narrowly tuned receptor that prefers medium-length, odd-chained diamines. Although a pronounced tuning to chain length is commonly found for olfactory receptors (26, 27), TAAR13c is peculiar in its strong preference for odd-chained diamines. Odd- and even-chained diamines have significant differences in the relative orientation and positioning of the two amino groups, and their cognate olfactory receptors likely have negatively charged counterions in distinct locations of the agonist binding pocket. Interestingly, odd-chained and even-chained diamines did elicit comparable aversive behavior, which suggests the presence of additional zebrafish olfactory receptors activated by even-chained diamines, consistent with data from cross-adaptation studies (6).

Some estimates about the conceivable size of the cadaverine receptor repertoire can be derived from our quantitative analysis of sensory neuron responses. We find that many receptor neurons show increased pERK levels at high cadaverine concentrations, consistent with the presence of several olfactory receptors that can detect cadaverine. However, at low concentrations an extremely sparse population of receptor neurons (0.3 cells per lamella, about 100 cells per olfactory rosette) is activated, corresponding to the lower limit of cell numbers found for individual olfactory receptor genes (cf. ref. 15). Moreover, the large majority of these cells expresses TAAR13c, consistent with this receptor being a major component of high affinity cadaverine detection. Further investigation, in particular TAAR13c loss-of-function analysis, will be required to delineate the exact role of TAAR13c in generating avoidance behavior to diamines.

The dose-dependence of cadaverine-evoked avoidance behaviors, c-Fos and pERK induction, and TAAR13c activation are all understandably different, because stimulus application, signal detection threshold, and signal/noise ratio are specific to each method. Receptor affinities can be much lower in heterologous systems than in vivo (28–30), where expression of receptors and signaling components are presumably optimized. Nevertheless, the threshold of cadaverine detection by TAAR13c of 3 μM is very similar to in vivo thresholds observed for the intact olfactory system (6, 31) and to thresholds measured for isolated olfactory sensory neurons (2). Although it is difficult to estimate naturally occurring cadaverine concentrations close to dead fish, the cadaverine concentration we measured in rotten zebrafish extracts was several orders of magnitude higher than the TAAR13c activation threshold, and presumably high enough to allow detection of that odor source from some distance. Importantly, the behavioral response in the two-choice assay is maximal at the same low concentration of cadaverine, which elicits neuronal activity predominantly in TAAR13c-expressing cells. Thus, the available data are consistent with TAAR13c being a significant part of the receptor repertoire that detects cadaverine present in ecologically relevant sources.

TAAR13c arose during teleost evolution and orthologs are not found in rodents and humans who also detect cadaverine. Thus, cadaverine-activated olfactory receptors in mammals may present a case of convergent evolution, either within the vertebrate TAAR family or between different olfactory receptor families (cf. ref. 27). In vitro studies did not identify a high-affinity cadaverine receptor among mouse, rat, or human TAARs (18), although cadaverine reportedly activates TAAR-containing glomeruli in mice at high concentrations (8). Other mammalian TAARs also detect aversive amines; for example, isoamylamine (TAAR3) and 2-phenylethylamine (TAAR4), both likewise

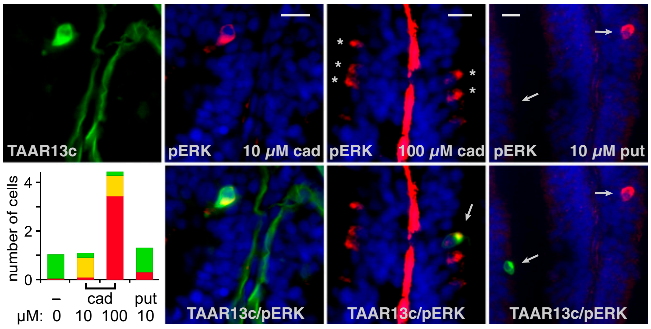

Fig. 5. Cadaverine activates TAAR13c-expressing neurons. Zebrafish were exposed to cadaverine (cad) and putrescine (put) at concentrations indicated and processed for concomitant IHC of TAAR13c (green fluorescence) and pERK (red fluorescence). DAPI was used as nuclear counterstain (blue). Sometimes the basal lamina was stained unspecifically (green and red stripes in the center of some lamellae). Asterisks, pERK^{+} cells; arrows, colabeled cells (yellow) and pERK^{+}/TAAR13c^{-} cells (red). (Scale bars: 10 μm.) (*Lower Left*) Quantitative evaluation, values are given as normalized cell numbers (120–250 cells per condition were analyzed); green bar, TAAR13c^{+}/pERK^{-} cells; yellow bar, double label; red bar, TAAR13c^{-}/pERK^{+} cells.

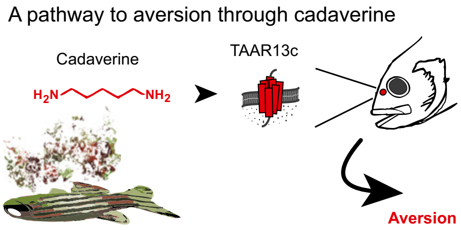

- Zebrafish olfactory receptor TAAR13c is a cadaverine receptor
- TAAR13c prefers odd-numbered, medium length diamines
- Decaying fish extracts activate TAAR13c due to cadaverine
- Cadaverine activates TAAR13c-expressing olfactory receptor neurons
- Cadaverine triggers innate avoidance behavior in zebrafish.

Fig. 6. Graphical summary of key findings.

produced by decarboxylation of amino acids (16, 18, 19, 32). Indeed, amines are an odor group that is chemically suited both to aquatic and airborne detection. Interestingly, trimethylamine, a TAAR5 agonist, is an aversive odor to humans and rats (20, 33) but attractive to mice (20). This finding is reminiscent of cadaverine, which is attractive to goldfish (2) but aversive to zebrafish (present results).

Taking these data together, we have shown that TAAR13c emerges as a sensitive olfactory receptor for the death-associated odor cadaverine, both in isolation and as part of a complex mixture. Cadaverine at low concentrations activates a sparse population of TAAR13c-expressing olfactory sensory neurons and elicits powerful and innate avoidance behavior in zebrafish, a vertebrate model system. See Fig. 6 for a graphical summary of key findings. Such an association of odors and cognate receptors with a powerful avoidance response provides a molecular basis for studying neural circuits connecting sensation with perception of odor valence.

Materials and Methods

TAAR Cloning. TAAR13c cDNA (National Center for Biotechnology Information accession no. NM_001083040.1) was cloned from zebrafish genomic DNA using standard methods. For other clones, primer, and vector information, see *SI Materials and Methods*.

TAAR Phylogenetic Analysis. The TAAR gene dataset was from ref. 17. For algorithms used, see *SI Materials and Methods*.

TAAR Functional Assays. The reporter assay was performed as described previously (16). Details for assay and receptor sequences are provided in *SI Materials and Methods*.

Antibody Generation. A unique peptide of 16 amino acids served as immunogen for TAAR13c. Details are provided in *SI Materials and Methods*.

Western Blot. The Western blot was performed as described previously (34). Details are provided in *SI Materials and Methods*.

Immunohistochemistry. Standard procedures were used. Protocols are provided in *SI Materials and Methods*.

Immunohistochemistry Combined with in Situ Hybridization. In situ hybridizaiton-IHC was performed as described previously (35). Protocols and details for antibody and probe are supplied in *SI Materials and Methods*.

Behavioral Analysis. Fish motion was tracked pre- and poststimulus addition. Two set-ups were used: single arena and two channel. Details of set-ups and analysis are provided in *SI Materials and Methods*.

Quantitative LC/MS Analysis of Diamines. Protocols for sample preparation, processing, and analysis are provided in *SI Materials and Methods*.

ACKNOWLEDGMENTS. We thank Walter Nadler for help with programming; Yuichiro Oka for critical review of the manuscript; Wayne Korzan, Matthias Gruhn, and Kim Korsching for technical advice; Jamie Lemon and Priyanka Maity for technical support; and Ansgar Bueschges for housing our behavioral set-up. This work was supported by Deutsche Forschungsgemeinschaft Award KO-1046/3 (to S.I.K.); an International Graduate School in Genetics and Functional Genomics stipend (to A.H. and L.R.S.); an International Graduate School in Development Health and Disease stipend (to G.A.); a Boehringer Ingelheim travel grant (to L.R.S.); and a grant (Award Number R01DC010155) from the National Institute on Deafness and Other Communicative Disorders (to S.D.L.).

1. Heale VR, Petersen K, Vanderwolf CH (1996) Effect of colchicine-induced cell loss in the dentate gyrus and Ammon's horn on the olfactory control of feeding in rats. *Brain Res* 712(2):213–220.
2. Rolen SH, Sorensen PW, Mattson D, Caprio J (2003) Polyamines as olfactory stimuli in the goldfish *Carassius auratus*. *J Exp Biol* 206(Pt 10):1683–1696.
3. Hamana K, Matsuzaki S (1984) Unusual polyamines in slime molds Physarum polycephalum and *Dictyostelium discoideum*. *J Biochem* 95(4):1105–1110.
4. Burger BV, et al. (2008) Chemical characterization of territorial marking fluid of male Bengal tiger, *Panthera tigris*. *J Chem Ecol* 34(5):659–671.
5. Pinel JP, Gorzalka BB, Ladak F (1981) Cadaverine and putrescine initiate the burial of dead conspecifics by rats. *Physiol Behav* 27(5):819–824.
6. Michel WC, Sanderson MJ, Olson JK, Lipschitz DL (2003) Evidence of a novel transduction pathway mediating detection of polyamines by the zebrafish olfactory system. *J Exp Biol* 206(Pt 10):1697–1706.
7. Nara K, Saraiva LR, Ye X, Buck LB (2011) A large-scale analysis of odor coding in the olfactory epithelium. *J Neurosci* 31(25):9179–9191.
8. Pacifico R, Dewan A, Cawley D, Guo C, Bozza T (2012) An olfactory subsystem that mediates high-sensitivity detection of volatile amines. *Cell Rep* 2(1):76–88.
9. Yoshihara Y (2009) Molecular genetic dissection of the zebrafish olfactory system. *Results Probl Cell Differ* 47:97–120.
10. Lieschke GJ, Currie PD (2007) Animal models of human disease: Zebrafish swim into view. *Nat Rev Genet* 8(5):353–367.
11. Gerlach G, Atema J, Kingsford MJ, Black KP, Miller-Sims V (2007) Smelling home can prevent dispersal of reef fish larvae. *Proc Natl Acad Sci USA* 104(3):858–863.
12. Guthrie KM, Anderson AJ, Leon M, Gall C (1993) Odor-induced increases in c-fos mRNA expression reveal an anatomical "unit" for odor processing in olfactory bulb. *Proc Natl Acad Sci USA* 90(8):3329–3333.
13. Mirich JM, Illig KR, Brunjes PC (2004) Experience-dependent activation of extracellular signal-related kinase (ERK) in the olfactory bulb. *J Comp Neurol* 479(2):234–241.
14. Weth F, Nadler W, Korsching S (1996) Nested expression domains for odorant receptors in zebrafish olfactory epithelium. *Proc Natl Acad Sci USA* 93(23):13321–13326.
15. Sato Y, Miyasaka N, Yoshihara Y (2007) Hierarchical regulation of odorant receptor gene choice and subsequent axonal projection of olfactory sensory neurons in zebrafish. *J Neurosci* 27(7):1606–1615.
16. Liberles SD, Buck LB (2006) A second class of chemosensory receptors in the olfactory epithelium. *Nature* 442(7103):645–650.
17. Hussain A, Saraiva LR, Korsching SI (2009) Positive Darwinian selection and the birth of an olfactory receptor clade in teleosts. *Proc Natl Acad Sci USA* 106(11):4313–4318.
18. Ferrero DM, et al. (2012) Agonists for 13 trace amine-associated receptors provide insight into the molecular basis of odor selectivity. *ACS Chem Biol* 7(7):1184–1189.
19. Ferrero DM, et al. (2011) Detection and avoidance of a carnivore odor by prey. *Proc Natl Acad Sci USA* 108(27):11235–11240.
20. Li Q, et al. (2013) Synchronous evolution of an odor biosynthesis pathway and behavioral response. *Curr Biol* 23(1):11–20.
21. Huang ES (2003) Construction of a sequence motif characteristic of aminergic G protein-coupled receptors. *Protein Sci* 12(7):1360–1367.
22. Mietz JL, Karmas E (1978) Polyamine and histamine content of rockfish, salmon, lobster, and shrimp as an indicator of decomposition. *J Assoc Off Anal Chem* 61(1):139–145.
23. Mori K, Sakano H (2011) How is the olfactory map formed and interpreted in the mammalian brain? *Annu Rev Neurosci* 34:467–499.
24. Speca DJ, et al. (1999) Functional identification of a goldfish odorant receptor. *Neuron* 23(3):487–498.
25. Demaria S, et al. (2013) Role of a ubiquitously expressed receptor in the vertebrate olfactory system. *J Neurosci* 33(38):15235–15247.
26. Fuss SH, Korsching SI (2001) Odorant feature detection: Activity mapping of structure response relationships in the zebrafish olfactory bulb. *J Neurosci* 21(21):8396–8407.
27. Saito H, Chi Q, Zhuang H, Matsunami H, Mainland JD (2009) Odor coding by a mammalian receptor repertoire. *Sci Signal* 2(60):ra9.
28. Mombaerts P (2004) Genes and ligands for odorant, vomeronasal and taste receptors. *Nat Rev Neurosci* 5(4):263–278.
29. Oka Y, et al. (2006) Odorant receptor map in the mouse olfactory bulb: In vivo sensitivity and specificity of receptor-defined glomeruli. *Neuron* 52(5):857–869.
30. Krautwurst D, Yau KW, Reed RR (1998) Identification of ligands for olfactory receptors by functional expression of a receptor library. *Cell* 95(7):917–926.
31. Friedrich RW, Korsching SI (1997) Combinatorial and chemotopic odorant coding in the zebrafish olfactory bulb visualized by optical imaging. *Neuron* 18(5):737–752.
32. Kobayakawa K, et al. (2007) Innate versus learned odour processing in the mouse olfactory bulb. *Nature* 450(7169):503–508.
33. Mitchell SC, Smith RL (2001) Trimethylaminuria: The fish malodor syndrome. *Drug Metab Dispos* 29(4 Pt 2):517–521.
34. Ahuja G, et al. (2013) Zebrafish crypt neurons project to a single, identified mediodorsal glomerulus. *Sci Rep* 3:2063.
35. Oka Y, Saraiva LR, Korsching SI (2012) Crypt neurons express a single V1R-related ora gene. *Chem Senses* 37(3):219–227.

Supporting Information

Hussain et al. 10.1073/pnas.1318596110

SI Materials and Methods

Trace Amine-Associated Receptor Cloning. Trace amine-associated receptor (TAAR)13c cDNA (National Center for Biotechnology Information accession no. NM_001083040.1) was amplified from zebrafish genomic DNA using specific PCR primers with flanking restriction sites NotI (5′) and EcoRI (3′):

5′: ATTTGCGGCCGCCATGGATTTATCATCACAAGAA,

3′: CCGGAATTCTCAAACCGTAAATAAATTGAT.

The PCR product was digested with NotI and EcoRI, and ligated into pcDNA3.1(-) expression vectors with or without a sequence encoding the first 20 amino acids of bovine rhodopsin (1, 2). The construct without the rhodopsin tag did not show any activity in the functional assays, presumably because of inefficient transport to the plasma membrane.

Other genes used in this study were TAAR1 (NM_001082904), TAAR10 (NM_001083038.2), TAAR11 (NM_001083077), TAAR12f (NM_001082907), TAAR13a (NW_001878149), TAAR13b (NM_001083042), TAAR13d (NM_001083041), TAAR15a (NM_001083039), TAAR16c (NW_001877318), and TAAR20t (NW_001877075.3). For phylogenetic position of genes, see Fig. 3.

TAAR Phylogenetic Analysis. A phylogenetic tree for *taar* genes was constructed using a modified maximum-likelihood method (PhyML-aLRT) with SPR setting for tree optimization and χ^2-based aLRT for branch support (3), and rendered using Treedyn (4). The gene set and alignment algorithm were as described previously (5), but only three mammalian species were included (mouse, rat, human).

TAAR Functional Assays. TAAR13c receptor activation was measured in a heterologous expression using a previously established cAMP-dependent assay (1). Half-maximal response (EC_{50}) values were determined within the concentration range of 0.3 μM to 1 mM, using a four parameter sigmoidal fit (6), and represent averages from four to six independent experiments, with individual values weighted by the variance of the respective curve fits. SE and degrees-of-freedom are calculated as appropriate for weighted averages. Fish extracts were prepared as described below for HPLC analysis. Expected responses for cadaverine and putrescine within fish extract were calculated using the sigmoidal regression curves obtained above.

Antibody Generation. We used a unique peptide consisting of 16 amino acids (NP_001076509.1, amino acids sequence from 234 to 249) as immunogen for TAAR13c (Fig. S1). Identity to other TAAR13 family members was in the range of 62–81%. Peptide synthesis and polyclonal antibody production (rabbit) were performed by Innovagen. Specificity of the antibody was established by Western blot with extracts from different tissues and competition with 10-fold molar excess of peptide immunogen (Fig. S1).

Western Blot. The Western blot with the adult zebrafish organs was performed as described previously (7). After the blocking step, the membrane was incubated with anti-TAAR13c antibody (1:100) or anti-pERK antibody (1:500) in blocking solution overnight at 4 °C. For the peptide competition assay, the anti-TAAR13c antibody was preincubated overnight at 4 °C with 10-fold molar access of immunization peptide. After three washes for 5 min each in PBST, the membrane was incubated in secondary antibody (1:5,000) for 1 h at room temperature. After three rinses in PBST, ECL reagent from Amersham (RPN2132) or Thermo Scientific (No. 34096) was used for developing the blot.

Immunohistochemistry. Individual zebrafish were placed in 20–30 mL of tank water in a 50-mL falcon tube and exposed to food odor, nothing, or diamine concentrations between 0.2 μM and 5 mM for 1 h (c-Fos) or 2–5 min (pERK) at room temperature. Fish were kept in a separate area to avoid any visual or physical stimuli and care was taken to minimize stress because of handling. After 1 h, fish were quickly killed by decapitation, the olfactory epithelium was dissected, and 8- to 10-μm fresh-frozen sections were obtained. Sections were fixed in 4% (wt/vol) PFA for 3–10 min at room temperature, washed three times for 10 min each in PBS 1× (pH 7.5), dried by incubation in acetone for 15 min at −20 °C, washed again three times for 5 min in PBST (PBS + 0.1% Triton-X100) and blocked in 5% normal goat serum in PBST for at least 1 h at room temperature. The tissue was then incubated with primary antibody (rabbit polyclonal anti–c-Fos antibody K-25, 1: 200 dilution, Santa Cruz or mouse anti-pERK antibody, 1:100 dilution, Cell Signaling) in blocking solution overnight at 4 °C. After extensive washing in PBST (3× 10 min), the sections were incubated with 1:200 dilution of secondary goat antibodies (anti-rabbit antibodies coupled to Alexa-488,A11008, Invitrogen or Alexa-594, A11037, Invitrogen or anti-mouse antibodies coupled to Alexa-594, Invitrogen, A11005) in PBST for 2 h at room temperature. Sections were washed three times with PBST, incubated with DAPI or 1:1,000 dilution of propidium iodide (Sigma-Aldrich) for 30 min in the dark at room temperature, washed three times with PBST, mounted, and embedded in Vectashield (Vector). Nuclear localization of c-Fos was established by costaining with propidium iodide, and the frequency of immunopositive nuclei was determined by randomized evaluation. Some pERK experiments were evaluated without randomization, and results of these analyses were not distinguishable from those of randomized evaluation.

Immunohistochemistry Combined with in Situ Hybridization. *Taar13c* cRNA riboprobe (bases 1–601) was prepared using standard methods. Pretreatment of sections, probe hybridization, and stringent washing were performed as described previously (8), except that Proteinase K treatment was omitted. For high stringency conditions the final washes were performed at 65 °C in 0.2× SSC, and for low stringency salt concentration was raised to 0.7× SSC. Afterward, sections were blocked in 1% blocking reagent (Roche) in PBS for 1 h. The slides were then incubated with sheep anti-DIG Fab fragments conjugated with alkaline phosphatase (AP, Roche; 1:200) together with rabbit anti-Taar13c antibody (1:100) in the blocking solution at 4 °C overnight. After washing three times in PBS, sections were treated with the secondary antibody (1:200) in PBS for 2 h at room temperature. Hybridized probes were visualized by enzymatic reaction of AP with HNPP Fluorescent Detection Set (Roche). After evaluating the success of the staining, slides were washed in PBS, mounted with VectaShield with DAPI (Vector), and observed and photographed with a fluorescent microscope (BZ-9000, Keyence).

Behavioral Analysis. Individual adult zebrafish between 6 and 12 mo of age (Ab/Tü strain) were tested 2 h after feeding and in the light phase of the diurnal cycle. For generation of transiently anosmic fish, both nostrils were glued with Histoacryl (Braun) and the fishes were allowed a resting period of 24 h before being tested. Anosmic fish showed normal motility ($P = 0.71$, $n = 6$). Before the test, fish were habituated for 45 min to an elongated tank (10× 100 cm, 9 L fresh filtered water). Fish movements were video recorded (30 frames per second) from above for 5 min before and after stimulus addition (180 μL odor or tank water as control) by an experimenter not visible to the fish. In initial experiments stimulus diffusion was examined by addition of dye, which spread to about one-quarter of the tank after 5 min. The 5-min trial period covers most of the observed avoidance behavior and was therefore chosen for quantification.

Fish movements were tracked using WINANALYZE automated motion tracker (www.winanalyze.com) (9), and the tracking was visually monitored. Distance to stimulus application site, velocity, and angular movement were visualized as histogram and as function of time, as well as averaged over time, using Excel (Microsoft) and OpenOffice (Apache). Total track length and the spatial patterns of tracks showed great intertrial and interfish variability, but were mostly very similar between the two 5-min periods of control experiments (Table S1). Distance relative to the odor source was determined for each frame and averaged separately before and after stimulus addition. Mean displacement was calculated as a difference of average location and expressed as percent of total tank length (TL). It should be noted that the maximal possible displacement starting from a random track is equivalent to 0.5 TL. Significance was evaluated by Student *t* test (two-sided, unpaired).

Close approach to the site of stimulus application was defined as distances smaller than 5% TL and time spent in close approach was measured as number of video frames fulfilling this criterion. For intertrial comparison, the difference of such frames before and after stimulus addition was calculated and normalized to the number of frames before stimulus addition. Significance was evaluated by Student *t* test (two-sided, unpaired).

Intertrial times of 1 to 2 h led to severely impaired evasive behavior in the subsequent trial. Thus, the minimal intertrial time period was set to 2 d, and no adaptation was observed under these conditions. Stimuli were applied in random order. Fish food odor was prepared by incubating fish food in water [10% (wt/vol) Tetramin, 2 h] and removal of solid debris by centrifugation.

For some experiments zebrafish avoidance behavior was analyzed in a Y-shaped tank (10), with two separate inflow channels (each 5 × 13 cm) and a mixing zone (10 × 11 cm). In this set-up, a more stringent upper limit for the actual stimulus concentration encountered by the fish can be determined. The following modifications were made for these experiments: Fishes were kept unfed for 24 h, then individual fish were habituated to the set-up for at least 45 min. Flow rate was adjusted to 350 mL/min for each channel independently via pump. At this rate the fish investigated freely each channel as well as the mixing zone. In initial experiment dye was added to one channel, which gradually spread in the mixing zone, but never entered back into the other channel. Fish movements were recorded for 4 min before and after switching one channel to stimulus solution. To ensure that fish would actively sample both compartments during the test phase, we only evaluated experiments, for which the fish in the prestimulus phase spent at least 20% of their time in the lesser visited side. No consistent bias for one channel was observed. Fish movements were tracked using LoliTrack v3 automated motion tracker (www.loligosystems.com) (11) and the tracking was visually monitored. Time spent in each compartment was analyzed using Open Office (Apache) and the avoidance index was determined: $\mathrm{AI} = [(t_a - t_p)/(\mathrm{t_a} + \mathrm{t_p})_{\mathrm{cad.}} - (t_a - t_p)/(t_a + t_p)_{\mathrm{water}}]$, where t_a = prestimulus, t_p = stimulus period, $_{\mathrm{cad.}}$= cadaverine, and $_{\mathrm{water}}$ = water channel. The value range for AI is between 1 (complete aversion) and −1 (complete attraction), starting with random movement in the prestimulus period.

Quantitative LC/MS Analysis of Diamines. Adult zebrafish were killed, incubated in PBS (6.3 mL/g) for 0 min ("fresh") or 1 wk at room temperature ("rotten"), homogenized, and centrifuged to remove debris. Extracts were further diluted 100-fold in PBS and analyzed by LC/MS using a Luna C18 column (Phenomenex, 4.6 × 100 mm) on an Agilent 1200 HPLC instrument (Agilent Technologies). Samples were eluted using a linear gradient [0–60% (vol/vol)] of solvent A (acetonitrile plus 0.1% formic acid) in solvent B (water plus 0.1% formic acid). The samples were analyzed in tandem by mass spectroscopy on an Agilent 6130 Quadrupole LC/MS system (Agilent Technologies). The numbers of ion counts with the mass-charge ratio (m/z) corresponding to putrescine, cadaverine, diaminohexane, diaminoheptane, diaminooctane, agmatine, cystamine, histamine, and cysteamine were separately graphed over time and compared with internal standards for quantitation. The detection limit was 0.5 mM.

1. Liberles SD, Buck LB (2006) A second class of chemosensory receptors in the olfactory epithelium. *Nature* 442(7103):645–650.
2. Krautwurst D, Yau KW, Reed RR (1998) Identification of ligands for olfactory receptors by functional expression of a receptor library. *Cell* 95(7):917–926.
3. Guindon S, et al. (2010) New algorithms and methods to estimate maximum-likelihood phylogenies: Assessing the performance of PhyML 3.0. *Syst Biol* 59(3):307–321.
4. Chevenet F, Brun C, Bañuls AL, Jacq B, Christen R (2006) TreeDyn: Towards dynamic graphics and annotations for analyses of trees. *BMC Bioinformatics* 7:439.
5. Hussain A, Saraiva LR, Korsching SI (2009) Positive Darwinian selection and the birth of an olfactory receptor clade in teleosts. *Proc Natl Acad Sci USA* 106(11):4313–4318.
6. Williams T, Kelley C (1987) Gnuplot. Available at www.gnuplot.info. Accessed January 2, 2011.
7. Ahuja G, et al. (2013) Zebrafish crypt neurons project to a single, identified mediodorsal glomerulus. *Sci Rep* 3:2063.
8. Weth F, Nadler W, Korsching S (1996) Nested expression domains for odorant receptors in zebrafish olfactory epithelium. *Proc Natl Acad Sci USA* 93(23):13321–13326.
9. Neumeister H, Cellucci CJ, Rapp PE, Korn H, Faber DS (2004) Dynamical analysis reveals individuality of locomotion in goldfish. *J Exp Biol* 207(Pt 4):697–708.
10. Gerlach G, Atema J, Kingsford MJ, Black KP, Miller-Sims V (2007) Smelling home can prevent dispersal of reef fish larvae. *Proc Natl Acad Sci USA* 104(3):858–863.
11. Schack HB, Malte H, Madsen PT (2008) The responses of Atlantic cod (*Gadus morhua* L.) to ultrasound-emitting predators: stress, behavioural changes or debilitation? *J Exp Biol* 211(Pt 13):2079–2086.

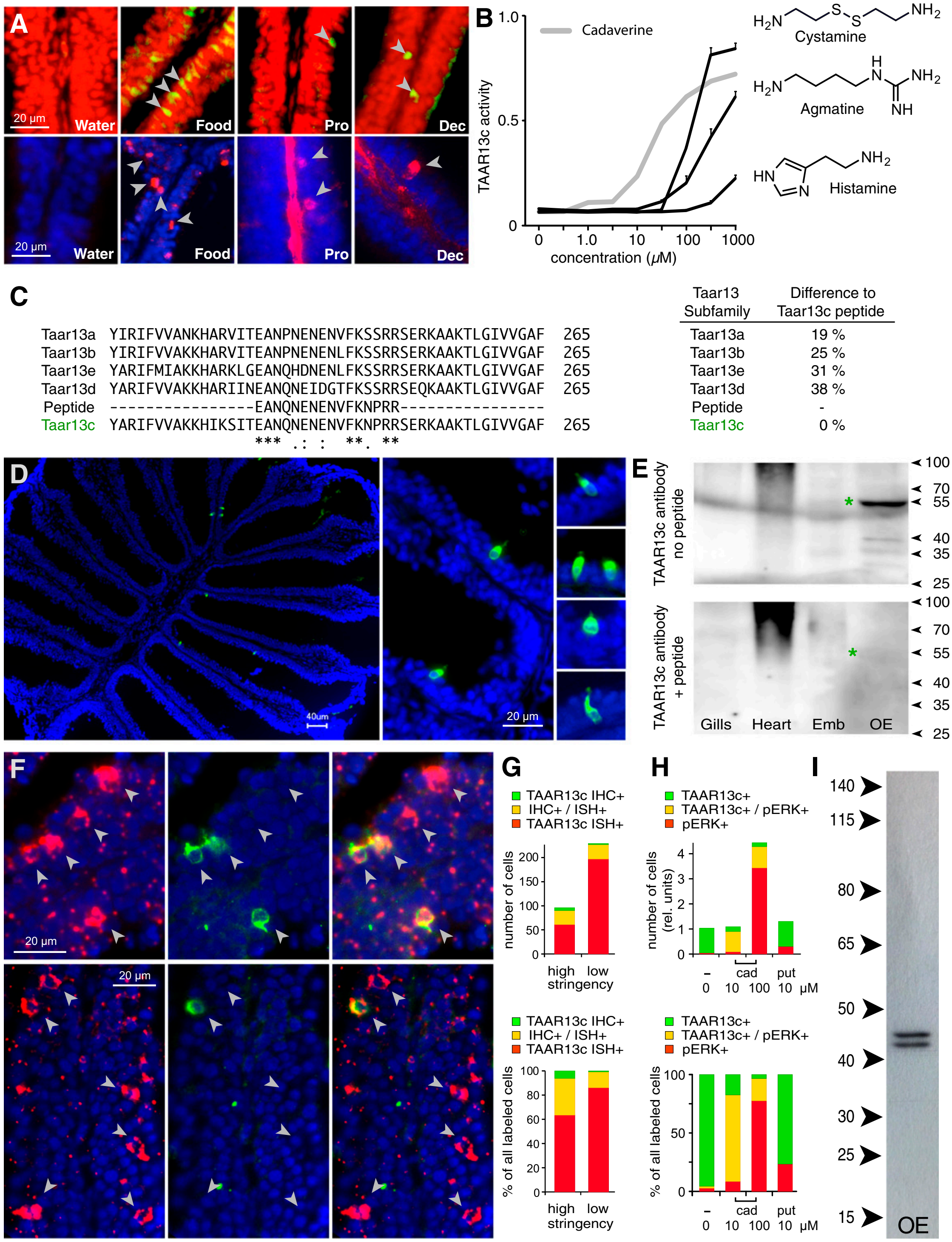
A
20 µm
Water
Food
Pro
Dec
20 µm
Water
Food
Pro
Dec
B
1.0
0.5
0
TAAR13c activity
Cadaverine
0
1.0
10
100
1000
concentration (µM)
H_2N Cystamine NH_2
Agmatine
Histamine
C
Taar13a YIRIFVVANKHARVITEANPNENENVFKSSRRSERKAAKTLGIVVGAF 265
Taar13b YIRIFVVAKKHARVITEANPNENENLFKSSRRSERKAAKTLGIVVGAF 265
Taar13e YARIFMIAKKHARKLGEANQHDNENLFKSSRRSERKAAKTLGIVVGAF 265
Taar13d YARIFVVAKKHARIINEANQNEIDGTFKSSRRSEQKAAKTLGIVVGAF 265
Peptide ----------------EANQNENENVFKNPRR---------------
Taar13c YARIFVVAKKHIKSITEANQNENENVFKNPRRSERKAAKTLGIVVGAF 265
*** .: : **. **
Taar13 Subfamily
Difference to Taar13c peptide
Taar13a 19 %
Taar13b 25 %
Taar13e 31 %
Taar13d 38 %
Peptide -
Taar13c 0 %
D
40um
20 µm
E
TAAR13c antibody no peptide
TAAR13c antibody + peptide
100
70
55
40
35
25
Gills
Heart
Emb
OE
F
20 µm
20 µm
G
TAAR13c IHC+
IHC+ / ISH+
TAAR13c ISH+
number of cells
200
150
100
50
0
high
low
stringency
% of all labeled cells
100
80
60
40
20
0
high
low
stringency
H
TAAR13c+
TAAR13c+ / pERK+
pERK+
number of cells (rel. units)
4
3
2
1
0
–
cad
put
0
10
100
10 µM
% of all labeled cells
100
50
0
I
140
115
80
65
50
40
30
25
15
OE

Fig. S1. Additional data. (*A*) Diamines elicit c-Fos and pERK increase in olfactory sensory neurons. (*Upper*) Zebrafish ($n = 12$) were exposed to stimuli indicated (2 or 5 mM for diamines). c-Fos immunohistochemistry (green) and nuclear staining (propidium iodide, red), enabled visualization of c-Fos$^+$ nuclei (yellow), some emphasized by gray arrow heads. (*Lower*) Zebrafish ($n = 8$) were exposed to stimuli indicated (1 mM). Some pERK-labeled cells (red) are emphasized by gray arrow heads; nuclear counterstain (DAPI, blue). Red central stripes in some panels, unspecific label in the basal lamina outside the sensory region. (*B*) Dose-dependent activation of TAAR13c by dibasic ligands cystamine, agmatine, and histamine. HEK293 cells were transfected with TAAR13c plasmid and a reporter gene, incubated with chemicals at concentrations indicated, and assayed for reporter gene activity. Values are in relative units. A representative experiment is shown ($n = 3 \pm$ SEM). No responses to diamines were observed in cells transfected with reporter gene alone. Only activation by cystamine is saturable. For comparison, the dose–response curve of cadaverine is shown (gray). (*C*) Sequence alignment of the peptide sequence used for the generation of TAAR13c antibody with the corresponding segments from the four other members of the TAAR13 subfamily. Difference to the peptide sequence is shown as percentage (*Right*). (*D*) Anti-TAAR13c antibody labels a sparse population of olfactory sensory neurons (green) in horizontal sections of olfactory epithelium. (*Left*) A complete horizontal section contains only six TAAR13c$^+$ olfactory sensory neurons; (*Center* and *Right*) TAAR13c$^+$ cells at higher magnifications. Counterstain by DAPI (blue). (*E*) Western blot analysis of protein extracts from gills, heart, 5 d postferitilization embryo (Emb), and olfactory epithelium (OE), using anti-

Legend continued on following page

TAAR13c antibody. (*Upper*) The antibody recognizes a specific protein with apparent molecular weight of 55 kDa in the olfactory extract lane; (*Lower*) no such band was observed after preincubation of anti-TAAR13c antibody with 10× molar excess of peptide. Note that the high molecular weight band in heart (absent in OE) is not eliminated by preincubation with peptide. Arrowheads, molecular weight of reference proteins in kilodaltons. (*F* and *G*) Concomitant immunohistochemical detection of TAAR13c (green fluorescence) and Taar13c riboprobe (red fluorescence) in zebrafish olfactory rosettes. DAPI was used as nuclear counterstain (blue). Washes were performed at low (0.7× SSC, 65 °C) and high stringency (0.2× SSC, 65 °C). Quantification of these results is shown in *G*. Color code as indicated; ISH, in situ hybridization; IHC, immunohistochemistry. Several-fold more cells are labeled by the Taar13c riboprobe at low stringency (*Upper*), resulting in a smaller percentage of all labeled cells for the double-labeled neurons (*Lower*). (*H*) Quantification of TAAR13c/pERK colocalization. Zebrafish were exposed to cadaverine (cad) and putrescine (put) at concentrations indicated and processed for concomitant immunohistochemical detection of TAAR13c and pERK. Results were quantified, color code as indicated. (*Upper*) Number of cells normalized per TAAR13c^{+} cell; (*Lower*) cell populations are expressed as percent of all labeled cells. (*I*) Western blot analysis of protein extract from OE, using anti-pERK antibody. The antibody recognizes two specific bands with molecular weight corresponding to pERK1 and pERK2. Arrowheads, molecular weight of reference proteins in kilodaltons.

Table S1. Odor-induced behavioral responses of zebrafish

Odor (1-mM stimulus)	Displacement[*] [(post − pre), TL], mean ± SEM	*P* value	Close approach[†] [(post − pre)/pre], mean ± SEM	*P* value[‡]	*P* value[§]	Track length ratio (post/pre)[¶]	*P* value
Water (negative control)	0.04 ± 0.04	—	−0.21 ± 0.35	NS	NA	0.91 ± 0.04	—
Food extract (positive control)	−0.25 ± 0.06	<0.01	3.6 ± 1.5	<0.05	NA	0.89 ± 0.07	0.76
1,3-Diaminopropane	−0.01 ± 0.01	NS	0.15 ± 0.36	NS	NA	0.99 ± 0.05	0.35
1,4-Diaminobutane (putrescine)	0.21 ± 0.04	<0.01	−0.66 ± 0.05	$<10^{-6}$	$<10^{-4}$	0.92 ± 0.08	0.88
1,5-Diaminopentane (cadaverine)	0.28 ± 0.05	<0.01	−0.84 ± 0.08	$<10^{-5}$	<0.03	1.14 ± 0.11	0.08
1,6-Diaminohexane	0.25 ± 0.03	<0.01	−0.72 ± 0.09	$<10^{-4}$	<0.01	1.01 ± 0.07	0.26
1,7-Diaminoheptane	0.20 ± 0.02	<0.01	−0.60 ± 0.06	$<10^{-6}$	<0.001	0.92 ± 0.07	0.91
1,8-Diaminooctane	0.17 ± 0.04	<0.05	−0.72 ± 0.11	$<10^{-4}$	<0.03	0.93 ± 0.04	0.74
1,10-Diaminodecane	−0.04 ± 0.05	NS	0.95 ± 0.93	NS	NA	0.95 ± 0.07	0.53

[*] Overall displacement of fish is quantified as (mean distance to odor source after stimulus addition) minus (mean distance to odor source before stimulus addition) and is expressed relative to tank length. Maximal possible displacement for fish with random movement before stimulus addition amounts to 0.5 TL; positive values correspond to avoidance. *P* value is for Student *t* test against water, NS, not significant.

[†] Close approach time is measured as number of video frames in which the fish approaches the stimulus application site closer than 5% of tank length. Normalized difference in close approach time is given as ([time in close approach post stimulus] − [time in close approach pre stimulus])/[time in close approach prestimulus]. Negative values indicate avoidance.

[‡] Significance for the difference between pre- and postclose approach time; *P* value determined by Student *t* test (two-sided).

[§] Significance for the difference between *post*-stimulus close approach time and zero close approach time (i.e., total avoidance); *P* value determined by Student *t* test (one-sided); NA, not applicable.

[¶] Fish track lengths were summarized over 9,000 frames (equals 5 min) before and after stimulus addition. Post/Pre ratios are shown, no significant change in track length and therefore velocity is seen. *P* values are determined by Student *t* test for the comparison with water (two-sided); none show significant differences.

Publication 4

Maik Behrens, Oliver Frank*, Harshadrai Rawel*, **Gaurav Ahuja*,** Christoph Potting, Thomas Hofmann, Wolfgang Meyerhof and Sigrun Korsching. *ORA1, a zebrafish olfactory receptor ancestral to all mammalian V1R genes, recognizes 4-hydroxyphenylacetic acid, a putative reproductive pheromone*. J Biol Chem.pii: jbc.M114.573162 (**2014**). *** Equal contribution**

http://www.jbc.org/content/early/2014/05/15/jbc.M114.573162

THE JOURNAL OF BIOLOGICAL CHEMISTRY VOL. 289, NO. 28, pp. 19778–19788, July 11, 2014
© 2014 by The American Society for Biochemistry and Molecular Biology, Inc. Published in the U.S.A.

ORA1, a Zebrafish Olfactory Receptor Ancestral to All Mammalian *V1R* Genes, Recognizes 4-Hydroxyphenylacetic Acid, a Putative Reproductive Pheromone

Received for publication, April 10, 2014 Published, JBC Papers in Press, May 15, 2014, DOI 10.1074/jbc.M114.573162

Maik Behrens[‡], Oliver Frank[§1], Harshadrai Rawel[¶1], Gaurav Ahuja[‖1], Christoph Potting[‖], Thomas Hofmann[§], Wolfgang Meyerhof[‡], and Sigrun Korsching[‖2]

From the [‡]Department of Molecular Genetics, German Institute of Human Nutrition Potsdam-Rehbruecke, Arthur-Scheunert-Allee 114-116, 14558 Nuthetal, the [§]Chair of Food Chemistry and Molecular Sensory Science, Technische Universität München, Lise-Meitner-Strasse 34, 85354 Freising, the [¶]Institute of Nutrition Science, University of Potsdam, Arthur-Scheunert-Allee 114-116, 14558 Nuthetal, and the [‖]Institute of Genetics, University at Cologne, Zülpicher Str. 47A, 50674 Cologne, Germany

Background: No ligands are known for any olfactory receptor of the *v1r*-related *ora* gene family.
Results: Zebrafish ORA1 recognizes with high sensitivity and specificity 4-hydroxyphenylacetic acid. This compound elicits oviposition behavior.
Conclusion: ORA1 was deorphanized with a ligand that may be a reproductive pheromone.
Significance: Pheromone reception conceivably might be the ancestral function of the *ora*/v1r family.

The teleost *v1r*-related *ora* genes are a small, highly conserved olfactory receptor gene family of only six genes, whose direct orthologues can be identified in lineages as far as that of cartilaginous fish. However, no ligands for fish olfactory receptor class A related genes (ORA) had been uncovered so far. Here we have deorphanized the ORA1 receptor using heterologous expression and calcium imaging. We report that zebrafish ORA1 recognizes with high specificity and sensitivity 4-hydroxyphenylacetic acid. The carboxyl group of this compound is required in a particular distance from the aromatic ring, whereas the hydroxyl group in the *para*-position is not essential, but strongly enhances the binding efficacy. Low concentrations of 4-hydroxyphenylacetic acid elicit increases in oviposition frequency in zebrafish mating pairs. This effect is abolished by naris closure. We hypothesize that 4-hydroxyphenylacetic acid might function as a pheromone for reproductive behavior in zebrafish. ORA1 is ancestral to mammalian V1Rs, and its putative function as pheromone receptor is reminiscent of the role of several mammalian V1Rs as pheromone receptors.

Pheromones play essential roles in many intraspecies communications, from mating preferences to control of aggression and individual recognition. Chemical signaling also occurs between species, *e.g.* for prey or predator detection. In mammals two large gene families are thought to be mainly responsible for detection of these signals, vomeronasal receptors type 1 and type 2 (V1R and V2R).[3] V2R receptors have been shown to recognize peptides (1, 2), whereas V1R ligands are found among low molecular weight molecules, such as steroids (Refs. 3 and 4, see also Ref. 5). We have recently shown that a small and highly conserved olfactory receptor gene family of just six *ora* genes (6) constitutes the ancestral repertoire, from which the large and dynamically evolving mammalian *v1r* families originate. All mammalian *v1r* genes are monophyletic with a single pair of *ora* genes, *ora1* and *ora2* (6), whose direct orthologues are present already in cartilaginous fish (7). In the light of such drastic differences in evolutionary characteristics for *v1r* and *v1r*-related *ora* genes it would be interesting to compare ORA ligands to those found for V1Rs. It is conceivable that ligands of the slowly evolving *ora* genes could be closer to those of ancestral *v1r* genes than the ligands of contemporary, rapidly evolving *v1r* genes themselves.

The zebrafish olfactory system is well characterized (Ref. 8 and references therein), and so we chose zebrafish *ora* genes for cloning and expression in a mammalian cell line. Activation of the receptors was analyzed by calcium imaging, using a variety of plausible assumptions as to potential ligands. Although none of these assumptions were borne out, eventually one led us on the track for a high affinity ligand of ORA1. We report the structure-activity tuning of ORA1, and show that the most effective ligand, 4-hydroxyphenylacetic acid, modulates reproductive behavior of zebrafish.

EXPERIMENTAL PROCEDURES

Cloning of Zebrafish ORA1 and ORA2 cDNA—*ora1* and *ora2* are monoexonic genes, whose full-length coding sequences were amplified from zebrafish genomic DNA, using the following primers: ORA1_FW 5′-TAGAATTCATGGACCT-GTGTGTCACCA-3′, ORA1_RV 5′-ATAGTTTAGCGGCCG-CCGTTCTTGCCGCTGGAGTT-3′, ORA2_FW 5′-CGGAATTCATGATTGCGGAGG-CTGTG-3′, ORA2_RV 5′-ATAGTTTAGCGGCCG-CCGTGCATGGTCTCTGGCTG-3′. Forward primers contain a 5′ EcoRI site and reverse primers contain a NotI site. After PCR amplification, reaction products were digested with EcoRI and NotI, and cloned into the EcoRI and NotI sites of the modified vector pcDNA5FRT PM (9), thereby adding an amino-terminal sst3 epitope to facilitate effi-

---

[1] These authors contributed equally to this article.

[2] To whom correspondence should be addressed. Tel.: 49-221-470-4843; Fax: 49-221-470-5172; E-mail: sigrun.korsching@uni-koeln.de.

[3] The abbreviations used are: V1R and V2R, vomeronasal 1 receptor and vomeronasal 2 receptor.

Downloaded from http://www.jbc.org/ at DEUTSCHE ZENTRALBIBLIOTHEK FUER MEDIZIN on November 13, 2014

cient cell surface localization and a carboxyl-terminal HSV (herpes simplex virus glycoprotein D) tag to enable immunological detection of the receptors.

Immunocytochemistry of ORA Constructs Transfected into HEK 293 Cells—Immunocytochemical detection of HEK 293T cells stably expressing the G protein-chimera Gα16gust44 was mainly done as described previously (10). Briefly, cells were seeded onto poly-D-lysine-coated glass coverslips in 24-well plates. Cells were transiently transfected with constructs coding for ORA1 or ORA2 using Lipofectamine 2000 (Invitrogen), and incubated for 24 h at 37 °C in 5% CO_2. Next, the cells were washed twice with PBS and placed for 30 min on ice to block endocytosis. For cell surface labeling biotinylated concanavalin A (Sigma) was applied at a dilution of 1:2,000 (1 h on ice). Repetitive washing with ice-cold PBS was followed by methanol/actone fixation (1:1 (v/v)) for 2 min. Following washing with PBS at room temperature, cells were incubated with 5% normal horse serum in PBS. Receptor proteins were detected with a 1:15,000 diluted anti-HSV antibody applied for 1 h at room temperature in blocking reagent (5% normal horse serum in PBS). Excess antibodies were removed by washing with PBS, before 1:2,000 diluted anti-mouse Alexa 488 and 1:1,000 diluted streptavidin Alexa 633 in PBS + 5% normal horse serum was applied for 1 h at room temperature. Finally, the glass coverslips were washed three times with PBS, once with deionized H_2O, and mounted with DAKO fluorescent mounting medium (DAKO). Images were taken by confocal laser scanning microscopy (Leica TCS SP2). For determination of expression rates 3 representative images per construct were taken and the number of green (= receptor expressing) and red (= total cell number) cells were counted.

Functional Calcium Imaging Experiments—The functional calcium imaging experiments were performed according to Ref. 10. Briefly, HEK 293T cells stably expressing the G protein-chimera Gα16gust44 were seeded onto 96-well plates coated with 10 μg/ml of poly-D-lysine. The next day cells were transiently transfected with ORA1, ORA2, or human bitter taste receptor TAS2R16 constructs using Lipofectamine 2000 (Invitrogen). After 24 h the cells were washed with buffer C1 (130 mM NaCl, 5 mM KCl, 10 mM Hepes, pH 7.4, 2 mM $CaCl_2$, 10 mM glucose), and loaded with the calcium-responsive dye Fluo-4 AM in the presence of 1 mM probenecide, an inhibitor of ABC transporter A1. To remove excessive fluorescence dye, cells were washed three times with buffer C1 and transferred into a fluorometric imaging plate reader (FLIPR, Molecular Devices) for measurement. Test substances were dissolved in C1 buffer and the changes in fluorescence after application of test substances were monitored. For the calculation of dose-response functions data from at least two independent experiments were obtained. For each experiment the signals of triplicate wells for each concentration were averaged and the corresponding fluorescence changes of mock-transfected cells were subtracted. Graphs and calculations of EC_{50} concentrations were performed using SigmaPlot. For the EC_{50} value determination nonlinear regression analysis was performed using the equation: $f(y) = (a - d)/1 + (x/EC_{50})^{nh} + d$.

Oxidation of L-Tyrosine and Related Compounds with Hydrogen Peroxide—To determine whether oxidative processes have resulted in the formation of agonistic compounds originating from "aged" L-tyrosine, we incubated candidate substances with hydrogen peroxide solution. 100 mg of freshly ordered L-tyrosine proved to be inactive on ORA1-transfected cells in functional calcium imaging experiments, as well as the same amount of L-dopamine and L-phenylalanine were mixed with 250 μl of 30% hydrogen peroxide solution (because of limited solubility 600 μl were used for L-phenylalanine) and incubated for several hours at room temperature. After this, the samples were subjected to brief centrifugation, the supernatants were diluted at least 10,000-fold and then taken for subsequent functional analyses. The remaining H_2O_2 (at most 1 mM or 0.003%) had no effect by itself.

HPLC Purification of Aged L-Tyrosine—Both analytical and preparative RP-HPLC of the samples was performed on a PRONTOSIL 120-3-C18, SC 150-ace-EPS column (150 × 4.6 mm, 3 μm; Bischoff Analysentechnik und -geraete GmbH, Leonberg, Germany) using a flow rate of 0.8 ml/min, UV detection at 280 nm, and a column temperature of 25 °C with a JASCO (Labor und Datentechnik GmbH, Gross-Umstadt, Germany) chromatographic system. The separation is based on the hydrophobic interactions of the analytes with the reverse phase filling of the column. A distilled water (acidified with 2% acetic acid; v/v)/methanol gradient was applied under the following conditions: 0–20% methanol, 2 min; 20–35% methanol, 18 min; 35–68% methanol, 2 min; 68% methanol, 3 min; 0–68% methanol, 3 min; 0% methanol, 12 min (regeneration/equilibration). The tyrosine samples (10 mg/ml) were dissolved in distilled water. The concentration was decreased in case of analytical HPLC. The injection volume of the samples was 10–20 μl. Altogether 10 fractions were collected. Fraction 2 was identified to contain pure tyrosine using an external standard and HPLC-MS (Shimadzu chromatographic LC-10 system equipped with a mass spectrometer LC-MS 2010 EV, Kyoto, Japan; MS conditions were as follows: Interface ESI, CDL temperature/heating block = 230 °C, nebulizing gas flow = 1.5 ml/min; detector voltage = 1.7 kV; interface voltage = 4.5 V; CDL voltage = 0. = V; Q-array voltage, DC = 20–30V, R_F = 85–125 V; scan modus, event time = 0.8 s, m/z = 120–550) performed under the same separation conditions as described above. The compound in fraction 6 could not be ionized under the applied MS conditions. The total peak area of the fractions was used to estimate the amount in fractions 2 and 6 using an external tyrosine standard. The relative composition was determined to be 67.6 and 5.2%, respectively.

Nuclear Magnetic Resonance (NMR) Spectroscopy—One- and two-dimensional ^1H and ^{13}C NMR spectra were acquired on a 500 MHz Avance III spectrometer (Bruker, Rheinstetten, Germany), respectively. Dimethyl sulfoxide-d_6 MeOD (9:1, v/v) was used as solvent and chemical shifts are reported in parts per million relative to the solvent signal. Homo- and heteronuclear correlation experiments were carried out using the pulse sequences taken from the Bruker software library. Data processing was performed by using TopSpin (2.1; Bruker, Rheinstetten, Germany) as well as Mestre-C (Mestrelab Research, A Coruña, Spain).

Downloaded from http://www.jbc.org/ at DEUTSCHE ZENTRALBIBLIOTHEK FUER MEDIZIN on November 13, 2014

Behavioral Assays—Analysis of aversion or attraction was performed as described (11). Individual adult zebrafish (Ab/Tü strain, 6 – 8 months old) were tested in an elongated tank (10 × 100 cm, 9 liters fresh filtered water) after 45 min of habituation. Fish movements were video recorded (30 frames/second) from the side for 5 min before and after stimulus addition (180 μl of odor or tank water as control) by an experimenter not visible to the fish. Fish movements were video recorded for 5 min before and after stimulus addition (180 μl of 1 mM 4-hydroxyphenylacetic acid or water) and tracked using LoliTrack version 3 automated motion tracker (12). Distance to the odor source and velocity were determined using Open Office (Apache). Mean displacement was calculated as a difference of average location and expressed as percent of total tank length. Significance was evaluated by Student's *t* test (two-sided, unpaired).

To examine oviposition (egg laying), zebrafish were kept gender-separated for 1–2 weeks prior to the experiment. In the evening preceding the experiment the breeding pairs were gently transferred to breeding tanks (20 × 10 cm, 600 ml of water), with female and male separated by a translucent divider. The next morning, one-half hour into the light cycle the divider was removed allowing the fish free movement. Pairs without eggs after the 90-min contact time were then supplemented with various concentrations of 4-hydroxyphenylacetic acid in 10 mM Tris, pH 7.4, or with buffer alone. The pairs were monitored for the presence of eggs 90 min after the stimulus. For generation of transiently anosmic fish, both nostrils were glued with Histoacryl® (Braun) and the fish were allowed a resting period of 24 h before being tested. Anosmic fish showed normal motility. Significance was estimated by χ-square analysis.

RESULTS

ORA1 and ORA2 Are Efficiently Expressed and Localize to the Plasma Membrane—We have chosen zebrafish as the species to search for ORA1/ORA2 agonists, because in this species the expression of all *ora* family members in olfactory sensory neurons has been shown (6). For heterologous expression we selected a system that has been very efficient for functional expression of bitter taste receptors (13), which are the closest homologues of the *ora/v1r* family (6). In short, the full-length receptor sequence is fused to an N-terminal sst3 tag serving as signal sequence (14) and a C-terminal hsv-epitope to enable detection (15). The constructs were transiently expressed in HEK 293T cells stably transfected with the broadly reactive G protein, Gα16gust44 (16, 17). G protein-coupled chemoreceptors are sometimes poorly transported to the plasma membrane in heterologous systems (see Refs. 18 –20), and we therefore analyzed the intracellular distribution of ORA1/ORA2 by immunocytochemical detection. The receptors were visualized using an antibody against the C-terminal hsv-epitope and the cell surface was stained by concanavalin A, which serves both as general cell marker and as label for plasma membrane (for details see "Experimental Procedures").

Both ORA receptors are robustly and reproducibly expressed. Nearly two-thirds of all cells express each receptor (Fig. 1*A*), and a large fraction of the expressed protein appears to be localized at the level of the plasma membrane as seen by the superposition of the receptor signals with those of the cell surface label (Fig. 1*A*). Thus, an essential prerequisite for functional characterization is fulfilled for both ORA1 and ORA2.

ORA1 but Not ORA2 Reacts to a Mixture of Amino Acids—Previous studies have demonstrated that amino acids and pheromones represent preferred olfactory stimuli for fish (21–23). We have tested both types of potential ligands, using as positive control cells expressing the bitter taste receptor TAS2R16 stimulated with the bitter compound D-(−)-salicin (9). None of the pheromones tested, among them those known to activate some zebrafish glomeruli (21), could activate either ORA1 or ORA2 (Table 1).

In contrast, the mixture of all 20 proteinogenic L-amino acids elicited a strong calcium signal for ORA1-transfected cells at 1 mM concentration per amino acid with a time course resembling that of the positive control (Fig. 1*B*). Stimulation of transfected cells with buffer alone had no effect, and likewise stimulation of mock-transfected cells (empty expression vector) with the full 20 amino acid mixture elicited no response (Fig. 1*B*). Thus the signal obtained for ORA1 appears to be a specific receptor-mediated response to the amino acid mixture. Ora2-transfected cells were not activated by the mixture (Fig. 1*B*).

ORA1 Activation Is Caused by a L-Tyrosine Contaminant—To identify which of the 20 L-amino acids are able to activate ORA1, we next separately used each of the amino acids at the same concentration (1 mM) (Fig. 1*C*). Only one amino acid, tyrosine, mimicked the response elicited by the mixture of amino acids, whereas the other 19 amino acids had no effect (Fig. 1*C*), suggesting that ORA1 activation in the previous experiment had been solely due to the presence of the L-tyrosine reagent.

However, when we attempted to validate this result using other lots of tyrosine we did not observe any activation of ORA1 (Fig. 2*A*). This excludes L-tyrosine as ligand and suggests a contaminant as the active compound. Because the first, active lot had aged for a prolonged period at +4 °C and indeed exhibited an off-color, we suspected contamination by some degradation product as the active ingredient, which presumably was only present in trace amounts and therefore likely to be a high potency agonist.

The Active Compound Is Generated by Oxidation of Tyrosine—We first examined whether the active ingredient might have formed by oxidation of tyrosine, a process expected to happen upon prolonged storage. We reacted fresh L-tyrosine with 30% hydrogen peroxide and tested the reaction product at different dilutions. Indeed, even at 1:10,000 dilution a strong signal was generated, similar to the signal elicited by the aged tyrosine lot (Fig. 2*A*), and in stark contrast to the complete inability of the fresh tyrosine itself to activate ORA1 (Fig. 2*A*). When the closely related substances L-dopamine and L-phenylalanine were subjected to the same oxidation procedure, no response was elicited either for the fresh (Table 1) or the oxidized compounds (Fig. 2*A*). Furthermore, hydrogen peroxide by itself had no effect (Fig. 2*A*). The outcome of this experiment suggested that the active substance in the aged L-tyrosine indeed originated from oxidation of L-tyrosine.

Purification and Identification of the Active Compound by HPLC and LC-MS—To identify the active compound or compounds, we first performed an analytical HPLC separation of

Downloaded from http://www.jbc.org/ at DEUTSCHE ZENTRALBIBLIOTHEK FUER MEDIZIN on November 13, 2014

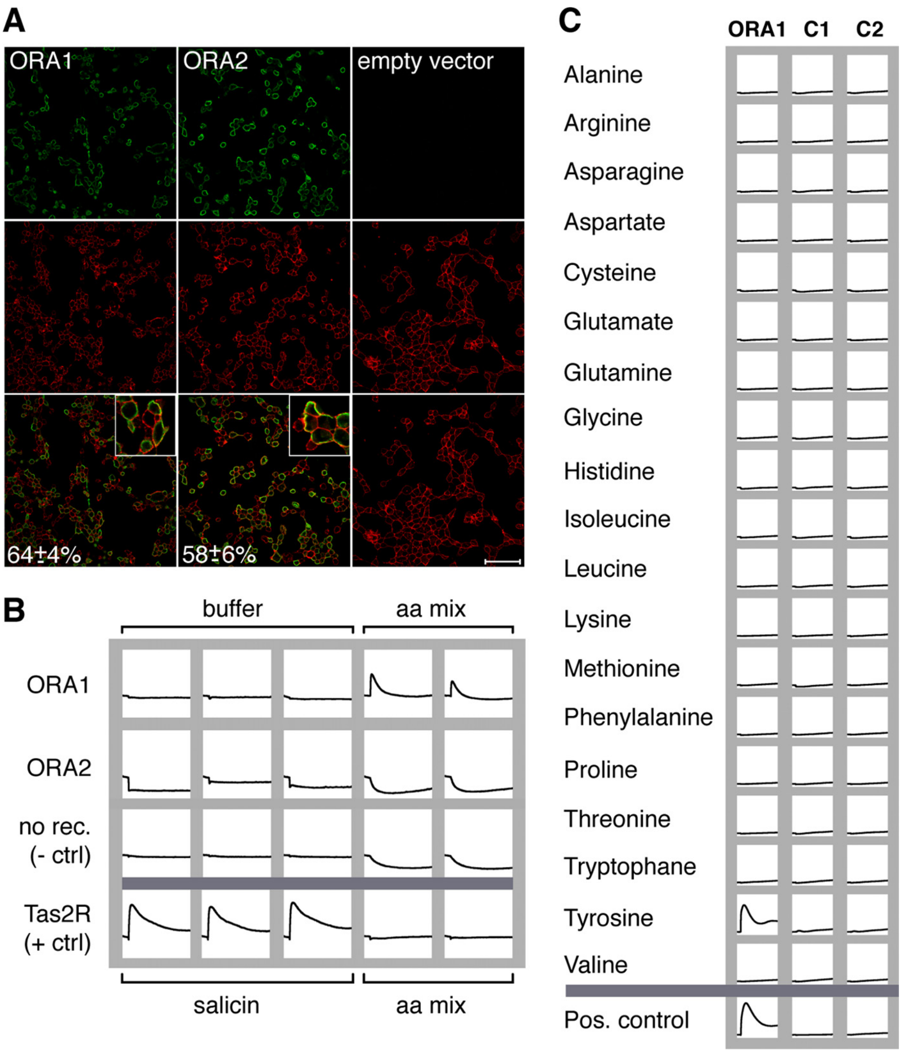

FIGURE 1. **Activation of ORA receptors by amino acids.** *A,* ORA receptors localize to the plasma membrane. HEK 293T cells were transfected as indicated, and receptor protein was detected with an antibody against the C-terminal HSV epitope and Alexa 488-coupled secondary antibody (*green*, *upper row*). Cell surfaces are visualized using biotinylated concanavalin A in combination with streptavidin/Alexa 633 (*red label*, *middle row*). *Yellow* color in the overlay (*bottom row*) indicates close proximity of receptors with the plasma membrane. *Insets* show groups of cells magnified by a factor of three. Note the absence of green signals in cells transfected with empty vector (*third column*). Cells expressing the *ora* genes (*green*) were counted and expressed as percentage of total cells (*red*) ± S.D. *Scale bar*, 75 μm. *B,* ORA1 but not ORA2 is activated by an amino acid mixture. HEK 293T cells were transiently transfected with ORA1, ORA2, TAS2R16, or empty vector, loaded with Fluo-4 AM, and stimulated with a mixture of all 20 proteinogenic amino acids (final concentration 1 mM each). Changes in calcium levels were analyzed in a fluorometric imaging plate reader. Only ORA1-transfected cells show a response, comparable in size to that of the positive control (TAS2R16 and 10 mM of the agonist D-(−)-salicin (9)). Thus, ORA1 appears to be specifically activated by one or several amino acids present in the amino acid mixture. *C,* ORA1-expressing cells only respond to tyrosine. HEK 293T cells were transiently transfected with ORA1 or empty vector, loaded with the calcium-sensitive dye fluo-4 AM, and analyzed in a fluorometric imaging plate reader before and after application of single amino acids at 1 mM concentration each. Duplicate wells, one of which is shown here, were tested for each experimental condition. No change in fluorescence was seen for untransfected cells (*middle column*) or cells transfected with empty vector (*right column*). The ORA1 response to tyrosine is comparable in size and time course to that of the bitter taste receptor TAS2R16 to a strong agonist (D-(−)-salicin, 10 mM (9)).

aged tyrosine using a water/methanol gradient for elution from a reversed phase C_{18} column (Fig. 2*B*, for details see "Experimental Procedures"). Ten major peaks were collected, dried down, re-dissolved in 200 μl of H_2O, and tested at 1:6 dilution by functional calcium imaging of ORA1-expressing cells (Fig. 2*C*). ORA1 was activated by a single peak contained in fraction 6, and no signals were observed in all other factions, consistent with a single compound underlying the observed activation by aged tyrosine. Fraction 6 amounted to 5.2% of the total peak area, *i.e.* it constitutes a minor component of aged tyrosine.

To obtain enough material for structure determination the HPLC purification was scaled up to obtain about 10 mg of purified fraction 6. The exact mass was determined by LC-TOF/MS resulting in an elemental composition of $C_8H_8O_3$. LC-MS revealed an intense pseudo molecular ion $[M-H]^-$ with m/z 151.0 and additional LC-MS/MS experiments showed a daughter ion m/z 107.0, supporting the cleavage of a molecule of CO_2, *i.e.* the presence of a carboxylic group. Analysis of the ^1H NMR spectroscopic data showed a total of 3 resonance signals, two of them aromatic (6.67 and 7.02 ppm) and all three signals resulting from 2 protons each. The aromatic protons showed the typical coupling pattern of an *AA′XX′* spin system of a *para*-substituted aromatic ring. The third signal at 3.37 ppm was shown by DEPT-135 as well as heteronuclear single quantum coherence experiments to be derived from a methylene group. The complete assignment of the structure was achieved by

Downloaded from http://www.jbc.org/ at DEUTSCHE ZENTRALBIBLIOTHEK FUER MEDIZIN on November 13, 2014

TABLE 1
Binding spectrum of ORA1

Active Compounds	*EC_{50} (µM)*	*Max. amplitude (ΔF/F)*
4-hydroxyphenylacetic acid	1.9 ± 0.3	0.86 ± 0.03
4-toloylacetic acid	14.8 ± 1.8	0.54 ± 0.03
3,4-methylenedioxyphenylacetic acid	16.0 ± 3.6	0.54 ± 0.04
4-methoxyphenylacetic acid	16.5 ± 2.7	0.39 ± 0.05
4-chlorophenylacetic acid	16.6 ± 1.6	0.49 ± 0.02
3,4-dihydroxyphenylacetic acid	22.8 ± 2.7	0.36 ± 0.02
Phenylacetic acid	30.5 ± 2.8	0.52 ± 0.01
4-aminophenylacetic acid	91.7 ± 17.3	0.58 ± 0.02
3-(4-hydroxyphenyl)-propionic acid	191.8 ± 39.8	0.17 ± 0.01
4-hydroxyphenylacetamide	199.9 ± 52.2	0.39 ± 0.03
Methyl-4-hydroxyphenylacetic acid	221.0 ± 25.2	0.45 ± 0.02

Inactive Compounds	*Maximal concentration tested (mM)*		
Proteinogenic amino acids			
L-alanine	1	L-leucine	1
L-arginine	1	L-lysine	1
L-asparagine	1	L-methionine	1
L-aspartate	1	L-phenylalanine	1
L-cysteine	1	L-proline	1
L-glutamate	1	L-serine	1
L-glutamine	1	L-threonine	1
Glycine	1	L-tryptophane	1
L-histidine	1	L-tyrosine	1
L-isoleucine	1	L-valine	1
Other amino acids and derivatives			
4-amino-L-phenylalanine	10	D-tyrosine	1
4-hydroxy-L-phenylglycine	10	DL-m-tyrosine	1
5-hydroxy-L-tryptophane	0.03	DL-o-tyrosine	3
4-iodo-L-phenylalanine	0.3	L-tyrosine methylester	1
4-nitro-L-phenylalanine	1		
Steroids and prostaglandins			
4-androstene-3,17-dione	0.003	15-keto-prostaglandin F2α	0.003
4-Pregnen-17,20β-diol-3-one	0.003	Prostaglandin F2α	0.003
4-Pregnen-17,20β-diol-3-one-20-sulphate	0.003		
4-Pregnen-17,20β,21-triol-3-one	0.003		
Other compounds			
L-DOPA	1	4-phenylenediacetic acid	1
Dopamine	1	Serotonin	0.3
4-hydroxybenzoic acid	3	Skatole	0.01
Indole	0.1	Tyramine	1
Indole-3-carboxylic acid	0.2		

Downloaded from http://www.jbc.org/ at DEUTSCHE ZENTRALBIBLIOTHEK FUER MEDIZIN on November 13, 2014

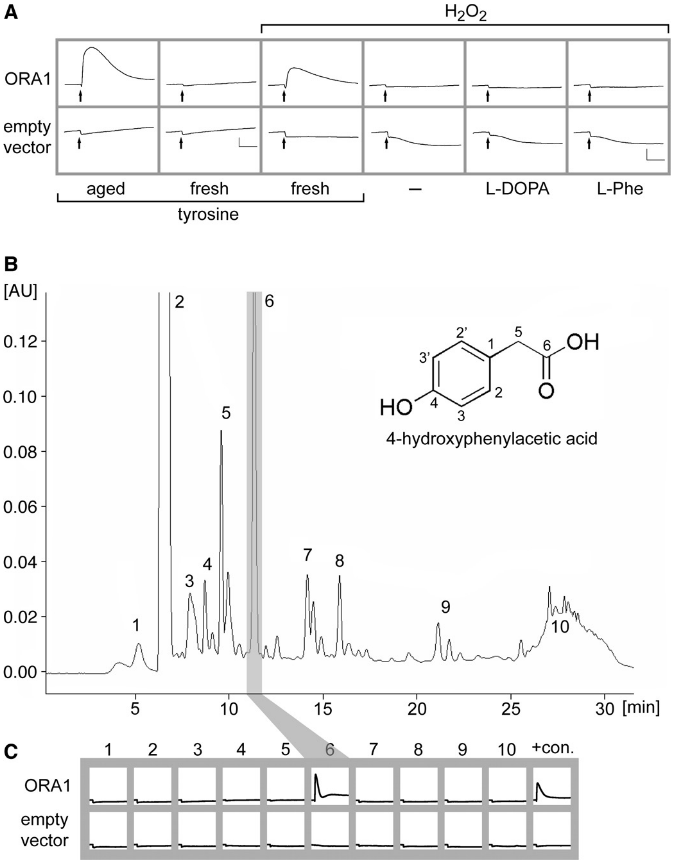

FIGURE 2. **ORA1 is activated by 4-hydroxyphenylacetic acid, a contaminant of aged tyrosine.** *A, top row*, cells were transfected with ORA1, and challenged with 100 μM of different stimuli as indicated. Calcium traces are averaged from 3 wells. Only aged tyrosine (*first column*), *i.e.* the tyrosine lot used in Fig. 1, and oxidized fresh tyrosine (*third column*) were active, but fresh tyrosine itself (*second column*) was not. Hydrogen peroxide itself, L-dopamine (*L-DOPA*), and L-phenylalanine (*L-Phe*) had no effect. *Bottom row*, cells transfected with empty vector showed no response to any of the stimuli. Shown are calcium traces averaged from 2 wells. Scaling: *y* axis = relative units, *x* axis = 1 min. *B*, a single active compound is detected in aged L-tyrosine. 100 μg of aged tyrosine was separated by HPLC fractionation using a water/methanol gradient with UV detection at 280 nm. Ten fractions corresponding to peak absorbance rates (labeled 1–10) were collected at the following time points during the run: *1*, 3.4–5.6 min; *2*, 6.0–6.9 min; *3*, 7.5–8.2; *4*, 8.2–9.2 min; *5*, 9.2–10.2 min; *6*, 10.7–11.5 min; *7*, 13.7–14.9 min; *8*, 15.5–17.4; *9*, 20.6–23 min; *10*, 25–29.5 min. *y* axis, absorbance units (*AU*); *x* axis, run time (min). *Inset of B*, chemical characterization of fraction 6 showed 4-hydroxyphenylacetic acid as the main compound. The carbon atoms of 4-hydroxyphenylacetic acid are labeled by arbitrary numbers to allow easy association with the following analytical, mass spectrometry, and NMR data that resulted in unambiguous identification: UV-visible (0.1% aqueous HCOOH)/MeOH; 6/4, v/v): λ_{max} = 228, 276 nm; LC/TOF-MS: $C_8H_8O_3$; LC/MS (ESI$^-$): 151.1 (100; [M-H]$^-$); ^{1}H NMR (500 MHz; dimethyl sulfoxide-d_6/MeOD; 9/1, v/v; COSY): δ 3.37 [s, 2H, H-C(**5**)], 6.67 [m, 2H, H-C(**3**,**3′**)], 7.02 [m, 2H, H-C(**3**,**3′**)]; ^{13}C NMR (125 MHz; dimethyl sulfoxide-d_6/MeOD; 9:1, v/v; DEPT-135, heteronuclear single quantum coherence, heteronuclear multiple bond correlation): δ 40.3 (CH$_2$, C(**5**)), 114.8 (CH, C(**3**, **3′**)), 125.6 (C, C(**1**)), 130.1 (CH, C(**2**, **2′**)), 155.8 (C, C(**4**)), 173.2 (C, C(**6**)). *C*, each of the collected fractions was dried, redissolved, and used to stimulate ORA1-transfected HEK 293T cells. Only fraction 6 resulted in fluorescence changes. *Last column*, 100 μM unpurified aged L-tyrosine served as positive control (*+con.*). Cells transfected with empty vector showed no response to any fraction. Scaling: *y* axis, arbitrary units; *x* axis 9 min.

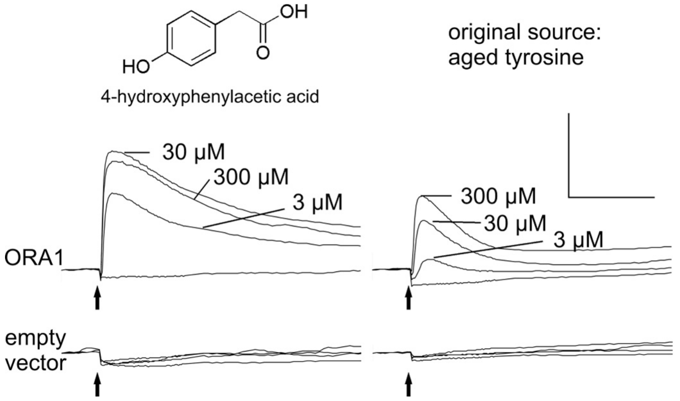

FIGURE 3. **Concentration-dependent saturable activation of ORA1 by 4-hydroxyphenylacetic *acid*.** HEK 293T cells transfected with ORA1 or empty vector were stimulated with different concentrations of 4-hydroxyphenylacetic acid, and calcium responses were imaged. For each concentration an average trace of three identically treated wells is shown (*left panel*). No response is seen for ORA1-transfected cells stimulated with buffer and for empty vector-transfected cells in all conditions (*bottom panels*). Note that ORA1-transfected cells are at least 10-fold more sensitive to 4-hydroxyphenylacetic acid than to aged tyrosine. *Scale bar*: *y* axis, arbitrary units; *x* axis, 2 min.

means of heteronuclear multiple bond correlation optimized for $^{2,3}J_{C,H}$ couplings. As an example, the carbonyl group resonating at 173.2 ppm showed a correlation signal with the protons of the methylene group, indicating a -CH$_2$COOH configuration and the carbon C(5) of the latter showed a cross-peak with the aromatic ring protons H-C(2,2′) via a $^3J_{C,H}$ coupling, suggesting this acetyl group as ring substituent. The signal at 155.8 ppm is well in line with a quaternary carbon substituted in the *para*-position with a phenolic system and showed the expected correlations with protons H-C(2,2′) and H-C(3,3′), see Fig. 2*B* for nomenclature. Taking all spectroscopic data into consideration, the degradation product of L-tyrosine could be unequivocally identified as 4-hydroxyphenylacetic acid (Fig. 2*B*). Furthermore, spectroscopic data of commercially available 4-hydroxyphenylacetic acid showed an exact match with those of the fraction 6 compound.

Validation of 4-Hydroxyphenylacetic Acid as ORA1 Ligand—Calcium imaging of ORA1-transfected cells was performed with different concentrations of commercial 4-hydroxyphenylacetic acid in the 3–300 μM range. Responses were dose-dependent and saturated at 30 μM, at least an order of magnitude lower than the original source, aged tyrosine (Fig. 3). This ratio was consistent with the result from the HPLC separation, which showed that 4-hydroxyphenylacetic acid was a contaminant in the original source, well below 10%.

The absence of signals in cells transfected with empty vector (Fig. 3) attests to the specificity of the functional data for ORA1-transfected cells. From the results of all the functional experiments we concluded that 1) 4-hydroxyphenylacetic acid is a high potency agonist for the receptor ORA1, and 2) that relatively minor structural changes destroy the agonistic properties suggesting a pronounced selectivity of this receptor.

Activation of ORA1 by 4-Hydroxyphenylacetic-related Compounds—To better understand the molecular features required for ORA1 agonists, we measured dose-response relationships for a variety of compounds structurally related to 4-hydroxyphenylacetic acid (Fig. 4, Table 1). Among this group, no better agonist than 4-hydroxyphenylacetic acid was found, which remains by far the best agonist exhibiting the lowest threshold concentration (approximately 0.1 μM), the lowest EC$_{50}$ concentration (1.9 ± 0.3 μM S.E.), and the largest maximal signal amplitude ($\Delta F/F > 0.8$).

Downloaded from http://www.jbc.org/ at DEUTSCHE ZENTRALBIBLIOTHEK FUER MEDIZIN on November 13, 2014

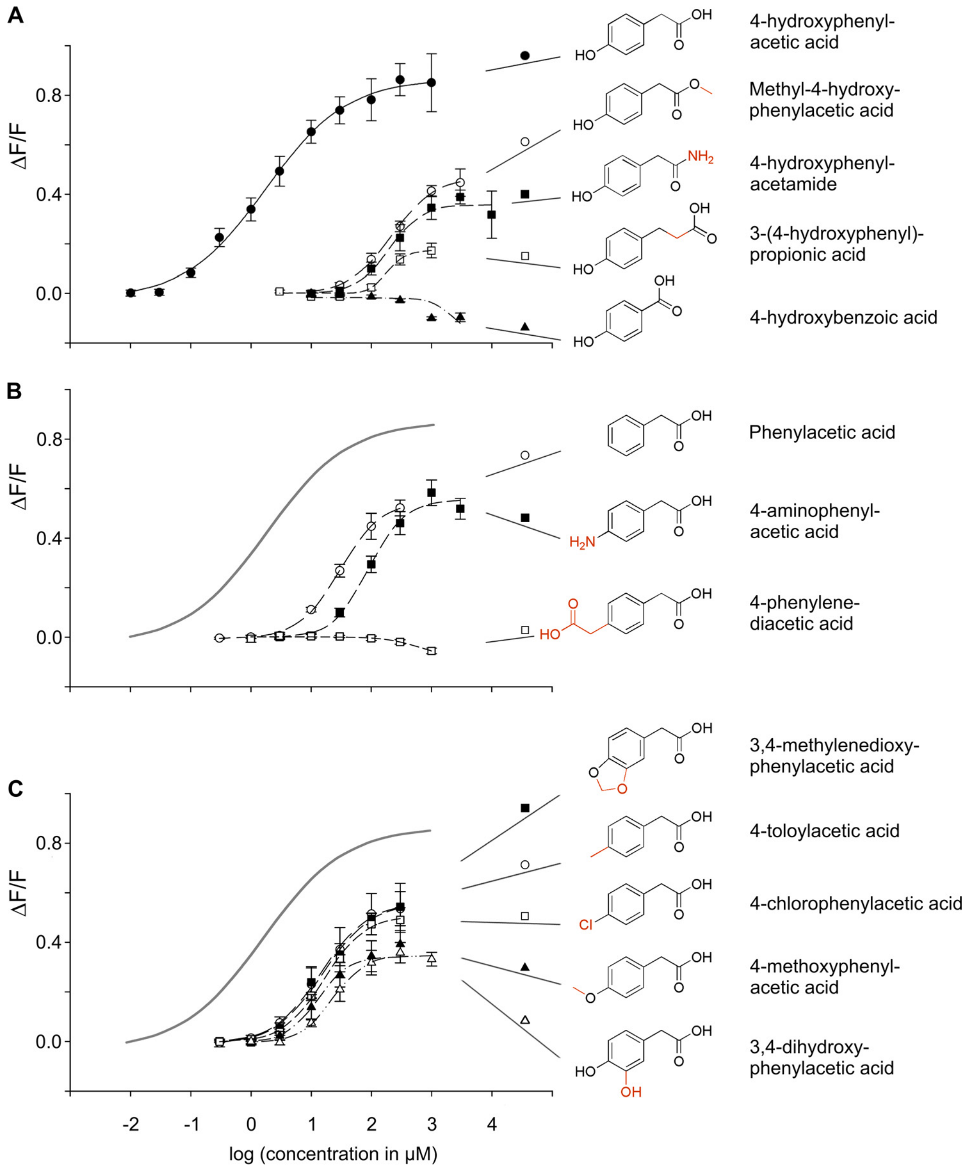

FIGURE 4. **Agonist selectivity and efficacy of ORA1.** HEK 293T Gα16gust44 cells were transfected with ORA1 cDNA and stimulated with increasing concentrations of compounds related to 4-hydroxyphenylacetic acid to monitor the corresponding dose-response functions. Resulting calcium signals were measured by fluorometric detection. *y* axis, Δ*F*/*F*; *x* axis, decadic logarithm of the concentration given in micromolar. Structural formulas of the substances are shown to the *left* of their names. *A*, 4-hydroxyphenylacetic acid activates ORA1 with an EC_{50} value of 1.9 ± 0.3 μM and a maximal signal amplitude above 0.8 Δ*F*/*F*. Structural alterations at the carboxyl group shift the dose-response curve to varying degrees to the *right* as well as reduce the maximal signal amplitude. *B*, structural alterations at the *para*-hydroxyl group shift the dose-response curve to the *right* as well as reduce the maximal signal amplitude. For comparison, the calculated dose-response curve for the optimal agonist, 4-hydroxyphenylacetic acid, is depicted in *gray*. *C*, 10-fold reduction in affinity by a positive inductive or mesomeric effect in *para*-position. For comparison, the calculated dose-response curve for the optimal agonist, 4-hydroxyphenylacetic acid, is depicted in *gray*.

Downloaded from http://www.jbc.org/ at DEUTSCHE ZENTRALBIBLIOTHEK FUER MEDIZIN on November 13, 2014

Of 55 compounds tested, only 11 4-hydroxyphenylacetic acid-related compounds activated ORA1 and showed a dose-dependent response (Fig. 4, Table 1). The efficacy as estimated by the maximal signal amplitude of these compounds was clearly lower, maximally 60% of the value observed for 4-hydroxyphenylacetic acid (Table 1), suggesting that all represent partial agonists. The potency, as estimated by the EC_{50} value, varied about 100-fold, with that of 4-hydroxyphenylacetic acid about an order of magnitude higher than that of the next best agonists (Table 1). Interestingly, the potencies do not correlate well with maximal signal amplitudes (Table 1), suggesting that potency and efficacy can vary independently for this receptor.

The Carboxyl Group Is Required in a Particular Distance to the Aromatic Ring Structure—Amidation or methylation of the carboxyl group increases the EC_{50} value 100-fold, *i.e.* decreases the affinity by 2 orders of magnitude (4-hydroxyphenylacetamide and methyl-4-hydroxyphenylacetic acid, respectively, see Fig. 4*A*, Table 1). Slightly increasing the distance from the ring by intercalating a methylene group (3-(4-hydroxyphenyl)-propionic acid) reduces the affinity by the same amount, but in addition impairs the maximal signal amplitude massively, down to 0.1 Δ*F*/*F*. Decreasing the distance of the carboxyl group from the ring abolishes the activity completely (4-hydroxybenzoic acid). Thus, the negative charge of the carboxyl group is required at a particular distance from the ring for efficient binding and in particular signal transduction. This hypothesis is supported by our observation that many related compounds, which were completely unable to activate ORA1 (Table 1), show modifications in this part of the molecular structure, *e.g.* the addition of a charged group (4-hydroxy-L-phenylglycine).

The para-Hydroxy Group Is Not Absolutely Required—Omitting the *para*-hydroxy group (phenylacetic acid) results in about an order of magnitude reduced potency and only 60% of maximal signal amplitude (Fig. 4*B*, Table 1). However, many variations of the *para*-substituent reduce the potency more severely. For example, a negative mesomeric and inductive effect in the *para*-position by exchanging the hydroxyl group with an amino group (4-aminophenylacetic acid) leads to a 50-fold reduction in potency (Fig. 4*B*, Table 1). Introducing a bulky (and charged) substituent in the *para*-position eliminates the activity completely (4-phenylenediacetic acid, Fig. 4*B*).

A positive inductive or mesomeric effect at the *para*-position is only marginally better than omitting the *para*-substituent completely, as seen by the activities of 4-chlorophenylacetic acid, 4-toloylacetic acid, 3,4-methylenedioxyphenylacetic acid, 3,4-dihydroxyphenylacetic acid, and 4-methoxyphenylacetic acid (Fig. 4*C*, Table 1). Interestingly, all five compounds possess undistinguishable EC_{50} values (Table 1), suggesting that the exact shape and size of the *para*-substituent is not important. The latter two compounds exhibit reduced maximal signal amplitudes compared with the first three compounds (Fig. 4*B*, Table 1). This uncoupling of affinity and efficacy would be consistent with the *p*-substituent boosting the efficacy of the ligand. Taken together, the *para*-hydroxyl group is not required *per se* for activity, but enhances potency and efficacy massively.

4-Hydroxyphenylacetic Acid Modulates Zebrafish Reproductive Behavior—The high sensitivity of ORA1 for 4-hydroxyphenylacetic acid suggests that this compound might be a relatively close fit to the endogenous ligand, if not an endogenous ligand itself. Its potency is over 10-fold better compared with that of a recently identified ligand-receptor pair that signals aversion to decaying flesh (11). This would be consistent with ORA1 serving as pheromone receptor, which generally exhibit higher sensitivity than "normal" olfactory receptors (*cf.* Refs. 21 and 24). Thus, we embarked on a search for innate zebrafish behavior elicited by 4-hydroxyphenylacetic acid.

First, we investigated whether a point source of 4-hydroxyphenylacetic acid in a stationary tank would elicit attraction or avoidance behavior (11). For these experiments 180 μl of 4-hydroxyphenylacetic acid solution (1 mM) was added to the tank by an experimenter hidden from sight for the zebrafish. Using the identical setup the same ligand concentration has been found to elicit maximal aversion behavior for the above mentioned ligand/receptor pair with 10-fold lower affinity (*cf.* Fig. 5*B*). However, 4-hydroxyphenylacetic acid did not result in detectable attraction or avoidance behavior (Fig. 5, *A* and *B*). Furthermore, average velocity, a measure of agitation, did not change after a 4-hydroxyphenylacetic acid stimulus was given, and no incidents of freezing, a fear response, were observed (Fig. 5, *A* and *C*).

Second, we considered a possible function of 4-hydroxyphenylacetic acid as a signal in social interactions, and tested zebrafish pairs with 100 μM 4-hydroxyphenylacetic acid (final concentration). We noted chasing behavior and in one case oviposition after contact with the odor in the case of female/male pairs of zebrafish. This suggested to us that 4-hydroxyphenylacetic acid might be involved in regulation of reproductive behavior. It is well known that several reproductive hormones and their metabolites including prostaglandins and steroids and so far unidentified compounds do double duty as odors that signal the reproductive state of the female to the male and vice versa (see Ref. 22).

We then investigated a possible effect of 4-hydroxyphenylacetic acid on oviposition behavior by exposing pairs of female and male zebrafish to different concentrations of 4-hydroxyphenylacetic acid. Because pairing of zebrafish by itself can induce oviposition, we kept the pairs together for 90 min before stimulus or control solution was added. Under the experimental conditions used, this resulted in oviposition during the first 90 min in 5% of cases ($n = 66$). A similar frequency of 8% ($n = 25$) was observed for control pairs not exposed to stimulus during the next 90 min. This frequency was used as a conservative estimate of the background egg-laying frequency for the next 90 min. We report that oviposition frequency increased severalfold after addition of 100 μM (final concentration) 4-hydroxyphenylacetic acid. This increase was blocked after closing the nostrils of the female with tissue glue (Fig. 5*D*). Both the increase and the block were significant (χ square test, $n = 10$, $p < 0.001$, and $n = 7$, $p < 0.02$, respectively). The induced oviposition persists at 4-hydroxyphenylacetic acid concentrations of 30 and 10 μM (Fig. 5*D*), although the number of eggs laid appeared to decrease with decreasing concentration. The eggs appeared partially immature and contained a higher than normal percentage of opaque (dead) eggs. We hypothesize that this could be due to the 4-hydroxyphenylacetic acid stimulus occurring out of physiological context in our experimental situation. We conclude that 4-hydroxyphenylacetic acid at low concentrations can elicit a physiological response as part of a reproductive behavior repertoire.

DISCUSSION

Our deorphanization of ORA1 constitutes the first instance of a ligand identification for any member of the *ora* family of olfactor receptor genes. In fact, ORA1 is only the third deorphanized fish olfactory receptor overall, with the other two receptors belonging to other families (11, 25). The small family of just six *ora* genes is remarkable for its high degree of conservation and its rather constant family size, both different from all other olfactory receptor gene families analyzed so far. Furthermore, *ora* genes are under strong negative selection and teleost ORA receptors possess direct orthologs even in cartilaginous fish (7), *i.e.* before the evolutionary divergence in teleosts and tetrapods. Thus, the *ora* family is ancestral to the mammalian and more generally tetrapod *v1r* receptor gene repertoires. The *v1r* receptors form a monophyletic tree with two of the six *ora* genes, *ora1* and *ora2*. Therefore, fish *ora1* and *ora2* genes may remain closer to the ancestral *v1r* genes than the contemporary *v1r* genes themselves, which show a very dynamic evolution, and exhibit many gene birth and death events. We have therefore attempted deorphanization of zebrafish ORA1 and ORA2

Downloaded from http://www.jbc.org/ at DEUTSCHE ZENTRALBIBLIOTHEK FUER MEDIZIN on November 13, 2014

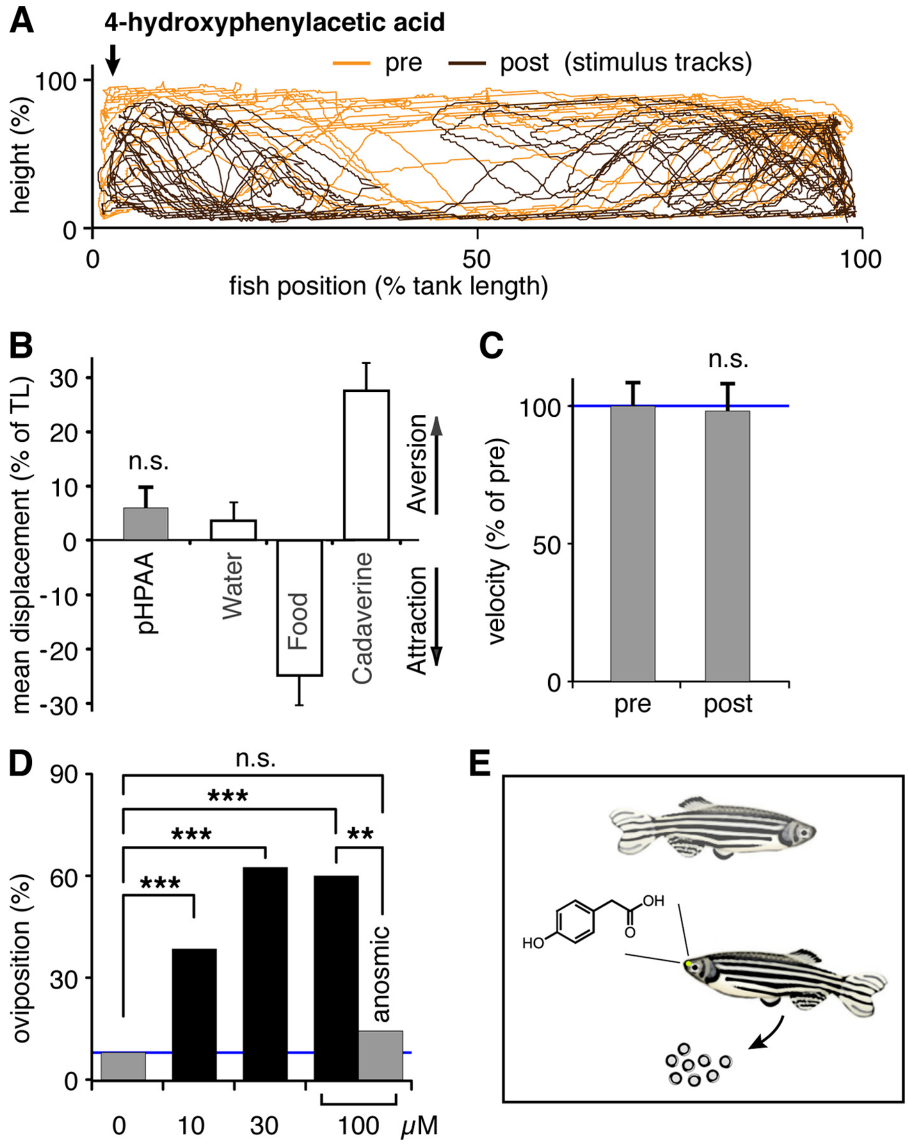

FIGURE 5. **Zebrafish behavioral responses to 4-hydroxyphenylacetic acid.** *A,* fish were exposed to a point source (*arrow*) of 4-hydroxyphenylacetic acid (1 mM), and their movements were video tracked 5 min before and after stimulus addition. A representative track is shown, *orange*, prestimulus; *brown*, poststimulus. *B,* quantitative evaluation of tracks shows no evidence for attraction or aversion by 4-hydroxyphenylacetic acid (*pHPAA*), *n.s.*, not significant. For comparison, attraction by food extract (*food*) and aversion to cadaverine is shown, raw data for these panels, see Ref. 11. *C,* no difference in motility was seen after exposure to 4-hydroxyphenylacetic acid. Motility is measured as average velocity and expressed as percent of the prestimulus value. *D,* oviposition frequency of zebrafish mating pairs is increased after exposure to 4-hydroxyphenylacetic acid, final concentrations as indicated. *Blue line* indicates control value (*left gray bar*). All three concentrations of 4-hydroxyphenylacetic acid are active, ***, $p < 0.001$. Naris closure (*right gray bar*) abolishes the increase in oviposition events, **, $p < 0.02$. *E,* schematic representation of the olfactory-mediated response of zebrafish mating pairs to 4-hydroxyphenylacetic acid.

receptors, and have been successful for ORA1, for which we identified and characterized several agonists.

We have shown ORA1 to be a highly sensitive and specific receptor for 4-hydroxyphenylacetic acid. An extensive search of structurally related compounds yielded no compound with similar or better potency and agonist efficacy. Albeit we cannot exclude the existence of structurally unrelated agonists, within the range of chemical structures analyzed, 4-hydroxyphenylacetic acid emerges as the optimal activator for ORA1. The best agonists among related compounds were about 10-fold less potent and exhibited less than two-thirds of the efficacy compared with 4-hydroxyphenylacetic acid. This large difference is consistent with the hypothesis that 4-hydroxyphenylacetic acid may be the physiologically relevant ligand for ORA1.

4-Hydroxyphenylacetic acid is detected by ORA1 with at least an order of magnitude higher sensitivity than typical food odors, such as amino acids (EC$_{50}$ values between 10 and 100 μM *in vivo* (24, 26, 27)) or the death-signaling odor cadaverine (11), even though measurements in heterologous systems may exhibit lower sensitivities for odorants than are observed *in vivo* (see *e.g.* Refs. 28 and 29). This high sensitivity is consistent with a pheromonal function for 4-hydroxyphenylacetic acid, because pheromones are expected to be detected at lower concentrations than normal odorants (21).

4-Hydroxyphenylacetic acid is a biogenic compound, which occurs in several metabolic pathways including a minor catabolic pathway for tyrosine (transamination, decarboxylation, and oxidation of the resulting aldehyde to the corresponding

Downloaded from http://www.jbc.org/ at DEUTSCHE ZENTRALBIBLIOTHEK FUER MEDIZIN on November 13, 2014

acid (*e.g.* Ref. 30 and Brenda-enzymes). 4-Hydroxyphenylacetic acid is produced in species as diverse as humans, insects, fungi, and bacteria (Refs. 31–34, respectively). It is present in micromolar concentrations in several bodily secretions including urine, feces (31), and saliva (35), and has been suggested as an antimicrobial agent (32–34), and also as component of a sexual display pheromone in felines (36).

Here we show that 4-hydroxyphenylacetic acid can modulate oviposition, a reproductive behavior, in zebrafish. This modulation appears to be mediated via the sense of smell, because it is abolished by naris closure. So far mostly various steroids and prostaglandins have been discussed as reproductive pheromones in fish species, but many pheromones remain unidentified up to now (22). We propose that 4-hydroxyphenylacetic acid may be in this category. Although we cannot exclude that 4-hydroxyphenylacetic acid may be mimicking a so far unknown endogenous steroid or prostaglandin, several known steroid and prostaglandin pheromones (21, 22) could not activate ORA1 in our assays.

ORA1 appears to be a plausible candidate for mediating the pheromonal effect of 4-hydroxyphenylacetic acid due to its high affinity and specificity. Further experiments will be required to firmly demonstrate this link and to rule out (or establish) the presence of other olfactory receptors for 4-hydroxyphenylacetic acid. Thus, the data presented here give a first glimpse onto a putative novel reproductive pheromone. Unfortunately, a thorough examination of this intriguing possibility is beyond the scope of the present study.

Currently, both the olfactory sensory neuron type, in which *ora1* is expressed, and its signal transduction mechanism are not known. Four morphologically and functionally different types of olfactory sensory neurons have been described so far in teleost fishes (37). Of these, crypt neurons can be excluded (38, 39), and ciliated neurons appear unlikely (39), which leaves the newly discovered kappe neurons (37) or microvillous neurons (39). The latter possibility would be analogous to the expression of *v1r* in microvillous neurons. Of the G proteins expressed in the olfactory epithelium of zebrafish (40), Gα_i has been shown to correlate with crypt neurons (38, 39), and Gα_{olf} is assumed to be specific for ciliated neurons, which leaves one of the two Gα_o proteins expressed in zebrafish olfactory sensory neurons as possibilities (40).

Our results reported here, the high specificity of ORA1 toward 4-hydroxyphenylacetic acid, together with the low threshold of detection, and the activity of this odor in enhancing a reproductive function (Fig. 5*E*), are consistent with the hypothesis that 4-hydroxyphenylacetic acid may have a pheromone function in zebrafish, and thus suggest ORA1 as a potential pheromone receptor. It is intriguing to speculate that despite the drastic differences in the evolutionary dynamics of *v1r* and *ora* genes and notwithstanding the opposing requirements for odors posed by aquatic and terrestrial habitats, a function as pheromone receptor may be shared as well as ancestral for these two orthologous gene families.

Acknowledgments—We thank Ulrike Redel, Peggy Grossmann, and Mehmet Saltürk for excellent technical assistance. Luis Saraiva was involved in an early phase of this project.

REFERENCES

1. Leinders-Zufall, T., Ishii, T., Mombaerts, P., Zufall, F., and Boehm, T. (2009) Structural requirements for the activation of vomeronasal sensory neurons by MHC peptides. *Nat. Neurosci.* **12,** 1551–1558
2. Haga, S., Hattori, T., Sato, T., Sato, K., Matsuda, S., Kobayakawa, R., Sakano, H., Yoshihara, Y., Kikusui, T., and Touhara, K. (2010) The male mouse pheromone ESP1 enhances female sexual receptive behaviour through a specific vomeronasal receptor. *Nature* **466,** 118–122
3. Isogai, Y., Si, S., Pont-Lezica, L., Tan, T., Kapoor, V., Murthy, V. N., and Dulac, C. (2011) Molecular organization of vomeronasal chemoreception. *Nature* **478,** 241–245
4. Boschat, C., Pélofi, C., Randin, O., Roppolo, D., Lüscher, C., Broillet, M. C., and Rodriguez, I. (2002) Pheromone detection mediated by a V1r vomeronasal receptor. *Nat. Neurosci.* **5,** 1261–1262
5. Del Punta, K., Leinders-Zufall, T., Rodriguez, I., Jukam, D., Wysocki, C. J., Ogawa, S., Zufall, F., and Mombaerts, P. (2002) Deficient pheromone responses in mice lacking a cluster of vomeronasal receptor genes. *Nature* **419,** 70–74
6. Saraiva, L. R., and Korsching, S. I. (2007) A novel olfactory receptor gene family in teleost fish. *Genome Res.* **17,** 1448–1457
7. Venkatesh, B., Lee, A. P., Ravi, V., Maurya, A. K., Lian, M. M., Swann, J. B., Ohta, Y., Flajnik, M. F., Sutoh, Y., Kasahara, M., Hoon, S., Gangu, V., Roy, S. W., Irimia, M., Korzh, V., Kondrychyn, I., Lim, Z. W., Tay, B. H., Tohari, S., Kong, K. W., Ho, S., Lorente-Galdos, B., Quilez, J., Marques-Bonet, T., Raney, B. J., Ingham, P. W., Tay, A., Hillier, L. W., Minx, P., Boehm, T., Wilson, R. K., Brenner, S., and Warren, W. C. (2014) Elephant shark genome provides unique insights into gnathostome evolution. *Nature* **505,** 174–179
8. Friedrich, R. W. (2013) Neuronal computations in the olfactory system of zebrafish. *Annu. Rev. Neurosci.* **36,** 383–402
9. Bufe, B., Hofmann, T., Krautwurst, D., Raguse, J. D., and Meyerhof, W. (2002) The human TAS2R16 receptor mediates bitter taste in response to β-glucopyranosides. *Nat. Genet.* **32,** 397–401
10. Behrens, M., Brockhoff, A., Batram, C., Kuhn, C., Appendino, G., and Meyerhof, W. (2009) The human bitter taste receptor hTAS2R50 is activated by the two natural bitter terpenoids andrographolide and amarogentin. *J. Agric. Food Chem.* **57,** 9860–9866
11. Hussain, A., Saraiva, L. R., Ferrero, D. M., Ahuja, G., Krishna, V. S., Liberles, S. D., and Korsching, S. I. (2013) High-affinity olfactory receptor for the death-associated odor cadaverine. *Proc. Natl. Acad. Sci. U.S.A.* **110,** 19579–19584
12. Schack, H. B., Malte, H., and Madsen, P. T. (2008) The responses of Atlantic cod (*Gadus morhua* L.) to ultrasound-emitting predators: stress, behavioural changes or debilitation? *J. Exp. Biol.* **211,** 2079–2086
13. Meyerhof, W., Batram, C., Kuhn, C., Brockhoff, A., Chudoba, E., Bufe, B., Appendino, G., and Behrens, M. (2010) The molecular receptive ranges of human TAS2R bitter taste receptors. *Chem. Senses* **35,** 157–170
14. Ammon, C., Schäfer, J., Kreuzer, O. J., and Meyerhof, W. (2002) Presence of a plasma membrane targeting sequence in the amino-terminal region of the rat somatostatin receptor 3. *Arch. Physiol. Biochem.* **110,** 137–145
15. Kreuzer, O. J., Krisch, B., Déry, O., Bunnett, N. W., and Meyerhof, W. (2001) Agonist-mediated endocytosis of rat somatostatin receptor subtype 3 involves β-arrestin and clathrin coated vesicles. *J. Neuroendocrinol.* **13,** 279–287
16. Bufe, B., Breslin, P. A., Kuhn, C., Reed, D. R., Tharp, C. D., Slack, J. P., Kim, U. K., Drayna, D., and Meyerhof, W. (2005) The molecular basis of individual differences in phenylthiocarbamide and propylthiouracil bitterness perception. *Curr. Biol.* **15,** 322–327
17. Ueda, T., Ugawa, S., Yamamura, H., Imaizumi, Y., and Shimada, S. (2003) Functional interaction between T2R taste receptors and G-protein α subunits expressed in taste receptor cells. *J. Neurosci.* **23,** 7376–7380
18. Saito, H., Kubota, M., Roberts, R. W., Chi, Q., and Matsunami, H. (2004) RTP family members induce functional expression of mammalian odorant receptors. *Cell* **119,** 679–691
19. Loconto, J., Papes, F., Chang, E., Stowers, L., Jones, E. P., Takada, T., Kumánovics, A., Fischer Lindahl, K., and Dulac, C. (2003) Functional expression of murine V2R pheromone receptors involves selective associa-

Downloaded from http://www.jbc.org/ at DEUTSCHE ZENTRALBIBLIOTHEK FUER MEDIZIN on November 13, 2014

tion with the M10 and M1 families of MHC class Ib molecules. *Cell* **112,** 607–618

20. Behrens, M., Bartelt, J., Reichling, C., Winnig, M., Kuhn, C., and Meyerhof, W. (2006) Members of RTP and REEP gene families influence functional bitter taste receptor expression. *J. Biol. Chem.* **281,** 20650–20659
21. Friedrich, R. W., and Korsching, S. I. (1998) Chemotopic, combinatorial, and noncombinatorial odorant representations in the olfactory bulb revealed using a voltage-sensitive axon tracer. *J. Neurosci.* **18,** 9977–9988
22. Stacey, N., and Sørensen, P. (2005) Reproductive pheromones. In *Behaviour and Physiology of Fish* (Sloman, K. A., Wilson, R. W., and Balshine, S., eds) pp. 359–412, Elsevier, Amsterdam
23. Yamamoto, Y., Hino, H., and Ueda, H. (2010) Olfactory imprinting of amino acids in lacustrine sockeye salmon. *PLoS One* **5,** e8633
24. Friedrich, R. W., and Korsching, S. I. (1997) Combinatorial and chemotopic odorant coding in the zebrafish olfactory bulb visualized by optical imaging. *Neuron* **18,** 737–752
25. Cao, Y., Oh, B. C., and Stryer, L. (1998) Cloning and localization of two multigene receptor families in goldfish olfactory epithelium. *Proc. Natl. Acad. Sci. U.S.A.* **95,** 11987–11992
26. Michel, W. C., and Lubomudrov, L. M. (1995) Specificity and sensitivity of the olfactory organ of the zebrafish, *Danio rerio*. *J. Comp. Physiol. A* **177,** 191–199
27. Fuss, S. H., and Korsching, S. I. (2001) Odorant feature detection: activity mapping of structure response relationships in the zebrafish olfactory bulb. *J. Neurosci.* **21,** 8396–8407
28. Mombaerts, P. (2004) Genes and ligands for odorant, vomeronasal and taste receptors. *Nat. Rev. Neurosci.* **5,** 263–278
29. Oka, Y., Katada, S., Omura, M., Suwa, M., Yoshihara, Y., and Touhara, K. (2006) Odorant receptor map in the mouse olfactory bulb: *in vivo* sensitivity and specificity of receptor-defined glomeruli. *Neuron* **52,** 857–869
30. Gossauer, A. (2006) *Struktur und Reaktivitaet der Biomolekuele: Eine Einfuehrung in die organische Chemie*, 1st ed., Helvetica Chimica Acta, Zurich
31. Li, M., Wang, B., Zhang, M., Rantalainen, M., Wang, S., Zhou, H., Zhang, Y., Shen, J., Pang, X., Zhang, M., Wei, H., Chen, Y., Lu, H., Zuo, J., Su, M., Qiu, Y., Jia, W., Xiao, C., Smith, L. M., Yang, S., Holmes, E., Tang, H., Zhao, G., Nicholson, J. K., Li, L., and Zhao, L. (2008) Symbiotic gut microbes modulate human metabolic phenotypes. *Proc. Natl. Acad. Sci. U.S.A.* **105,** 2117–2122
32. Dettner, K., and Schwinger, G. (1980) Defensive substances from pygidial glands of water beetles. *Biochem. Syst. Ecol.* **8,** 89–95
33. Ko, H. S., Jin, R. D., Krishnan, H. B., Lee, S. B., and Kim, K. Y. (2009) Biocontrol ability of Lysobacter antibioticus HS124 against Phytophthora blight is mediated by the production of 4-hydroxyphenylacetic acid and several lytic enzymes. *Curr. Microbiol*. **59,** 608–615
34. Ohtani, K., Fujioka, S., Kawano, T., Shimada, A., and Kimura, Y. (2011) Nematicidal activities of 4-hydroxyphenylacetic acid and oidiolactone D produced by the fungus *Oidiodendron* sp. *Z. Naturforsch C* **66,** 31–34
35. Takahama, U., Oniki, T., and Murata, H. (2002) The presence of 4-hydroxyphenylacetic acid in human saliva and the possibility of its nitration by salivary nitrite in the stomach. *FEBS Lett.* **518,** 116–118
36. Pageat, P., and Gaultier, E. (2003) Current research in canine and feline pheromones. *Vet. Clin. North Am. Small Anim. Pract.* **33,** 187–211
37. Ahuja, G., Nia, S. B., Zapilko, V., Shiriagin, V., Kowatschew, D., Oka, Y., and Korsching, S. I. (2014) Kappe neurons, a novel population of olfactory sensory neurons. *Sci. Rep.* **4,** 4037
38. Ahuja, G., Ivandic, I., Saltürk, M., Oka, Y., Nadler, W., and Korsching, S. I. (2013) Zebrafish crypt neurons project to a single, identified mediodorsal glomerulus. *Sci. Rep.* **3,** 2063
39. Oka, Y., Saraiva, L. R., and Korsching, S. I. (2012) Crypt neurons express a single V1R-related *ora* gene. *Chem. Senses* **37,** 219–227
40. Oka, Y., and Korsching, S. I. (2011) Shared and unique G alpha proteins in the zebrafish *versus* mammalian senses of taste and smell. *Chem. Senses* **36,** 357–365

Downloaded from http://www.jbc.org/ at DEUTSCHE ZENTRALBIBLIOTHEK FUER MEDIZIN on November 13, 2014

Publication 5

Gaurav Ahuja # and Sigrun Korsching. Zebrafish Olfactory Receptor ORA1 Recognizes a Putative Reproductive Pheromone. Communicative & Integrative Biology, Doi:10.4161/19420889.2014.970501 **(2014).** # Corresponding author

http://www.tandfonline.com/doi/full/10.4161/19420889.2014.970501#.VGUaf4WpqPI

Communicative & Integrative Biology 7:5, 1–4; October 1, 2014; © 2014 Published with license by Taylor & Francis Group, LLC

Downloaded by [87.78.185.224] at 12:54 13 November 2014

Zebrafish olfactory receptor ORA1 recognizes a putative reproductive pheromone

Gaurav Ahuja* and Sigrun Korsching
Institute for Genetics; University at Cologne; Cologne, Germany

Keywords: calcium imaging, heterologous expression, oviposition, pheromone, tyrosine, V1R-like, zebrafish

Abbreviations: V1Rs, Vomeronasal receptor, type 1; V2Rs, Vomeronasal receptor, type 2; VSNs, vomeronasal sensory neurons; ora, olfactory receptor class A-related; pHPAA, p-hydroxyphenylacetic acid; EC50, half-maximal response.

© Gaurav Ahuja and Sigrun Korsching

*Correspondence to: Gaurav Ahuja; Email: gahuja@smail.uni-koeln.de

Submitted: 09/02/2014

Accepted: 09/03/2014

http://dx.doi.org/10.4161/19420889.2014.970501

Addendum to: ORA1, a Zebrafish Olfactory Receptor Ancestral to All Mammalian V1R Genes, Recognizes 4-Hydroxyphenylacetic Acid, a Putative Reproductive Pheromone J. Biol. Chem. 2014 289: 19778–19788. First Published on May 15, 2014, doi:10.1074/jbc.M114.573162.

This is an Open Access article distributed under the terms of the Creative Commons Attribution-Non-Commercial License (http://creativecommons.org/licenses/by-nc/3.0/), which permits unrestricted non-commercial use, distribution, and reproduction in any medium, provided the original work is properly cited. The moral rights of the named author(s) have been asserted.

Teleost *v1r*-related *ora* genes constitute a small and highly conserved olfactory receptor gene family, and their direct orthologs are present in lineages as distant as cartilaginous fishes. Recently, the first member of the *ora* gene family was deorphanized. ORA1 detects p-hydroxyphenylacetic acid with high sensitivity and specificity. This compound elicits olfactory-mediated oviposition behavior in adult zebrafish mating pairs, suggesting a potential function as a reproductive pheromone for pHPAA itself or a related substance. This association of an odor and its cognate receptor with an oviposition response may provide a molecular basis for studying neural circuits involved in fish reproduction.

Pheromones are chemical signals produced by a species and recognized by the olfactory system of the conspecific to mediate behavioral functions such as mating preferences and individual recognition. In mammals, vomeronasal sensory neurons (VSNs) express members of 2 large olfactory receptor gene families, *v1r* and *v2r*, which are thought to mediate pheromone detection.[1] V2Rs recognize peptides, whereas V1R ligands are found among low molecular weight molecules, such as steroids.[1-3] The mammalian *v1r* receptor family is large, with over 100 genes in rodent species, and undergoes frequent species-specific expansions.[4] Interestingly, all mammalian *v1r* genes are monophyletic with only 2 teleost *ora* genes, *ora1* and *ora2*.[5] In drastic contrast to the rapidly evolving mammalian *v1r* genes, the teleost *ora* gene family is highly conserved between all teleost species analyzed, and consists of the same 6 genes, with an occasional gene loss.[5] Even in cartilaginous fishes some direct orthologs are observed.[6] Thus it was unclear, whether teleost *ora* genes, despite their different evolutionary dynamics, might also have a pheromonal function like their mammalian counterparts. Two research groups teamed up a while ago to attempt deorphanization of teleost *ora* genes, the Korsching lab in Cologne and the Meyerhof lab in Potsdam. Recently they reported the deorphanization of ORA1, which they found to detect p-hydroxyphenylacetic acid (pHPAA) with high sensitivity and specificity.[7] Moreover, behavior analysis suggested that pHPAA induces olfactory-mediated oviposition behavior in adult zebrafish pairs[7], which implies its possible function as a putative fish pheromone.

A Convoluted Path toward Identification of an Olfactory Ligand

The search for an ORA1 ligand turned out to be quite the detective story. In the end, a contaminant of the initially suspected 'ligand' was identified as a sensitive and specific agonist. Initial screening for ligand identification was performed with known odors for fish, including amino acids and some reproductive pheromones.[8-10] Interestingly, all tested pheromones failed to activate ORA1, whereas a strong activation response was elicited with a mixture of the 20 proteinogenic L-amino acids. Testing of the individual amino acids indicated that activation was due to L-tyrosine alone. Alas, this was an old lot of tyrosine, and a freshly prepared lot of L-tyrosine failed to reproduce the

Downloaded by [87.78.185.224] at 12:54 13 November 2014

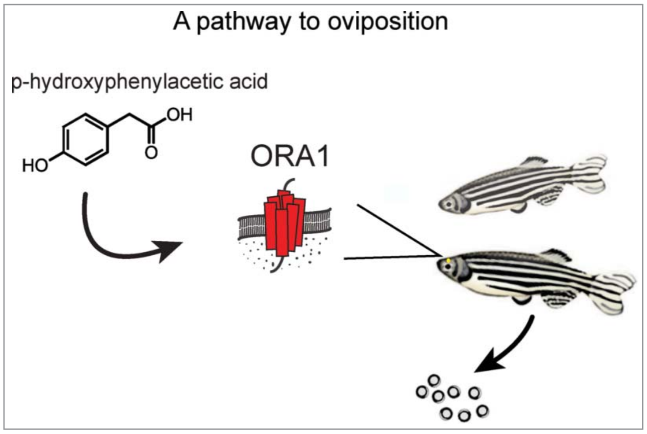

Figure 1. Graphical representation of key findings. Calcium imaging in a heterologous expression assay identified p-hydroxyphenylacetic acid as a agonist of ORA1 receptor. Perception of p-hydroxyphenylacetic acid by the olfactory system of female zebrafish in the presence of a male can induce oviposition.

activation response. This suggested to the researchers that the active compound might be a degradation product of L-tyrosine. In fact, tyrosine is known to be sensitive to oxidation upon prolonged storage. Therefore, to test this hypothesis, a fresh lot of L-Tyrosine was oxidized by incubation with hydrogen peroxide, and indeed strong agonist activity was observed in the reaction product (hydrogen peroxide itself had no activity). This suggested that the active substance in the aged L-tyrosine originated from oxidative decay of L-tyrosine. Subsequently, analytical HPLC chromatography on a reverse phase column showed the agonist activity in a single peak. To hunt the agonist down, Meyerhof and Korsching solicited the help of the Rawel group in Berlin to obtain sufficient HPLC-purified material for subsequent structural analysis. For structure determination these groups joined efforts with the Hofmann group in Munich, which used a combination of LC-TOF/MS and proton NMR to unravel the structure. The contaminant was finally identified as pHPAA, and functional testing of the synthetic compound elicited a strong activation response even at very low concentrations, with a half-maximal response (EC_{50}) at 2 μM.

Could pHPAA be the Endogenous Ligand?

Dose response analysis suggested that pHPAA is recognized by ORA1 with much higher affinity compared to food odors such as amino acids[9,11,12] or even the death-associated odor cadaverine.[13] Furthermore, thorough testing of many structurally related compounds did not reveal any substance with better potency or efficacy for ORA1. Any modification of the carboxyl group such as amidation or methylation reduced the affinity at least 2 orders of magnitude, and shortening the distance of the carboxyl group to the benzene ring by eliminating a methylene group abolished agonist activity altogether. Somewhat less severe constraints were observed for the para hydroxy group, whose elimination results only in a one order of magnitude loss for the affinity. However, a bulky group in this position such as an acetyl group destroys agonist activity completely. Interestingly, the efficacy, i.e. the maximal response, varied somewhat independently from the affinity, as estimated by EC_{50} determination. Both efficacy and affinity were maximal for pHPAA. So, could the authors have hit on the endogenous ligand for the ORA1 receptor?

Any endogenous signaling molecule should fulfill 2 requirements: firstly there should be a biosynthetic path generating the molecule, and secondly it should have a biological function. pHPAA is a product of a minor catabolic pathway for tyrosine,[14] which would seem to fulfill the first requirement. Indeed it has been reported that pHPAA is produced by diverse organisms, such as humans, insects, fungi and bacteria. As for the second requirement, biological functions for pHPAA have been reported in a variety of species, ranging from an antimicrobial property[15] for defense in several species to a component of sexual display pheromone in felines.[16] Unfortunately, none of these species included fish, and so the authors set out in search of a possible behavioral answer to pHPAA.

What is the Impact of pHPAA on Zebrafish Behavior?

The authors had recently shown an aversive response of zebrafish to the death-associated odor cadaverine,[13] and so began to search for either aversive or attractive responses to pHPAA. However, none of the motion parameters analyzed showed significant differences in the presence of pHPAA. Again, an accidental observation came to the help of the researchers. When adult fish were tested in pairs, they noticed sometimes deposition of eggs (oviposition). The effect turned out to be highly significant in mixed gender pairs, and also was observed at similarly low concentrations as the ligand activation of the ORA1 receptor.

Admittedly, pHPAA does not show much similarity to known classes of teleost fish reproductive pheromones, which comprise several steroids and their sulfated metabolites, as well as some prostaglandins. Furthermore, those steroids and prostaglandins tested as possible agonists did not activate ORA1.[8,17] However, knowledge of fish reproductive pheromones is still sketchy, and it is known that some components are still unidentified.[8,18] Thus the findings discussed here allow the fascinating interpretation that the authors have chanced onto a novel biological class of reproductive pheromones (**Fig. 1**). Of course, much remains to be done to shore up this hypothesis and to rule out more mundane alternative explanations.

What Do We Know About the Cells Expressing ORA1?

The characteristic sparse expression pattern of olfactory receptor genes in

Downloaded by [87.78.185.224] at 12:54 13 November 2014

distributed neurons within the sensory surface is also observed for zebrafish ORA1.[5] However, the cell type and the signal transduction cascade of ORA1 expressing neurons are still elusive. Four different types of olfactory sensory neurons are known in zebrafish, ciliated and microvillous neurons as major populations[19] and small populations of crypt and kappe neurons.[20,21] These 4 cell types differ in molecular markers, but also in morphology and spatial distribution within the olfactory epithelium.[20-22] *In situ* hybridization showed ORA1-expressing neurons in apical positions within the olfactory lamellae, which seems to exclude the more basally located ciliated neurons.[5,23] Among the other 3 types, crypt neurons are known not to express ORA1,[22] which leaves microvillous neurons or kappe neurons as candidates. Both are present in the superficial layers.[20] However, it is also conceivable that yet another, so far undetected class of olfactory sensory neurons would express ORA1.

Olfactory receptors such as the *ora* genes belong to the superfamily of G protein-coupled receptors, and are expected to signal through trimeric G proteins. Recently a comprehensive evaluation of zebrafish G α proteins has shown the expression of *Go1*, *Go2*, *Gi*, and *Golf* in the olfactory epithelium.[24] Of these, one of the 2 *Go* isoforms, or possibly *Gi*, would be candidates for signal transduction of ORA1, since the association of *Golf* with ciliated neurons would seem to rule out an expression in ORA1-positive neurons.[25,26] Direct evidence will be provided by double labeling experiments using ORA1 *in situ* probe together with G protein or cell type-specific markers.

Open Questions

So far it is unclear whether the olfactory-mediated oviposition behavior elicited by pHPAA is driven by ORA1 as a sole or major receptor. Alternatively, additional receptors may be contributing to this phenotype. To address this question, double labeling experiments with ORA1 probe and established neuronal activity markers could be performed. Neuronal activity markers such as cFOS, phospho-ERK, egr-1, c-jun and Arc have been successfully used in similar studies.[27] Moreover, new genome editing techniques like CRISPR/Cas or TALEN can be used to knock out ORA1 in zebrafish.[28] If pHPAA-mediated oviposition will be reduced or eliminated in such knock-outs, this would constitute strong evidence for the pHPAA effect being mediated by ORA1. CRISPR/Cas and TALEN may also be useful for knock-in of marker genes into the ORA1 locus, allowing to identify the ORA1 target glomerulus in the olfactory bulb. A knock-in of channel rhodopsin[29] in the ORA1 locus could rigorously restrict neuronal activation to only ORA1-expressing neurons, and thus would present another possibility to examine whether ORA1 activation by itself would be sufficient to generate the oviposition response. Beyond the olfactory bulb, it may be possible to map the pHPAA-activated neural circuits with single cell resolution in the intact zebrafish brain using a combination of high-speed light-sheet microscopy with genetically encoded calcium indicator (GCaMP5/6), *cf.*[30] Finally it will be interesting to examine, whether pHPAA is indeed the endogenous ligand of ORA1, in which case one would expect to find a biosynthetic pathway as well as a path to delivery of pHPAA in the context of mating behavior.

Disclosure of Potential Conflicts of Interest

No potential conflicts of interest were disclosed.

Acknowledgments

We would like to thank Maik Behrens, Oliver Frank, Harshadrai Rawel, Christoph Potting, Thomas Hofmann and Wolfgang Meyerhof for their contributions to the research depicted here.

References

1. Isogai Y, Si S, Pont-Lezica L, Tan T, Kapoor V, Murthy VN, Dulac C. Molecular organization of vomeronasal chemoreception. Nature 2011; 478:241-5; PMID: 21937988; http://dx.doi.org/10.1038/nature10437
2. Del Punta K, Leinders-Zufall T, Rodriguez I, Jukam D, Wysocki CJ, Ogawa S, Zufall F, Mombaerts P. Deficient pheromone responses in mice lacking a cluster of vomeronasal receptor genes. Nature 2002; 419:70-4; PMID:12214233; http://dx.doi.org/10.1038/nature00955
3. Boschat C, Pélofi C, Randin O, Roppolo D, Lüscher C, Broillet M-C, Rodriguez I. Pheromone detection mediated by a V1r vomeronasal receptor. Nat Neurosci 2002; 5:1261-2; PMID:12436115; http://dx.doi.org/10.1038/nn978
4. Korsching S. The molecular evolution of teleost olfactory receptor gene families. Results Probl Cell Differ 2009; 47:37-55; PMID:18956167; http://dx.doi.org/10.1007/400_2008_11
5. Saraiva LR, Korsching SI. A novel olfactory receptor gene family in teleost fish. Genome Res 2007; 17: 1448-57; PMID:17717047; http://dx.doi.org/10.1101/gr.6553207
6. Venkatesh B, Lee AP, Ravi V, Maurya AK, Lian MM, Swann JB, Ohta Y, Flajnik MF, Sutoh Y, Kasahara M, et al. Elephant shark genome provides unique insights into gnathostome evolution. Nature 2014; 505:174-9; PMID:24402279; http://dx.doi.org/10.1038/nature12826
7. Behrens M, Frank O, Rawel H, Ahuja G, Potting C, Hofmann T, Meyerhof W, Korsching S. ORA1, a zebrafish olfactory receptor ancestral to all mammalian V1R genes, recognizes 4-hydroxyphenylacetic acid, a putative reproductive pheromone. J Biol Chem 2014; 289:19778-88; PMID:24831010; http://dx.doi.org/10.1074/jbc.M114.573162
8. Sorensen PW, Hara TJ, Stacey NE. Sex pheromones selectively stimulate the medial olfactory tracts of male goldfish. Brain Res 1991; 558:343-7; PMID:1782551; http://dx.doi.org/10.1016/0006-8993(91)90790-3
9. Friedrich RW, Korsching SI. Combinatorial and chemotopic odorant coding in the zebrafish olfactory bulb visualized by optical imaging. Neuron 1997; 18:737-52; PMID:9182799; http://dx.doi.org/10.1016/S0896-6273(00)80314-1
10. Yamamoto Y, Hino H, Ueda H. Olfactory imprinting of amino acids in lacustrine sockeye salmon. PLoS One 2010; 5; e8633; PMID:20062811; http://dx.doi.org/10.1371/journal.pone.0008633
11. Fuss SH, Korsching SI. Odorant feature detection: activity mapping of structure response relationships in the zebrafish olfactory bulb. J Neurosci 2001; 21:8396-407; PMID:11606628
12. Michel WC, Lubomudrov LM. Specificity and sensitivity of the olfactory organ of the zebrafish, Danio rerio. J Comp Physiol A 1995; 177:191-9; PMID:7636767; http://dx.doi.org/10.1007/BF00225098
13. Hussain A, Saraiva LR, Ferrero DM, Ahuja G, Krishna VS, Liberles SD, Korsching SI. High-affinity olfactory receptor for the death-associated odor cadaverine. Proc Natl Acad Sci U S A 2013; 110:19579-84; PMID: 24218586; http://dx.doi.org/10.1073/pnas.1318596110
14. Gossauer A. Struktur und Reaktivitaet der Biomolekuele: Eine Ein- Fuehrung in Die Organische Chemie. Zurich: Helv Chim Acta, 2006; 1st ed.
15. Ohtani K, Fujioka S, Kawano T, Shimada AKY. Nematicidal activities of 4-hydroxyphenylacetic acid and oidiolactone D produced by the fungus Oidiodendron sp. Z Naturforsch C 2011; 66:31-4; PMID:21476434; http://dx.doi.org/10.5560/ZNC.2011.66c0031
16. Pageat P, Gaultier E. Current research in canine and feline pheromones. Vet Clin North Am- Small Anim Pract 2003; 33:187-211; PMID:12701508; http://dx.doi.org/10.1016/S0195-5616(02)00128-6
17. Friedrich RW, Korsching SI. Chemotopic, combinatorial, and noncombinatorial odorant representations in the olfactory bulb revealed using a voltage-sensitive axon tracer. J Neurosci 1998; 18:9977-88; PMID:9822753
18. Stacey N, Sorensen P. Reproductive pheromones. Fish Physiol 2005; 24:359-412; http://dx.doi.org/10.1016/S1546-5098(05)24009-8
19. Sato Y, Miyasaka N, Yoshihara Y. Mutually exclusive glomerular innervation by two distinct types of olfactory sensory neurons revealed in transgenic zebrafish. J Neurosci 2005; 25:4889-97; PMID:15901770; http://dx.doi.org/10.1523/JNEUROSCI.0679-05.2005

20. Ahuja G, Nia SB, Zapilko V, Shiriagin V, Kowatschew D, Oka Y, Korsching SI. Kappe neurons, a novel population of olfactory sensory neurons. Sci Rep 2014; 4:4037; PMID:24509431; http://dx.doi.org/10.1038/srep04037
21. Ahuja G, Ivandic I, Salturk M, Oka Y, Nadler W, Korsching SI. Zebrafish crypt neurons project to a single, identified mediodorsal glomerulus. Sci Rep 2013; 3:2063; PMID:23792970; http://dx.doi.org/10.1038/srep02063
22. Oka Y, Saraiva LR, Korsching SI. Crypt neurons express a single V1R-related ora gene. Chem Senses 2012; 37:219-27; PMID:22038944; http://dx.doi.org/10.1093/chemse/bjr095
23. Pfister P, Rodriguez I. Olfactory expression of a single and highly variable V1r pheromone receptor-like gene in fish species. Proc Natl Acad Sci U S A 2005; 102:5489-94; PMID:15809442; http://dx.doi.org/10.1073/pnas.0402581102
24. Oka Y, Korsching SI. Shared and unique G alpha proteins in the zebrafish versus mammalian senses of taste and smell. 2011; 36:357-65; PMID:21242316; http://dx.doi.org/10.1093/chemse/bjq138
25. Braubach OR, Fine A, Croll RP. Distribution and functional organization of glomeruli in the olfactory bulbs of zebrafish (Danio rerio). J Comp Neurol 2012; 520:2317-39; PMID:22581687; http://dx.doi.org/10.1002/cne.23075
26. Gayoso JÁ, Castro A, Anadón R, Manso MJ. Differential bulbar and extrabulbar projections of diverse olfactory receptor neuron populations in the adult zebrafish (Danio rerio). J Comp Neurol 2011; 519:247-76; PMID:21165974; http://dx.doi.org/10.1002/cne.22518
27. Bepari AK, Watanabe K, Yamaguchi M, Tamamaki N, Takebayashi H. Visualization of odor-induced neuronal activity by immediate early gene expression. BMC Neurosci 2012; 13:140; PMID:23126335; http://dx.doi.org/10.1186/1471-2202-13-140
28. Gaj T, Gersbach CA, Iii CFB. ZFN, TALEN, and CRISPR/Cas-based methods for genome engineering. Trends Biotechnol 2013; 31:397-405; PMID:23664777; http://dx.doi.org/10.1016/j.tibtech.2013.04.004
29. Yizhar O, Fenno LE, Davidson TJ, Mogri M, Deisseroth K. Optogenetics in neural systems. Neuron 2011; 71:9-34; PMID:21745635; http://dx.doi.org/10.1016/j.neuron.2011.06.004
30. Ahrens MB, Orger MB, Robson DN, Li JM, Keller PJ. Whole-brain functional imaging at cellular resolution using light-sheet microscopy. Nat Methods 2013; 10:413-20; PMID:23524393; http://dx.doi.org/10.1038/nmeth.2434

Downloaded by [87.78.185.224] at 12:54 13 November 2014

This page was intentionally left blank.

V. Discussion

Zebrafish crypt neurons project to a single, identified mediodorsal glomerulus

Of three types of olfactory sensory neurons present in vertebrates, the two major populations, ciliated and microvillous neurons, have been extensively studied due to the availability of suitable markers (Sato et al. 2005). In recent years, the third population, crypt neurons have developed considerable interest due to their peculiar morphology and also because they combine elements of the other two populations, ciliated and microvilllous receptor neurons (Hansen & Zeiske 1998). However, comparatively little is known about the third population, crypt neurons (Hansen & Zeiske 1998). So far no genetic markers for crypt neurons have been described and thus identification of these neurons depends on electron microscopy or TrkA- or S100-like immunoreactivity (Hansen & Zeiske 1998; Germana et al. 2004; Catania et al. 2003). However, there have been inconsistent reports using S100-like immunoreactivity. (Oka et al. 2012) showed that different results could be obtained depending on the fixation conditions, and established the optimal conditions for the specific labeling of crypt neurons as omitting the fixation step. However, tissue preservation is unavoidably compromised under these conditions, and attempts to use S100-like immunoreactivity to elucidate the neuronal circuits formed by crypt neurons have remained inconclusive (Sato et al. 2005; Braubach et al. 2012; Gayoso et al. 2012; Gayoso et al. 2011).

In a double transgenic line which labels both ciliated and microvillous sensory neurons with reporter fluorescent dyes, fluorescence was noticably absent from all 6 glomeruli of the mediodorsal cluster (Sato et al. 2005). Consequently, these six glomeruli were initially thought to be the target glomeruli of crypt neurons. Several years later, even larger target regions for crypt neurons were suggested based on backtracing experiments with DiI, a lypophilic tracer (Gayoso et al. 2012). In these studies, injections performed into the dorsomedial and dorsolateral fields of the olfactory bulb both resulted in labeled crypt neurons. Similarly, attempts to use the crypt neuron marker S100-like immunoreactivity in the olfactory bulb clearly pointed to both dorsomedial and dorsolateral sites, under standard immunostaining conditions (Braubach et al. 2012; Gayoso et al. 2012). Taken together, all these attempts to localize the target glomerulus/ glomeruli either by using unspecific antibodies or diffusible backtracing dyes, might overestimate the spatial extent of the target region.

Recently Oka, Saraiva and Korsching reported that a single olfactory receptor, the *v1r*-like *ora4* gene, is expressed in all crypt neurons as defined by quantitative morphological assessment (Oka et al. 2012). Therefore I hypothesized that crypt neurons might possess a single target glomerulus, in accordance with the axonal convergence principle established for ciliated neurons. To test this hypothesis I investigated the suitability of TrkA-immunoreactivity (Catania et al. 2003) as specific marker for crypt neurons. As mentioned above, S100-immunoreactivity is not suitable for this purpose as it is not restricted to crypt neurons under standard histological conditions.

In this study, I have characterized TrkA-immunoreactivity as a specific and robust marker for crypt neurons. TrkA-immunoreactivity specifically labels crypt neurons soma, axons and terminals. The absence of TrKA transcript and protein in the olfactory epithelium suggests the reactivity of anti-TrkA antibody to some unknown antigen, creating limitations to use it as a genetic marker. However, dense and specific labeling of crypt neuron axons and terminals, under standard histological conditions, makes anti-TrKA antibody suitable to determine its target region in the olfactory bulb. By using this marker, I have shown that crypt neurons project exclusively to a single glomerulus of the mediodorsal cluster. The glomerulus is identified and named as mdg2, in accordance to the nomenclature by (Braubach et al. 2012). Moreover, I have obtained supporting results by another, independent technique, axonal backtracing, which showed that the majority of the population backtraced from mdg2 were crypt neurons, whereas no such cells were labeled by backtracing from neighboring glomeruli **(Figure 4)**.

These findings showing a single target glomerulus for crypt neurons depend on the assumption that entire crypt neuron population is labeled by TrkA-immunoreactivity. Crypt neurons were defined by their characteristic morphology at the electron microscopy level. However, it is not possible to reliably quantify the total number of crypt neurons per olfactory epithelium by electron microscopy (Hansen & Zeiske 1998). Hence one cannot rule out the possibility of the existence of some cryptic cell population which are both S100 and TrkA-like immunoreactivity negative. However, several arguments make such a possibility unlikely. Firstly, if such population exists then they would be expected to have their projections in the those glomeruli which are negative for fluorescent staining in double transgenic fish (Tg(*TRPC2:Venus*); Tg(*OMP:lyn-mRFP*)). Furthermore, the cell population labeled by backtracing from a closely neighboring glomerulus, mdg3, were microvillous neurons (based on morphometric analysis). Moreover, a small population of non-crypt cells (based on morphology and spatial distribution) obtained from DiI injection in mdg2, suggesting nearby glomeruli take projections from microvillous neurons. Lastly, a recent publication (Braubach et al. 2012), showed the projection of Go-like immunoreactivity-positive neurons to mdg5 of the mediodorsal cluster. These neurons have non-crypt morphology and in fact constitute a novel population, as discussed below.

All this evidence suggests that *ora4*-expressing crypt neurons project to a single mediodorsal glomerulus (Oka et al. 2012; Ahuja et al. 2013). Since the *ora* gene family consists of six members, there are 6 glomeruli in the mediodorsal cluster, and one *ora* gene, *ora4*, projects to one of the glomeruli in the mediodorsal cluster, mdg2, it will be interesting to see, whether the entire mediodorsal cluster receives projections from *ora* gene-expressing OSNs.

Identification of a single glomerulus for crypt neurons is consistent with the concept of a novel ‘one cell type – one receptor’ mode of expression for crypt neurons (Oka et al. 2012), which is distinct from and goes beyond the ‘one neuron – one receptor’ mode of expression established for ciliated and microvillous olfactory receptor neurons. Here I extend this observation to a ‘one cell type – one receptor – one glomerulus’ concept, which is reminiscent of the specialized subsystems present in insect pheromone detection (Hildebrand 1995).

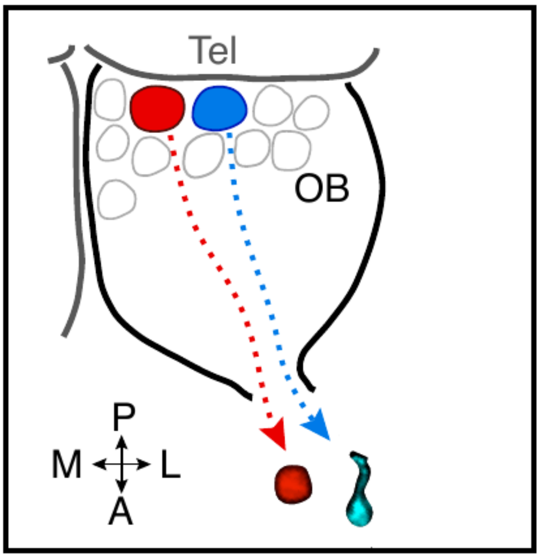

Figure 4: Schematic representation of backtracing results for the crypt neuron and a neighboring glomerulus, mdg2 region and dlg region, respectively. The scheme illustrates that mdg2 of the mediodorsal cluster obtains projections from the crypt neurons, whereas the neighboring glomerulus of the dorso-lateral cluster takes projections from ciliated

neurons (modified from (Ahuja et al. 2013)).

Kappe neurons, a novel population of olfactory sensory neurons

A recent publication suggested that Go-like immunoreactivity labels a mixture of crypt and non-crypt neurons, nevertheless projects to a single glomerulus of the mediodorsal cluster, mdg5 (Braubach et al. 2012). I thought to investigate these findings because it is interesting to know if the neurons innervating a single glomerulus could be morphologically and presumably functionally heterogeneous – a violation of the well-established rule of axonal convergence of same receptor-expressing neurons into a homogeneous glomerulus (Mombaerts 2006). Secondly in that study double labeling with a crypt neuron marker was not attempted, and shape and spatial position of cells labeled by Go-like immunoreactivity were not quantitatively assessed.

I have carefully addressed this question by performing thorough quantitative analysis of several morphological parameters coupled with double labeling experiments with established markers for all three known populations of olfactory sensory neurons (Hansen & Zeiske 1998). My results show that Go-like immunoreactivity labeled neurons do not express any markers for ciliated, microvillous and crypt neurons and indeed possess a distinct shape and spatial position compared to these three populations. This led to the identification and characterization of a novel fourth class of olfactory receptor neurons, which we named as *kappe* neurons, due to the presence of cap-like structure (kappe is German for cap) apically localized on these neurons (Ahuja et al. 2014) *cf.* **(Figure 5)**. It is not clear whether kappe neurons exist in other teleost fishes since Go-like immunoreactivity shows heterogenous results (Ferrando et al. 2006; Hansen et al. 2004). In some fishes, Go-like immunoreactivity is known to label a small subset of microvillous-like neurons (Hansen & Zielinski 2005) and in other species it is known to label crypt-like neurons (Hansen et al. 2003). The situation is additionally complicated because Go-like immunoreactivity might not always label Go protein (Ahuja et al. 2014; Hansen et al. 2004). Indeed, the subcellular distribution of Go-immunoreactivity in dendrite, cytoplasm, axon and axon terminals of kappe neurons is unexpectedly broad, since G proteins often are preferentially localized to the apical, signal-transducing part of the cell. Furthermore, *in situ* hybridization with Go probe on adult zebrafish olfactory epithelium showed a large and broadly distributed cell population (Oka & Korsching 2011), inconsistent with the expression pattern obtained from Go-like immunoreactive kappe neurons. This evidence suggests that Go-immunoreactivity could be due to cross-reactivity with an unknown antigen. Incidentally, this would be similar to the situation for both crypt neuron markers, anti-TrkA or anti-S100 antibodies (Oka et al. 2012; Ahuja et al. 2013). A further analysis of kappe neurons will require the identification of the cross-reacting antigen, which will allow the use of molecular and genetic tools.

In conclusion, kappe neurons and crypt neurons project to a single glomerulus - mdg5 and mdg2 of the mediodorsal cluster, respectively (Ahuja et al. 2014; Ahuja et al. 2013). It will be interesting to see whether the remaining four glomeruli of the mediodorsal cluster also might get input by specialized small neuronal populations like the crypt and kappe neurons.

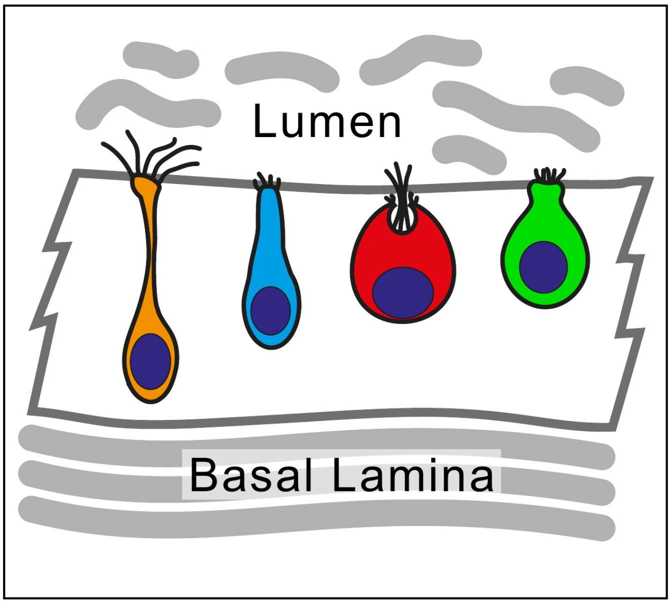

Figure 5: Schematic representation of four types of olfactory sensory neurons and their laminar positions. Ciliated neurons (orange) have round somata and slender dendrites that terminate in bundles of cilia on the epithelial surface. Their nuclei position is relatively basal along the laminar height in comparison to other OSN types. Microvillous neurons (blue) have bundles of microvilli on their apical surface. Crypt neurons (red) are globular-shaped and carry both microvilli and cilia on their apical surface. They are located more apical than microvillous neurons. Go-immunoreactivity positive kappe neurons (green) are pear-shaped with an apical appendage resembling a cap (German: Kappe), have no cilia, and are located even more apical than crypt neurons (modified from (Ahuja et al. 2014)).

Zebrafish olfactory receptor ORA1 recognizes a putative reproductive pheromone

The *v1r*-related *ora* gene family is the latest of all teleost olfactory receptor gene families to be characterized. In mammals, the *v1r* gene family undergoes frequent species-specific expansions and can reach over 100 genes in rodent species (Gaillard et al. 2004). Interestingly, all mammalian *v1r* genes are monophyletic with only two teleost *ora* genes, *ora1* and *ora2* (Saraiva & Korsching 2007). In drastic contrast to the rapidly evolving mammalian *v1r* genes, the teleost *ora* gene family is highly conserved between all teleost species analyzed, and consists of the same six genes, with an occasional gene loss (Saraiva & Korsching 2007). Even in cartilaginous fishes some direct orthologs are observed (Venkatesh et al. 2014). Thus it was unclear, whether teleost *ora* genes, despite their different evolutionary dynamics, might also have a pheromonal function like their mammalian counterparts (Saraiva & Korsching 2007; Isogai et al. 2011). Therefore, to address this question, two research groups teamed up a while ago to attempt deorphanization of teleost *ora* genes, the Korsching lab in Cologne and the Meyerhof lab in Potsdam. They have deorphanized ORA1, which we found to detect p-hydroxyphenylacetic acid (pHPAA) with high sensitivity and specificity (Behrens et al. 2014). In order to understand the physiological importance of this compound, I have performed attraction-aversion behavioral analysis, by using point source stimulus in a tank apparatus (Hussain et al. 2013). However, none of the motion parameters analyzed showed significant differences in the presence of pHPAA. An accidental observation helped me to understand the physiological role of pHPAA. When I tested pairs of adult fish, sometimes I noticed deposition of eggs (oviposition). Careful examination of this behavior suggested that the effect is highly significant in mixed gender pairs, and that low concentrations of pHPAA can elicit oviposition (Behrens et al. 2014). Moreover, the transient anosmic female fish paired with a normosmic male failed to produce similar results, suggesting the pHPPA-induced oviposition behavior depends on female olfactory perception. Admittedly, pHPAA does not show much similarity to known classes of teleost fish reproductive pheromones, which comprise several steroids and their sulfated metabolites, as well as some prostaglandins (Stacey & Sorensen 2005). Furthermore, those steroids and prostaglandins tested as possible agonists did not activate ORA1 in heterologous system (Friedrich & Korsching 1998; Stacey & Sorensen 2005; Behrens et al. 2014). However, knowledge of fish reproductive pheromones is still sketchy, and it is known that some components are still unidentified (Sorensen et al. 1991; Stacey &

Sorensen 2005). Thus the findings discussed here allow the interpretation that we have chanced onto a novel biological class of reproductive pheromones **(Figure 6)**. Of course, much remains to be done to shore up this hypothesis and to rule out more mundane alternative explanations. This includes the *in-vivo* validation of the contribution of ORA1 receptor for such inducible oviposition behavior and also the identification of the ORA1-expressing cell type, transducing Gα protein and glomerular projection of ORA1 expressing olfactory sensory neurons. Identification of a physiological source of pHPAA would rule out the always present concern that pHPAA just mimicks an endogenous compound. One should also expect some difference in olfactory processing of pHPAA between the sexes, if the hypothesis of a new reproductive pheromone is appropriate.

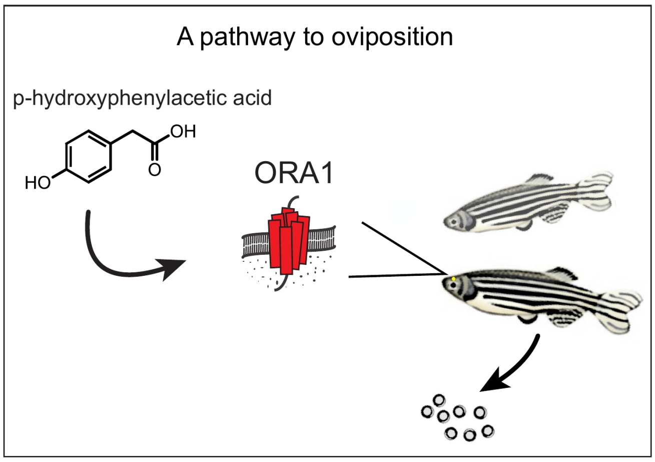

Figure 6: Graphical representation illustrating perception of p-hydroxyphenylacetic acid by the olfactory system of female zebrafish in the presence of a male can induce oviposition. Taken from (Ahuja & Korsching 2014).

High-affinity olfactory receptor for the death-associated odor cadaverine

Cadaverine and putrescine are death-associated odors produced by microbe-mediated decarboxylation of basic amino acids. Different innate behaviors (attraction or aversion) are known for different species towards these amines i.e. attraction in goldfish and rats and aversion in humans (Heale et al. 1996; Rolen et al. 2003; Hamana & Matsuzaki 1984). Olfactory receptors for these diamines have been unknown in any species, until Prof. Korsching's lab, in collaboration with Prof. Liberles group from Harvard, has identified TAAR13c as cadaverine receptor (Hussain et al. 2013) by using a heterologous ligand detection assay (Liberles & Buck 2006). They have examined various genes of the *taar* gene family (which are expected to detect amines) and could identify one receptor, i.e. TAAR13c which recognizes both cadaverine (with high affinity) and putrescine (with comparatively lower affinity). TAAR13c has distinct molecular recognition properties which endow sensitivity for diamines but not monoamines. Structure activity analysis indicates an unusual divalent ligand binding pocket requiring two remote positive charges for activation. Furthermore, TAAR13c is strongly activated by primary amines and indeed is phylogenetically closer to those rodent *taars* that prefer primary over tertiary amines (Hussain et al. 2013a). TAAR13c arose during teleost evolution and orthologs are absent in rodents and humans who also detect cadaverine. Thus, cadaverine-activated olfactory receptors in mammals may present a case of convergent evolution, either within the vertebrate *taar* family or between different olfactory receptor families (Saito et al. 2009).

Deorphanization of TAAR13c had been performed in vitro, and therefore it was necessary to examine, whether the same ligands are recognized in vivo, and whether TAAR13c constitutes a major receptor for cadaverine or, alternatively might be one of many cadaverine receptors. To tackle these questions I have established a neural activation marker, p-ERK, in zebrafish and I have developed a behavioral setup that allows defined concentrations of stimulus to be used. By implementing these methods, I have performed *in vivo* validation of the receptor ligand previously identified *in vitro*.

I observed that higher concentrations of cadaverine activate many olfactory receptor neurons, and only a small subset of these neurons carry TAAR13c receptor (Hussain et al. 2013). However, tenfold lower concentrations mainly elicit phosphorylation of ERK in an extremely sparse population of receptor neurons (about 100 cells/whole olfactory epithelium) and indeed the large majority of these neurons carry the TAAR13c receptor (Hussain et al. 2013). I have tested the same low concentration in an behavior experiment testing for aversion/attraction using a 2 channel flow apparatus, and have found that this low concentration (10µM) of cadaverine can induce pronounced aversion behavior in adult zebrafish. However, further investigation, in particular TAAR13c loss-of-function analysis, will be required to delineate the exact role of TAAR13c in generating avoidance behavior to diamines.

Taken together, we have shown that TAAR13c emerges as a sensitive olfactory receptor for the death-associated odor cadaverine, both in isolation and as part of a complex mixture. Cadaverine at low concentrations both activates a sparse population of TAAR13c-expressing olfactory sensory neurons and elicits powerful and innate avoidance behavior in zebrafish, a vertebrate model system **(Figure 7)**. Such an association of odor and cognate receptor with a powerful avoidance response provides a molecular basis for studying neural circuits connecting sensation with perception of odor valence.

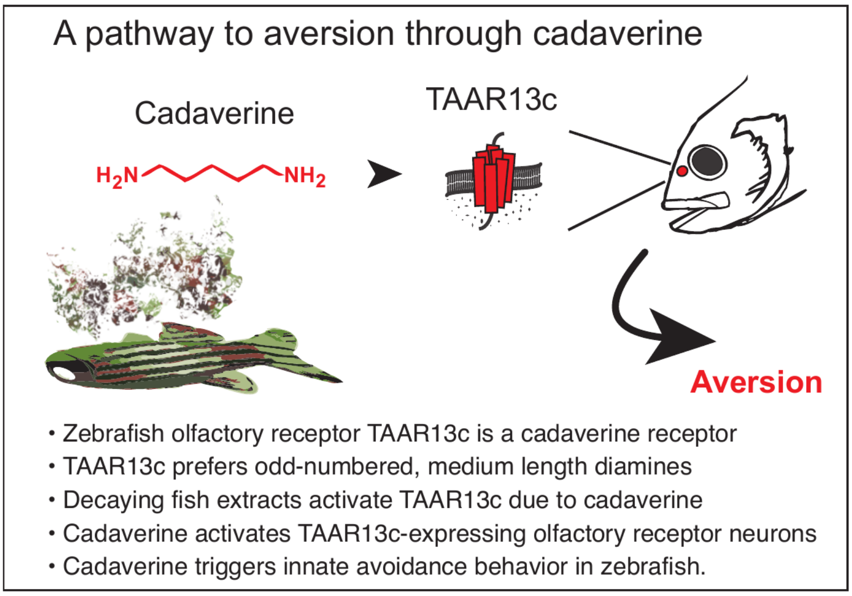

- Zebrafish olfactory receptor TAAR13c is a cadaverine receptor
- TAAR13c prefers odd-numbered, medium length diamines
- Decaying fish extracts activate TAAR13c due to cadaverine
- Cadaverine activates TAAR13c-expressing olfactory receptor neurons
- Cadaverine triggers innate avoidance behavior in zebrafish.

Figure 7: Graphical summary of key findings in (Hussain et al. 2013). Figure taken from (Hussain et al. 2013).

Coding strategies in small olfactory subsystems may be different from those employed in large subsystems

With my observation that zebrafish crypt neurons project to a single, identified mediodorsal glomerulus (Ahuja et al. 2013) and the previous knowledge that all crypt neurons express the same receptor, ORA4, a novel coding strategy was revealed, which we suggested to designate as the 'one cell type – one receptor – one glomerulus' strategy. Furthermore, the novel population of olfactory sensory neurons I identified, *kappe* neurons, also projects to a single target glomerulus (Ahuja et al. 2014), suggesting that they may also exhibit a similar coding strategy, although currently their receptor/receptors are unknown.

A distinct behavioral response may be generated by activation of a single high- affinity receptor

For two high-affinity olfactory receptors I have shown that a distinctive behavior could be elicited at very low concentrations of their optimal ligand (aversion for cadaverine (Hussain et al. 2013), oviposition for pHPAA (Behrens et al. 2014), respectively). For cadaverine and its cognate receptor, TAAR13c, I could show that at the same low concentration the large majority of neurons activated by cadaverine expresses TAAR13c, suggesting that TAAR13c is the major or maybe even the only receptor carrying the avoidance response to cadaverine.

These results provide an excellent starting point to examine the molecular basis of neural circuits connecting sensation, perception, and innate behavior.

VI. References

Ahuja, G. et al., 2014. Kappe neurons, a novel population of olfactory sensory neurons. *Scientific reports*, 4, p.4037.

Ahuja, G. et al., 2013. Zebrafish crypt neurons project to a single, identified mediodorsal glomerulus. *Sci Rep*, 3, p.2063.

Ahuja, G. & Korsching, S., 2014. Zebrafish olfactory receptor ORA1 recognizes a putative reproductive pheromone. *Communicative &amp; Integrative Biology*, 0(0), pp.1–4.

Alioto, T.S. & Ngai, J., 2006. The repertoire of olfactory C family G protein-coupled receptors in zebrafish: candidate chemosensory receptors for amino acids. *BMC genomics*, 7, p.309.

Babusyte, A. et al., 2013. Biogenic amines activate blood leukocytes via trace amine-associated receptors TAAR1 and TAAR2. *Journal of leukocyte biology*, 93, pp.387–94.

Baier, H., Rotter, S. & Korsching, S., 1994. Connectional topography in the zebrafish olfactory system: random positions but regular spacing of sensory neurons projecting to an individual glomerulus. *Proc Natl Acad Sci U S A*, 91(24), pp.11646–11650.

Behrens, M. et al., 2014. ORA1, a Zebrafish Olfactory Receptor Ancestral to All Mammalian V1R Genes, Recognizes 4-Hydroxyphenylacetic Acid, a Putative Reproductive Pheromone. *The Journal of biological chemistry*, 289(28), pp.19778–88.

Belluscio, L. et al., 1998. Mice deficient in G(olf) are anosmic. *Neuron*, 20, pp.69–81.

Berghard, A. & Buck, L.B., 1996. Sensory transduction in vomeronasal neurons: evidence for G alpha o, G alpha i2, and adenylyl cyclase II as major components of a pheromone signaling cascade. *The Journal of neuroscience*, 16, pp.909–918.

Borowsky, B. et al., 2001. Trace amines: identification of a family of mammalian G protein-coupled receptors. *Proceedings of the National Academy of Sciences of the United States of America*, 98, pp.8966–8971.

Boschat, C. et al., 2002. Pheromone detection mediated by a V1r vomeronasal receptor. *Nature neuroscience*, 5, pp.1261–1262.

Boulay, F. et al., 1990. The human N-formylpeptide receptor. Characterization of two cDNA isolates and evidence for a new subfamily of G-protein-coupled receptors.

Biochemistry, 29, pp.11123–11133.

Bradaia, A. et al., 2009. The selective antagonist EPPTB reveals TAAR1-mediated regulatory mechanisms in dopaminergic neurons of the mesolimbic system. *Proceedings of the National Academy of Sciences of the United States of America*, 106, pp.20081–20086.

Braubach, O.R., Fine, A. & Croll, R.P., 2012. Distribution and functional organization of glomeruli in the olfactory bulbs of zebrafish (Danio rerio). *J Comp Neurol*, 520(11), pp.2317–39.

Brechbühl, J., Klaey, M. & Broillet, M.-C., 2008. Grueneberg ganglion cells mediate alarm pheromone detection in mice. *Science (New York, N.Y.)*, 321(5892), pp.1092–5.

Brechbühl, J., Moine, F. & Broillet, M.-C., 2013. Mouse Grueneberg ganglion neurons share molecular and functional features with C. elegans amphid neurons. *Frontiers in behavioral neuroscience*, 7(December), p.193.

Buck, L. & Axel, R., 1991. A novel multigene family may encode odorant receptors: a molecular basis for odor recognition. *Cell*, 65, pp.175–187.

Buck, L.B., 2004. Olfactory receptors and odor coding in mammals. *Nutrition reviews*, 62, pp.S184–S188; discussion S224–S241.

Buck, L.B., 2005. Unraveling the sense of smell (Nobel Lecture). In *Angewandte Chemie - International Edition*. pp. 6128–6140.

Catania, S. et al., 2003. The crypt neurons in the olfactory epithelium of the adult zebrafish express TrkA-like immunoreactivity. *Neurosci Lett*, 350(1), pp.5–8.

DeMaria, S. et al., 2013. Role of a ubiquitously expressed receptor in the vertebrate olfactory system. *J Neurosci*, 33(38), pp.15235–15247.

Dewan, A. et al., 2013. Non-redundant coding of aversive odours in the main olfactory pathway. *Nature*, 497(7450), pp.486–489.

Duda, T. & Sharma, R.K., 2008. ONE-GC membrane guanylate cyclase, a trimodal odorant signal transducer. *Biochemical and Biophysical Research Communications*, 367, pp.440–445.

Elsaesser, R. et al., 2005. Phosphatidyl-inositide signalling proteins in a novel class of sensory cells in the mammalian olfactory epithelium. *The European journal of* *neuroscience*, 21(10), pp.2692–700.

Elsaesser, R. & Paysan, J., 2007. The sense of smell, its signalling pathways, and the dichotomy of cilia and microvilli in olfactory sensory cells. *BMC Neurosci*, 8 Suppl 3, p.S1.

Ferrando, S. et al., 2006. Observations of crypt neuron-like cells in the olfactory epithelium of a cartilaginous fish. *Neuroscience letters*, 403(3), pp.280–282.

Ferrero, D.M. et al., 2012. Agonists for 13 trace amine-associated receptors provide insight into the molecular basis of odor selectivity. *ACS Chem Biol*, 7(7), pp.1184–1189.

Ferrero, D.M. et al., 2011. Detection and avoidance of a carnivore odor by prey. *Proc Natl Acad Sci U S A*, 108(27), pp.11235–11240.

Fleischer, J., Breer, H. & Strotmann, J., 2009. Mammalian olfactory receptors. *Frontiers in cellular neuroscience*, 3(August), p.9.

Fleischer, J., Mamasuew, K. & Breer, H., 2009. Expression of cGMP signaling elements in the Grueneberg ganglion. *Histochem Cell Biol*, 131(1), pp.75–88.

Friedrich, R.W. & Korsching, S.I., 1998. Chemotopic, combinatorial, and noncombinatorial odorant representations in the olfactory bulb revealed using a voltage-sensitive axon tracer. *J Neurosci*, 18(23), pp.9977–9988.

Friedrich, R.W. & Korsching, S.I., 1997. Combinatorial and chemotopic odorant coding in the zebrafish olfactory bulb visualized by optical imaging. *Neuron*, 18(5), pp.737–752.

Gaillard, I., Rouquier, S. & Giorgi, D., 2004. Olfactory receptors. *Cellular and molecular life sciences : CMLS*, 61(4), pp.456–69.

Gao, J.L. et al., 1998. Differential expansion of the N-formylpeptide receptor gene cluster in human and mouse. *Genomics*, 51, pp.270–276.

Gayoso, J. et al., 2012. Crypt cells of the zebrafish Danio rerio mainly project to the dorsomedial glomerular field of the olfactory bulb. *Chemical senses*, 37(4), pp.357–69.

Gayoso, J.Á. et al., 2011. Differential bulbar and extrabulbar projections of diverse olfactory receptor neuron populations in the adult zebrafish (Danio rerio). *The Journal of comparative neurology*, 519(2), pp.247–76.

Germana, A. et al., 2004. S100 protein-like immunoreactivity in the crypt olfactory neurons of the adult zebrafish. *Neurosci Lett*, 371(2-3), pp.196–198.

Gloriam, D.E.I. et al., 2005. The repertoire of trace amine G-protein-coupled receptors: Large expansion in zebrafish. *Molecular Phylogenetics and Evolution*, 35, pp.470–482.

Hamana, K. & Matsuzaki, S., 1984. Unusual polyamines in slime molds Physarum polycephalum and Dictyostelium discoideum. *J Biochem*, 95(4), pp.1105–1110.

Hamdani el, H. & Doving, K.B., 2006. Specific projection of the sensory crypt cells in the olfactory system in crucian carp, Carassius carassius. *Chem Senses*, 31(1), pp.63–67.

Hansen, a & Finger, T.E., 2000. Phyletic distribution of crypt-type olfactory receptor neurons in fishes. *Brain, behavior and evolution*, 55(2), pp.100–110.

Hansen, A. et al., 2003. Correlation between olfactory receptor cell type and function in the channel catfish. *J Neurosci*, 23(28), pp.9328–9339.

Hansen, A., Anderson, K.T. & Finger, T.E., 2004. Differential distribution of olfactory receptor neurons in goldfish: structural and molecular correlates. *The Journal of comparative neurology*, 477(4), pp.347–359. Hansen, A. & Zeiske, E., 1998. The peripheral olfactory organ of the zebrafish, Danio rerio: an ultrastructural study. *Chem Senses*, 23(1), pp.39–48.

Hansen, A. & Zielinski, B.S., 2005. Diversity in the olfactory epithelium of bony fishes: development, lamellar arrangement, sensory neuron cell types and transduction components. *Journal of neurocytology*, 34(3-5), pp.183–208.

Hashiguchi, Y. & Nishida, M., 2007. Evolution of trace amine-associated receptor (TAAR) gene family in vertebrates: Lineage-specific expansions and degradations of a second class of vertebrate chemosensory receptors expressed in the olfactory epithelium. *Molecular Biology and Evolution*, 24, pp.2099–2107.

Hayden, S. & Teeling, E.C., 2014. The molecular biology of vertebrate olfaction. *Anatomical record (Hoboken, N.J. : 2007)*, 297(11), pp.2216–26.

Heale, V.R., Petersen, K. & Vanderwolf, C.H., 1996. Effect of colchicine-induced cell loss in the dentate gyrus and Ammon’s horn on the olfactory control of feeding in rats.

Brain Res, 712(2), pp.213–220.

Hildebrand, J.G., 1995. Analysis of chemical signals by nervous systems. *Proc Natl Acad Sci U S A*, 92(1), pp.67–74.

Hussain, A. et al., 2013. High-affinity olfactory receptor for the death-associated odor cadaverine. *Proceedings of the National Academy of Sciences of the United States of America*, 110, pp.19579–84.

Hussain, A., Saraiva, L.R. & Korsching, S.I., 2009. Positive Darwinian selection and the birth of an olfactory receptor clade in teleosts. *Proceedings of the National Academy of Sciences of the United States of America*, 106(11), pp.4313–4318.

Ibarra-Soria, X., Levitin, M.O. & Logan, D.W., 2014. The genomic basis of vomeronasal-mediated behaviour. *Mammalian genome : official journal of the International Mammalian Genome Society*, 25(1-2), pp.75–86.

Isogai, Y. et al., 2011. Molecular organization of vomeronasal chemoreception. *Nature*, 478, pp.241–245.

Johnson, M. a et al., 2012. Neurons expressing trace amine-associated receptors project to discrete glomeruli and constitute an olfactory subsystem. *Proceedings of the National Academy of Sciences of the United States of America*, pp.2–7.

Juilfs, D.M. et al., 1997. A subset of olfactory neurons that selectively express cGMP-stimulated phosphodiesterase (PDE2) and guanylyl cyclase-D define a unique olfactory signal transduction pathway. *Proceedings of the National Academy of Sciences of the United States of America*, 94, pp.3388–3395.

Kaluza, J.F. et al., 2004. Olfactory Receptors in the Mouse Septal Organ. *Journal of Neuroscience Research*, 76, pp.442–452.

Kang, N. & Koo, J., 2012. Olfactory receptors in non-chemosensory tissues. *BMB Reports*, 45, pp.612–622.

Kociánová, I. et al., 2006. Structure of Masera's septal olfactory organ in cat (Felis silvestris f. catus) - Light microscopy in selected stages of ontogeny. *Acta Veterinaria Brno*, 75, pp.471–475.

Korsching, S., 2009. The Molecular Evolution of Teleost Olfactory Receptor Gene Families.

Kratzing, J.E., 1978. The olfactory apparatus of the bandicoot (Isoodon macrourus): fine structure and presence of a septal olfactory organ. *Journal of anatomy*, 125, pp.601–613.

Leinders-zufall, T. et al., 2014. A Family of Nonclassical Class I MHC Genes Contributes to Ultrasensitive Chemodetection by Mouse Vomeronasal Sensory Neurons. , 34(15), pp.5121–5133.

Leinders-Zufall, T. et al., 2007. Contribution of the receptor guanylyl cyclase GC-D to chemosensory function in the olfactory epithelium. *Proceedings of the National Academy of Sciences of the United States of America*, 104, pp.14507–14512.

Liberles, S.D., 2014. Mammalian pheromones. *Annual review of physiology*, 76, pp.151–75.

Liberles, S.D., 2009. Trace amine-associated receptors are olfactory receptors in vertebrates. *Ann N Y Acad Sci*, 1170, pp.168–172.

Liberles, S.D. & Buck, L.B., 2006. A second class of chemosensory receptors in the olfactory epithelium. *Nature*, 442(7103), pp.645–650.

Luu, P. et al., 2004. Molecular determinants of ligand selectivity in a vertebrate odorant receptor. *The Journal of neuroscience : the official journal of the Society for Neuroscience*, 24, pp.10128–10137.

Ma, M., 2012. Odor and pheromone sensing via chemoreceptors. *Advances in experimental medicine and biology*, 739, pp.93–106.

Meyer, M.R. et al., 2000. A cGMP-signaling pathway in a subset of olfactory sensory neurons. *Proceedings of the National Academy of Sciences of the United States of America*, 97, pp.10595–10600.

Migeotte, I., Communi, D. & Parmentier, M., 2006. Formyl peptide receptors: A promiscuous subfamily of G protein-coupled receptors controlling immune responses. *Cytokine and Growth Factor Reviews*, 17, pp.501–519.

Mombaerts, P., 2006. Axonal wiring in the mouse olfactory system. *Annu Rev Cell Dev Biol*, 22, pp.713–737.

Mombaerts, P. et al., 1996. Visualizing an olfactory sensory map. *Cell*, 87(4), pp.675–686.

Mori, K. & Sakano, H., 2011. How is the olfactory map formed and interpreted in the mammalian brain? *Annu Rev Neurosci*, 34, pp.467–499.

Munger, S.D. et al., 2010. An olfactory subsystem that detects carbon disulfide and mediates food-related social learning. *Current biology : CB*, 20(16), pp.1438–44.

Oka, Y. & Korsching, S.I., 2011. Shared and unique G alpha proteins in the zebrafish versus mammalian senses of taste and smell. *Chemical senses*, 36(4), pp.357–65.

Oka, Y., Saraiva, L.R. & Korsching, S.I., 2012. Crypt neurons express a single V1R-related ora gene. *Chem Senses*, 37(3), pp.219–227.

Omura, M. & Mombaerts, P., 2014. Trpc2-Expressing Sensory Neurons in the Main Olfactory Epithelium of the Mouse. *CellReports*, pp.1–13.

Panas, M.W. et al., 2012. Trace amine associated receptor 1 signaling in activated lymphocytes. *Journal of Neuroimmune Pharmacology*, 7, pp.866–876.

Parisi, V. et al., 2014. Immunohistochemical characterization of the crypt neurons in the olfactory epithelium of adult zebrafish. *Annals of anatomy = Anatomischer Anzeiger : official organ of the Anatomische Gesellschaft*, 196(4), pp.178–82.

Pfister, P. & Rodriguez, I., 2005. Olfactory expression of a single and highly variable V1r pheromone receptor-like gene in fish species. *Proceedings of the National Academy of Sciences of the United States of America*, 102, pp.5489–5494.

Del Punta, K. et al., 2002. Deficient pheromone responses in mice lacking a cluster of vomeronasal receptor genes. *Nature*, 419, pp.70–74.

Rivière, S. et al., 2009. Formyl peptide receptor-like proteins are a novel family of vomeronasal chemosensors. *Nature*, 459, pp.574–577.

Rodriguez, I. et al., 2002. Multiple new and isolated families within the mouse superfamily of V1r vomeronasal receptors. *Nature neuroscience*, 5, pp.134–140.

Rolen, S.H. et al., 2003. Polyamines as olfactory stimuli in the goldfish Carassius auratus. *J Exp Biol*, 206(Pt 10), pp.1683–1696.

Saito, H. et al., 2009. Odor coding by a Mammalian receptor repertoire. *Sci Signal*, 2(60), p.ra9.

Saraiva, L.R. & Korsching, S.I., 2007. A novel olfactory receptor gene family in teleost fish A novel olfactory receptor gene family in teleost fish. Genome Research, pp.1448–1457.

Sato, Y., Miyasaka, N. & Yoshihara, Y., 2005. Mutually exclusive glomerular innervation by two distinct types of olfactory sensory neurons revealed in transgenic zebrafish. *The Journal of neuroscience : the official journal of the Society for Neuroscience*, 25(20), pp.4889–4897.

Schmid, A. et al., 2010. Grueneberg ganglion neurons are finely tuned cold sensors. *The Journal of neuroscience : the official journal of the Society for Neuroscience*, 30(22), pp.7563–8.

Sorensen, P.W., Hara, T.J. & Stacey, N.E., 1991. Sex pheromones selectively stimulate the medial olfactory tracts of male goldfish. *Brain Res*, 558(2), pp.343–347.

Speca, D.J. et al., 1999. Functional identification of a goldfish odorant receptor. *Neuron*, 23(3), pp.487–498.

Stacey, N. & Sorensen, P., 2005. Reproductive Pheromones. *Fish Physiology*, 24, pp.359–412.

Strotmann, J. et al., 2004. Olfactory receptor proteins in axonal processes of chemosensory neurons. *The Journal of neuroscience : the official journal of the Society for Neuroscience*, 24, pp.7754–7761.

Sun, L. et al., 2009. Guanylyl cyclase-D in the olfactory CO2 neurons is activated by bicarbonate. *Proceedings of the National Academy of Sciences of the United States of America*, 106(6), pp.2041–6.

Vassar, R. et al., 1994. Topographic Organization of Sensory Projection to the Olfactory Bulb. *Cell*, 79, pp.981–991.

Venkatesh, B. et al., 2014. Elephant shark genome provides unique insights into gnathostome evolution. *Nature*, 505, pp.174–9.

Wagner, S. et al., 2006. A multireceptor genetic approach uncovers an ordered integration of VNO sensory inputs in the accessory olfactory bulb. *Neuron*, 50(5), pp.697–709.

Wakabayashi, Y. et al., 2007. Expression of a vomeronasal receptor gene (V1r) and G protein alpha subunits in goat, Capra hircus, olfactory receptor neurons. *J Comp Neurol*, 503, pp.371–380.

Walz, A. et al., 2007. Axonal wiring of guanylate cyclase-D-expressing olfactory neurons is dependent on neuropilin 2 and semaphorin 3F. *Development (Cambridge, England)*, 134, pp.4063–4072.

Wang, Z.-G. & Ye, R.D., 2002. Characterization of two new members of the formyl peptide receptor gene family from 129S6 mice. *Gene*, 299, pp.57–63.

Weth, F., Nadler, W. & Korsching, S., 1996. Nested expression domains for odorant receptors in zebrafish olfactory epithelium. *Proc Natl Acad Sci U S A*, 93(23), pp.13321–13326.

VII.Abstract

Olfaction or the sense of smell is phylogenetically ancient, and mediates many vital behaviors such as prey detection, predator evasion, reproduction and kin recognition. Basic principles of vertebrate olfaction, among them the so-called -'one neuron-one receptor' rule and the principle of axonal convergence, are conserved in zebrafish, a powerful vertebrate model system. Furthermore, zebrafish possess orthologs of all but one of the six olfactory receptor families described for mammals, and both main olfactory sensory neuron types, ciliated and microvillous neurons, are present in zebrafish, together with the corresponding signal transduction cascades.

Here I show that the principle of axonal convergence of same-receptor-expressing neurons is valid for crypt neurons, a poorly understood third type of olfactory neurons that expresses the V1R-related ORA4 as sole olfactory receptor. I could identify the crypt neuron target glomerulus as mdg2, one of six invariant glomeruli in the mediodorsal cluster of the olfactory bulb.Together with the expression of ORA4 in all crypt neurons, this finding reveals a novel coding strategy in vertebrate olfaction: 'one cell type – one target glomerulus'. In the course of these studies I discovered and characterized a novel, forth population of olfactory neurons, which we named *kappe* neurons for their cap-like apical protrusion. For another member of the *ora* gene family, the recently deorphanized ORA1 receptor, I have identified a putative biological function for the first time. I could show that low concentrations of para-hydroxyphenyl acetic acid, a high affinity ligand of ORA1, elicit increases in oviposition frequency in zebrafish mating pairs, raising the exciting possibility that para-hydroxyphenyl acetic acid might constitute a novel reproductive pheromone.

Whether the activation of a single olfactory receptor is sufficient to generate behavioral output, is currently an active field of research. However there are very few cases described, where this has been shown to be the case, chief among them the insect pheromone receptors. I could show that low concentrations of cadaverine, a high affinity ligand for a zebrafish trace amine-associated receptor, TAAR13c, are sufficient to elicit a distinct avoidance behavior, and that at the same low concentration most of the activated olfactory neurons expressed TAAR13c, using pERK levels as measure of neuronal activation. This result suggests that TAAR13c is the major and conceivably the only receptor eliciting sensitive avoidance behavior to cadaverine.

VIII. Zusammenfassung

Der Geruchssinn ist phylogenetisch alt und vermittelt viele überlebenswichtige Verhaltensweisen wie das Aufspüren von Beutetieren, das Wahrnehmen von Fressfeinden, die Fortpflanzung und die Erkennung von Artgenossen. Grundlegende Prinzipien des Geruchssinnes in Vertebraten, darunter die sogenannte „ein Neuron-ein Rezeptor“-Regel und das Prinzip der axonalen Konvergenz, sind auch für den Zebrabärbling gültig, der ein etabliertes Wirbeltiermodellsystem darstellt. Darüber hinaus besitzt der Zebrafisch Orthologe für fünf der sechs olfaktorischen Rezeptorfamilien, die für Säugetiere bekannt sind. Auch die beiden grossen Populationen olfaktorischer sensorischer Neuronen, ciliierte und mikrovilläre Neuronen, sind im Zebrabärbling vorhanden, zusammen mit den dazugehörigen Signaltransduktionskaskaden.

Ich konnte in dieser Arbeit zeigen, dass das Prinzip der axonalen Konvergenz von Neuronen, die den gleichen Rezeptor exprimieren, für Crypt-Neuronen gültig ist, die einen noch wenig verstandenen dritten Typus olfaktorischer Neurone darstellen und einen einzigen olfaktorischen Rezeptor, ORA4, exprimieren. Den Zielglomerulus von Crypt-Neuronen habe ich als mdg2 identifiziert, bei dem es sich um einen von sechs unveränderlichen Glomeruli in dem mediodorsalen Cluster des olfaktorischen Bulbus handelt. Zusammen mit der Expression von ORA4 in allen Crypt-Neuronen zeigt dieser Befund ein neue Kodierungsstrategie im olfaktorischen System von Vertebraten: „Ein Zelltyp-ein Zielglomerulus“. Im Verlauf dieser Untersuchungen habe ich eine neue, vierte Population olfaktorischer Neurone entdeckt und charakterisiert. Da diese Neuronen apikal eine Kappe-ähnliche Struktur aufweisen, wurden sie von uns als Kappe-Neuronen bezeichnet.

Für ein anderes Mitglied der *ora*-Genfamilie, den ORA1-Rezeptor, habe ich zum ersten Mal eine mutmaßliche biologische Funktion identifiziert. Diesem Rezeptor konnte kürzlich (4-Hydroxyphenyl)-essigsäure als hochaffiner Ligand zugeordnet werden, und ich konnte zeigen, dass niedrige Konzentrationen dieses Liganden bei Zebrafischpärchen die Eiablage steigern, was die aufregende Möglichkeit aufwirft, dass (4-Hydroxyphenyl)-essigsäure ein neuartiges Reproduktionspheromon darstellen könnte.

Ob die Aktivierung eines einzigen olfaktorischen Rezeptors ausreicht, um ein Verhalten hervorzurufen, ist eine gegenwärtig aktiv untersuchte Fragestellung. Es sind nur wenige Beispiele für ein solches monogenes Verhalten bekannt, in erster Linie die

Pheromonrezeptoren von Insekten. Ich konnte zeigen, dass niedrige Konzentrationen von Kadaverin, einem hochaffinen Liganden für einen *trace amine-associated receptor* des Zebrabärblings, TAAR13c, ausreichend sind, um im Zebrafisch Vermeidungsverhalten auszulösen. Durch Messung von pERK als Maß für die neuronale Aktivität konnte ich zeigen, dass bei der gleichen niedrigen Konzentration die meisten der aktivierten olfaktorischen Neurone TAAR13c exprimierten. Dieses Ergebnis deutet darauf hin, dass TAAR13c der Hauptrezeptor und möglicherweise bei geringen Konzentrationen der einzige Rezeptor ist, der die aversive Reaktion auf Kadaverin auslöst.

IX. Author Contributions

1. Ahuja G, Ivandic I, Saltuerk M, Oka Y, Nadler W, Korsching SI. (2013) ¨Zebrafish crypt neurons project to a single, identified mediodorsal glomerulus¨. Sci Rep. 3:2063.

#

Authorship Status	*First*
Designed Research	Yes
Performed Research	Yes
Analyzed Data	Yes
Designed Figures	Yes
Wrote Paper	No

2. Ahuja G, Bozorg Nia S, Zapilko V, Shiriagin V, Kowatschew D, Oka, Y, Korsching SI (2014) ¨Kappe neurons, a novel population of olfactory sensory neurons¨. Sci Rep. 4:4037.

#

Authorship Status	*First*
Designed Research	Yes
Performed Research	Yes
Analyzed Data	Yes
Designed Figures	Yes
Wrote Paper	No

3. Hussain A*., Saraiva L.R*., Ferrero D*., Ahuja G*, Krishna VS, Liberles SD, Korsching SI (2013) ¨High-affinity olfactory receptor for the death-associated odor cadaverine¨. Proc Natl Acad Sci U S A, 110(48):19579-84. * Equal contribution

#

Authorship Status	*First*
Designed Research	No
Performed Research	Yes
Analyzed Data	No
Designed Figures	Yes
Wrote Paper	Yes

4. Behrens M., Frank O*., Rawel H* ., Ahuja G*., Potting C, Hofmann T., Meyerhof W and Korsching S (2014). ¨ORA1, a zebrafish olfactory receptor ancestral to all mammalian V1R genes, recognizes 4-hydroxyphenylacetic acid, a putative reproductive pheromone¨. J Biol Chem.pii: jbc.M114.573162.. * Equal contribution.

Authorship Status	*Second*
Designed Research	Yes
Performed Research	Yes
Analyzed Data	Yes
Designed Figures	Yes
Wrote Paper	Yes

5. **Ahuja G**[$] and Korsching SI. Zebrafish Olfactory Receptor ORA1 Recognizes a Putative Reproductive Pheromone. Communicative & Integrative Biology, Doi:10.4161/19420889.2014.970501 (2014). [$] Corresponding author

#

Authorship Status	*Second*
Designed Figures	Yes
Wrote Review article	Yes

[#] This information is also available under the ¨authors contribution¨ section of the publications.

X. ERKLÄRUNG

Ich versichere, dass ich die von mir vorgelegte Dissertation selbstständig angefertigt, die benutzten Quellen und Hilfsmittel vollständig angegeben und die Stellen in der Arbeit -einschließlich Tabellen, Karten und Abbildungen -, die anderen Werken im Wortlaut oder dem Sinn nach entnommen sind, in jedem Einzelfall als Entlehnung kenntlich gemacht habe; dass diese Dissertation noch keiner anderen Fakultät oder Universität zur Prüfungvorgelegen hat; dass sie - abgesehen von den unten angegebenen Teilpublikationen – noch nicht veröffentlicht worden ist, sowie dass ich eine solche Veröffentlichung vor Abschluss des Promotionsverfahrens nicht vornehmen werde. Die Bestimmungen dieser Promotionsordnung sind mir bekannt. Die von mir vorgelegte Dissertation ist von Prof. Dr. S. I. Korsching betreut worden.

Köln, den 17. Nov, 2014

Teilpublikationen:

1. **Gaurav Ahuja** # and Sigrun Korsching. Zebrafish Olfactory Receptor ORA1 Recognizes a Putative Reproductive Pheromone. Communicative & Integrative Biology, doi:10.4161/19420889.2014.970501 **(2014).** # Corresponding author
2. Maik Behrens, Oliver Frank*, Harshadrai Rawel*, **Gaurav Ahuja*,** Christoph Potting, Thomas Hofmann, Wolfgang Meyerhof and Sigrun Korsching. *ORA1, a zebrafish olfactory receptor ancestral to all mammalian V1R genes, recognizes 4-hydroxyphenylacetic acid, a putative reproductive pheromone*. J Biol Chem.pii: jbc.M114.573162 **(2014).**
   * These authors contributed equally to this paper
3. **Gaurav Ahuja**, Shahrzad Bozorg Nia, Veronika Zapilko, Vladimir Shiriagin, Daniel Kowatschew, Yuichiro Oka & Sigrun I. Korsching. Kappe neurons, a novel population of olfactory sensory neurons. Sci. Rep. 4, 4037; doi:10.1038/srep04037 **(2014)**.
4. Ashiq Hussain*, Luis R. Saraiva*, David M. Ferrero*, **Gaurav Ahuja***, Venkatesh S. Krishna, Stephen D. Liberles, and Sigrun I. Korsching. *High-affinity olfactory receptor for the death-associated odor cadaverine*; PNAS, doi/10.1073/pnas.1318596110 **(2013)**.
   * These authors contributed equally to this paper
5. **Gaurav Ahuja**, Ivan Ivandic, Mehmet Saltuerk, Yuichiro Oka, Walter Nadler & Sigrun I. Korsching. Zebrafish crypt neurons project to a single, identified mediodorsal glomerulus. Sci. Rep. 3, 2063; doi:10.1038/srep02063 **(2013)**.

XI. Curriculum vitae

Gaurav Ahuja
Apartment no: 514, Zuelpicher Strasse 58d, 50674,Cologne
Mobile: +49-176-34168334; *Email:* gauravahuja77@gmail.com

Aim

To pursue intellectually stimulating and challenging research that will broaden the frontiers of biological sciences by working in tandem with an accomplished team.

Further Education

PhD student in the laboratory of Prof. Sigrun Korsching at Institute for Genetics (University of Cologne), Cologne, Germany. **(Oct 2010 - present)**

M.Sc. in Genomics at the Center for Excellence in Genomic Sciences, School of Biological Sciences, Madurai Kamaraj University Tamil Nadu, India with **first division degree with distinction**.**(2008 to 2010)**

B.Sc. in Biotechnology from the Department of Biotechnology, Jamia Millia Islamia (Central Government University), New Delhi with **first division degree with distinction**. **(2005 to 2008)**

Additional Research Experience

M.Sc. Dissertation at Madurai Kamaraj University under the supervision of Dr. G.Kumaresan on ¨Molecular Genomic identification of prevalence of stem cell or stem cell related signatures in gastric cancer Transcriptome¨. **(Sep 2009 to Apr 2010)**

M.Sc. Summer project at the Department of Genetics, University of Delhi, South Campus, New Delhi, under the supervision of Prof. Sheela Srivastava on ¨Production, purification and characterization of bacteriocin from lactic acid bacteria and related strains¨ (Head of the Department of Genetics). **(May 2009 to Jul 2009)**

B.Sc. Summer project on ¨Training in ‘Molecular and Immunological methods for the detection of hepatitis, HIV-AIDS & dengue in human blood samples¨, at National Institute of Communicable Diseases, Ministry of Health and family Welfare, Government of INDIA, New Delhi. **(May 2007 to Jul 2007)**

Industrial Research Experience

Industrial internship on ¨Fermentation of Beer and its autoclaving on a Large Scale¨ at Superior Industries PVT. LTD. (Faridabad, Haryana). (Ref No: SIL/PER/06-07/915). **(Dec 2006 to Jan 2007)**

Publications

1. **Gaurav Ahuja**, Vera Reichel, Adnan S. Syed, Yuichiro Oka and Sigrun Korsching. Fuzzy topology for zebrafish olfactory receptors of the V2R-related OlfC family. **(Manuscript in preparation)**

2. Luis R. Saraiva*, **Gaurav Ahuja***, Ivan Ivandic, Adnan S. Syed, John C. Marioni, Sigrun I. Korsching, and Darren W. Logan. Molecular and neuronal homology between the olfactory systems of zebrafish and mouse. **(Submitted)** * shared first authors.

3. **Gaurav Ahuja** # and Sigrun Korsching. Zebrafish Olfactory Receptor ORA1 Recognizes a Putative Reproductive Pheromone. Communicative & Integrative Biology, Doi:10.4161/19420889.2014.970501 **(2014).** # Corresponding author http://www.tandfonline.com/doi/full/10.4161/19420889.2014.970501#.VGUaf4WpqPI

4. Maik Behrens, Oliver Frank*, Harshadrai Rawel*, **Gaurav Ahuja*,** Christoph Potting, Thomas Hofmann, Wolfgang Meyerhof and Sigrun Korsching. *ORA1, a zebrafish olfactory receptor ancestral to all mammalian V1R genes, recognizes 4-hydroxyphenylacetic acid, a putative reproductive pheromone*. J Biol Chem.pii: jbc.M114.573162. (**2014**)http://www.jbc.org/content/early/2014/05/15/jbc.M114.573162
   *** shared second author**

5. **Gaurav Ahuja**, Shahrzad Bozorg Nia, Veronika Zapilko, Vladimir Shiriagin, Daniel Kowatschew, Yuichiro Oka & Sigrun I. Korsching. Kappe neurons, a novel population of olfactory sensory neurons. Sci. Rep. 4, 4037; DOI:10.1038/srep04037 **(2014)**. http://www.nature.com/srep/2014/140210/srep04037/full/srep04037.html

6. Ashiq Hussain*, Luis R. Saraiva*, David M. Ferrero*, **Gaurav Ahuja***, Venkatesh S. Krishna, Stephen D. Liberles, and Sigrun I. Korsching. *High-affinity olfactory receptor for the death-associated odor cadaverine*; PNAS, doi/10.1073/pnas.1318596110 (**2013**). *** Shared first authors**
   http://www.pnas.org/content/110/48/19579.abstract

7. **Gaurav Ahuja**, Ivan Ivandic, Mehmet Saltuerk, Yuichiro Oka, Walter Nadler & Sigrun I. Korsching. Zebrafish crypt neurons project to a single, identified mediodorsal glomerulus. Sci. Rep. 3, 2063; DOI:10.1038/srep02063 **(2013)**.
   http://www.nature.com/srep/2013/130624/srep02063/full/srep02063.html

Prizes, Awards, Scholarship, Fellowships

Second best oral presentation award at symposium ¨**Shaping Cells and Organisms**¨ organized by IGS DHD, Cologne **(Sept 2014).**

Best poster award at Neurovision 10, entitled ¨Deorhanizing crypt neurons, third type of olfactory sensory neurons¨ under category ¨Neuroanatomy & Neurogenetics¨ at Forschungszentrum Jülich, Germany **(Sept 2014)**.

Best poster award at Neurovision 9, 2013 entitled ¨High-affinity olfactory receptor for the death-associated odor cadaverine¨ at University of Cologne, Germany **(Nov 2013)**.

Best poster award (2nd position) at GSFBS Alumni-day program at University of Cologne, Germany.

Successfully completed PhD scholarship from **International Graduate School in Development Health and Disease (IGS DHD)**, University of Cologne, Germany **(Oct 2010).**

Two times qualified CSIR-JRF, Council for Scientific and Industrial Research-Junior research fellowship (All India rank= 222 and 33) in **2009 and 2010**, respectively.

Invited speaker

Invited for a oral presentation at Turkish-German Graduate workshop in molecular neuroscience, at Bogazici University, Istanbul, Turkey, 2014.

Invited for a oral talk at “Aqua Terr” at Madurai Kamaraj University, Tamil Nadu, India (Sept 2013)

Invited for a oral presentation at MBG-BRIDGE, at Bogazici University, Istanbul, Turkey, 2012.

Teaching Experience

Advance Biology faculty at Mordern Vidhya Niketan, Faridabad, Haryana, India **(Apr-Sep 2010)**

Part- time teaching experience in Biology for the students coming from a minority group at Salvation Inc., an international Humanitarian developmental agency, New Delhi. **(2006)**

Acquired Scientific Methods

Molecular Biology: Standard techniques, Cloning techniques, Proteomics, quantitative PCR PCR, *in situ* hybridization, Immunostaining, Western blotting.

Neurobiology: Neuronal tracings using retrograde labeling dyes, whole mount axon labeling using immunostanings.

Bioinformatics: Microarray data analysis, Data mining and phylogenetic analysis, Genome browsing.

Additional Skills

1. Sound knowledge of Linux, MAC and Windows operating systems.
2. Comfortable in using Open Office and MS office applications.
3. Experienced in using vector illustration programs e.g. Inkscape and Adobe Illustrator.

References

Prof. Dr. Sigrun Korsching, Institute for Genetics, University of Cologne, Cologne, Germany: Email Id: sigrun.korsching@uni-koeln.de

XII. Appendix

List of abbreviations

1. MOE : Main olfactory epithelium
2. VNO : Vomeronasal organ
3. GG : Grueneberg ganglion
4. SO : Septal organ
5. OR : Odorant receptor
6. TAAR : Trace amine-associated receptor
7. FPR : Formyl peptide receptor
8. ORA : Olfactory receptor classA-related
9. zOR : Zebrafish odorant receptor
10. OSN : Olfactory sensory neuron
11. OMP : Olfactory marker protein
12. TRPC2 : Transient receptor potential cation channel, subfamily C, member 2,
13. OB : Olfactory Bulb
14. GFP : Green fluorescent protein
15. V1R : Vomeronasal receptor, type 1
16. V2R : Vomeronasal receptor, type 2
17. MDG : Mediodorsal glomeruli
18. pHPAA : para-hydroxy phenyl acetic acid